

Dissertation  
submitted to the  
Combined Faculties for the Natural Sciences and for Mathematics  
of the Ruperto-Carola University of Heidelberg, Germany  
for the degree of  
Doctor of Natural Sciences

presented by  
Diplom-Biochemikerin Nadine Holter  
born in Miltenberg

Oral-examination: \_\_\_\_\_



Development of  
phasic and tonic inhibitory GABAergic currents  
in mouse dentate gyrus

Referees: Prof. Dr. Hilmar Bading  
Prof. Dr. Andreas Draguhn



The present thesis was prepared at the Institute for Physiology and Pathophysiology of the Ruperto-Carola University of Heidelberg from December 2005 to November 2008, the doctoral thesis supervisor was Prof. Dr. Andreas Draguhn.

### **Danksagung**

*An dieser Stelle möchte ich allen danken, die zum Gelingen meiner Doktorarbeit beigetragen haben. Mein Dank gilt im Besonderen:*

*Prof. Dr. Andreas Draguhn, meinem Doktorvater, für die Betreuung der vorliegenden Arbeit und für intensive Diskussionen.*

*Prof. Dr. Hilmar Bading für die Begutachtung dieser Arbeit.*

*Prof. Dr. Hannah Monyer für die Aufnahme in das Graduiertenkolleg 791 und die damit verbundene finanzielle, sowie ideelle Förderung. Catherine Munzig für die Unterstützung.*

*Allen Kollegen der Arbeitsgruppe Draguhn für ein einzigartiges Arbeitsumfeld. Besonders Dr. Claus Bruehl und Nadine Zuber für die Hilfestellung.*

*Meiner Familie für das Vertrauen und die Unterstützung. Tobias für intensive abendliche Diskussionen und ehrliche Kritik.*



Declarations according to § 8 (3) b) and c) of the doctoral degree regulations:

- a) I hereby declare that I have written the submitted dissertation myself and in this process have used no other sources or materials than those expressly indicated,
- b) I hereby declare that I have not applied to be examined at any other institution, nor have I used the dissertation in this or any other form at any other institution as an examination paper, nor submitted it to any other faculty as a dissertation.

.....  
date

.....  
signature

*Project-related publications:*

Holter NI, Zuber N, Bruehl C, & Draguhn A (2007). Functional maturation of developing interneurons in the molecular layer of mouse dentate gyrus. *Brain Res* **1186**, 56-64.

Holter NI, Zylla M, Zuber N & Draguhn A. Tonic GABAergic inhibition in maturing dentate granule cells. **In preparation.**

*Publication from another project:*

Holter NI\*, Grimm C\*, Draguhn A, and Bruehl C (2008) Compensatory increase in P/Q-calcium current-mediated synaptic transmission following chronic block of N-type channels. *Neurosci Lett*, **442 (1)**, 44-49.

\* both authors contributed equally



## *Abstract*

The present thesis describes functional and morphological properties of interneurons and granule cell in developing mouse dentate gyrus, with special focus on inhibitory GABAergic currents. The dentate gyrus is the main hippocampal input structure receiving strong excitatory cortical afferents via the perforant path. Therefore, inhibition at the 'hippocampal gate' is important, particularly during postnatal development, when the hippocampal network is prone to seizures.

During this critical period of development the intrinsic and synaptic properties of developing inhibitory interneurons were monitored in the molecular layer of mouse hippocampal slices. In this region, mainly calretinin-positive cells of multipolar appearance were found. These GABAergic interneurons showed maturational changes of their intrinsic and synaptic properties after the first postnatal week. The maturation of molecular layer interneurons went along with faster and larger action potentials, increased repetitive firing, and increased frequency of spontaneous postsynaptic inhibitory currents. All developmental changes in intrinsic and synaptic properties occurred between postnatal day 6-8 and postnatal day 9-11, indicating a rapid functional maturation at the end of the first postnatal week.

Age-dependent changes of intrinsic and synaptic properties were also found in developing dentate gyrus granule cells. Similar to interneurons, mature dentate gyrus granule cells exhibited faster and larger action potentials and showed an increased frequency of spontaneous postsynaptic inhibitory currents. Thus, the integration of granule cells in the inhibitory synaptic network of dentate gyrus took place after the second postnatal week.

The data shows a rapid functional maturation of intrinsic and synaptic properties of interneurons and granule cells in the dentate gyrus and an early integration into the synaptic networks. However, stratum molecular interneurons were integrated prior to granule cells in the dentate gyrus network, which is corresponding to their subsequent developmental appearance.

Besides the influence of phasic synaptic inhibitory currents, throughout postnatal development the dentate gyrus network was also shown to be inhibited by tonic GABAergic currents. In dentate gyrus granule cells, tonic inhibitory currents were mediated by GABA<sub>A</sub>-receptors containing  $\alpha_5$ - and  $\delta$ -subunits. These extrasynaptic receptors were activated through the GABA in the extracellular space. The ambient transmitter was delivered by synaptic GABA release and regulated through GABA uptake by the GABA transporter-1. The contribution of the main components to tonic inhibition was surprisingly stable during granule cell maturation.

Throughout postnatal development, tonic inhibition reduced excitability of dentate gyrus granule cells by increasing action potential threshold. It further regulated hippocampal network excitability by preventing overexcitation of the dentate gyrus upon stimulation of entorhinal cortex. Functionally, tonic inhibition was shown to influence the excitation/inhibition balance of both, the adult and the maturing dentate gyrus.



## Kurzfassung

Die vorliegende Arbeit beschreibt die funktionalen und morphologischen Eigenschaften von Interneuronen und Körnerzellen im sich entwickelnden Gyrus dentatus der Maus. Der Fokus liegt dabei auf den GABAergen inhibitorischen Strömen. Der Gyrus dentatus steht unter starker exzitatorischer Kontrolle durch den entorhinalen Cortex. Daher ist die Inhibition an der Eingangstruktur des Hippocampus wichtig, insbesondere während der postnatalen Entwicklung, in der das hippocampale Netzwerk besonders krampfanfällig ist.

Während dieser kritischen Entwicklungsperiode wurden Interneurone der molekularen Schicht des Gyrus dentatus beobachtet. An akuten Hirnschnitten des Hippocampus wurden die intrinsischen und synaptischen Eigenschaften der sich entwickelnden Interneurone untersucht. In der Molekularschicht des Gyrus dentatus waren hauptsächlich multipolare Calretinin-positive Zellen zu finden. Nach der ersten postnatalen Woche zeigten diese GABAergen Interneurone entwicklungsabhängige Änderungen in ihren intrinsischen und synaptischen Eigenschaften. Die Reifung der Interneurone in der Molekularschicht ging einher mit schnelleren und größeren Aktionspotenzialen, vermehrtem repetitiven Feuermuster und einer erhöhten Frequenz der spontanen inhibitorischen postsynaptischen Ströme. Diese entwicklungsabhängigen Veränderungen fanden alle zwischen dem postnatalen Tag 6-8 und postnatalen Tag 9-11 statt, was auf eine schnelle funktionelle Reifung der Interneurone am Ende der ersten Woche hinweist.

Vergleichbar mit den Interneuronen entwickelten sich die Körnerzellen des Gyrus dentatus in ihren intrinsischen und synaptischen Eigenschaften. Reifere Körnerzellen hatten schnellere und größere Aktionspotenziale und eine gesteigerte Frequenz spontaner postsynaptischer inhibitorischer Ströme. Die Einbindung der Körnerzellen in das synaptische Netzwerk des Gyrus dentatus fand erst nach der zweiten postnatalen Woche statt. Entsprechend der Reihenfolge ihrer Entstehung integrierten sich Interneurone und Körnerzellen nacheinander in das neuronale Netzwerk des Gyrus dentatus.

Die erhobenen Daten zeigen eine schnelle funktionelle Reifung der Interneurone und Körnerzellen im Gyrus dentatus in ihren intrinsischen und synaptischen Eigenschaften und auch eine frühe Einbindung in das synaptische Netzwerk.

Abgesehen von den phasischen synaptischen inhibitorischen Strömen war das Netzwerk des Gyrus dentatus während der Entwicklung auch durch tonische GABAerge Ströme beeinflusst. Tonische inhibitorische Ströme der Körnerzellen im Gyrus dentatus wurden durch die GABA<sub>A</sub>- Rezeptoren vermittelt, welche  $\alpha_5$ - and  $\delta$ - Untereinheiten enthielten. Diese extrasynaptischen Rezeptoren wurden durch GABA im extrazellulären Raum aktiviert. Der die Zellen umgebende Transmitter wurde durch synaptische GABA-Freisetzung bereit gestellt und durch GABA-Aufnahme mit Hilfe des GABA Transporters GAT-1 reguliert. Der Beitrag dieser Hauptkomponenten der tonischen Inhibition blieb während der Ausreifung der Körnerzellen überraschenderweise unverändert.

Während der postnatalen Entwicklung verminderte tonische Inhibition die Erregbarkeit der Körnerzellen durch ein Anheben der Aktionspotenzialschwelle. Weiterhin regulierte die tonische Inhibition die Erregbarkeit des hippocampalen Netzwerks, indem sie eine Übererregbarkeit des Gyrus dentatus nach Stimulation im entorhinalen Kortex verhinderte. Daher beeinflusste tonische Inhibition die Excitations/Inhibitions Balance auf funktioneller Ebene im adulten Gyrus dentatus ebenso wie im sich entwickelnden Gewebe.



## Contents

<b>Introduction</b> .....	<b>- 1 -</b>
The hippocampal formation .....	- 1 -
<i>Cellular architecture of the hippocampal formation</i> .....	- 1 -
<i>Fiber projections of the hippocampal formation</i> .....	- 1 -
<i>Fiber projections of the dentate gyrus</i> .....	- 2 -
<i>Physiological function of the hippocampal formation</i> .....	- 2 -
The dentate gyrus – cell types and development .....	- 4 -
<i>Dentate gyrus granule cells</i> .....	- 4 -
<i>Interneurons</i> .....	- 5 -
<i>Network patterns and development of network patterns</i> .....	- 5 -
<i>Chloride reversal potential and GABAergic postsynaptic potentials</i> .....	- 6 -
The GABAergic synapse .....	- 7 -
<i>GABA transporters</i> .....	- 8 -
<i>GABA<sub>A</sub>-receptors</i> .....	- 9 -
Phasic GABA <sub>A</sub> -receptor activation .....	- 10 -
<i>The functional role of phasic inhibition</i> .....	- 10 -
Tonic GABA <sub>A</sub> -receptor activation .....	- 11 -
<i>The delta-subunit</i> .....	- 12 -
<i>The alpha<sub>5</sub>-subunit</i> .....	- 13 -
<i>Functional role of tonic inhibition</i> .....	- 13 -
<b>Aims of the study</b> .....	<b>- 15 -</b>
<b>Experimental procedure</b> .....	<b>- 16 -</b>
Slice preparation .....	- 16 -
Electrophysiological experiments .....	- 17 -
Whole cell patch clamp recordings .....	- 17 -
<i>Recording electrodes and intracellular solutions</i> .....	- 17 -
<i>The ‘Whole cell patch-clamp’ technique</i> .....	- 18 -
<i>Function of a patch-clamp amplifier</i> .....	- 18 -
<i>Electrical properties of whole cell recording</i> .....	- 20 -

Limitations of the patch clamp technique .....	- 21 -
<i>The space clamp problem</i> .....	- 21 -
<i>Series resistance</i> .....	- 21 -
<i>Offset potentials</i> .....	- 21 -
Patch Clamp Setup .....	- 22 -
Recording protocols .....	- 22 -
<i>Action potentials</i> .....	- 22 -
<i>Spontaneous inhibitory postsynaptic currents – dentate gyrus interneurons</i> .....	- 22 -
<i>Excitatory synaptic currents – dentate gyrus interneurons</i> .....	- 23 -
<i>GABAergic inhibitory currents – dentate gyrus granule cells</i> .....	- 23 -
Extracellular recordings (population spikes) - dentate gyrus granule cells .....	- 23 -
Drugs .....	- 24 -
Temperature conditions.....	- 24 -
Data recording and analysis .....	- 24 -
Histochemical experiments .....	- 25 -
Histological analysis.....	- 25 -
<i>Molecular layer interneurons</i> .....	- 26 -
<i>Dentate gyrus granule cells</i> .....	- 26 -
Immunohistochemistry .....	- 27 -
<i>Protocol</i> .....	- 27 -
<i>Molecular layer interneurons</i> .....	- 27 -
<b>Results</b> .....	<b>- 28 -</b>
<b>Part 1</b> .....	<b>- 28 -</b>
<b>Functional maturation of developing interneurons in the molecular layer of mouse dentate gyrus</b>	
Passive intrinsic properties of molecular layer interneurons change with maturation.....	- 29 -
Active intrinsic properties of molecular layer interneurons change with maturation .....	- 30 -
Spontaneous synaptic properties of molecular layer interneurons .....	- 33 -
<i>Excitatory synaptic currents were largely absent</i> .....	- 33 -
<i>Inhibitory synaptic activity of molecular layer interneurons increased with maturation</i> .....	- 34 -
Morphology of recorded stratum molecular interneurons .....	- 36 -
Classification of interneurons in developing stratum molculare .....	- 36 -
<b>Part 2</b> .....	<b>- 39 -</b>
<b>Maturation of dentate gyrus granule cells during early postnatal development</b>	
Passive intrinsic properties of granule cells change with maturation .....	- 40 -
Active intrinsic properties of dentate granule cells change with maturation.....	- 40 -

Postnatal development of Inhibitory Postsynaptic Currents (IPSCs) .....	- 42 -
Maturation of dentate granule cells recorded at physiological conditions .....	- 44 -
<i>Effect of temperature on IPSCs in dentate granule cell layer</i> .....	- 44 -
<i>Effect of GABA on IPSCs in dentate granule cell layer</i> .....	- 45 -
<b>Part 3</b> .....	<b>- 46 -</b>
<b>Tonic inhibitory currents in mouse dentate gyrus granule cells during postnatal development</b>	
Detection and analysis of tonic inhibition .....	- 47 -
Tonic inhibitory currents at “physiological” recording conditions.....	- 49 -
<i>Effect of temperature on tonic inhibitory currents of dentate gyrus granule cells</i> .....	- 49 -
<i>Effect of the GABA-supplementation on tonic inhibitory currents of granule cells</i> .....	- 49 -
Tonic inhibitory currents of dentate gyrus granule cells.....	- 50 -
<i>Pharmacological separation of tonic and phasic inhibitory currents in granule cells</i> .....	- 50 -
Tonic inhibitory currents could be detected throughout postnatal development .....	- 51 -
Receptors contributing to tonic inhibitory currents during postnatal development .....	- 53 -
<i>GABA<sub>A</sub>-receptors and not glycine receptors are contributing to tonic inhibitory currents in dentate gyrus granule cells</i> .....	- 53 -
<i>GABA<sub>A</sub>-receptor <math>\alpha_5</math>- and <math>\delta</math>-subunits are mediating tonic inhibitory currents in dentate gyrus granule cells during development</i> .....	- 53 -
Sources of ambient GABA for tonic inhibitory currents of dentate gyrus granule cells .....	- 57 -
<i>Synaptically released transmitter GABA acts as a source for the ambient GABA in the extracellular space throughout postnatal development</i> .....	- 57 -
<i>Contribution of GABA transporter GAT-1 to tonic inhibition during postnatal development</i> ...	- 59 -
Tonic inhibitory currents control single cell excitability throughout postnatal development .....	- 61 -
Tonic inhibitory currents control network excitability throughout postnatal development.....	- 63 -
<b>Discussion</b> .....	<b>- 65 -</b>
Functional maturation of interneurons in molecular layer of dentate gyrus .....	- 66 -
Functional maturation of dentate gyrus granule cells .....	- 67 -
Tonic inhibitory currents in dentate gyrus granule cells during postnatal development .....	- 68 -
Technical issues related to the recordings and measurements in this study .....	- 70 -
Outlook.....	- 72 -
<b>References</b> .....	<b>- 73 -</b>
<b>Appendix</b> .....	<b>- 83 -</b>

## Abbreviations

aCSF	artificial cerebrospinal fluid
AMPA	$\alpha$ -Amino-3-hydroxy-5-methylisoxazole-4-propionic acid
AP	action potential
APV	DL-2-Amino-5-phosphonopentanoic acid
ATP	adenosin-triphosphate
BSA	bovine serum albumin
CA1/2/3	regions of the hippocampus (cornu ammonis)
CCK	cholecystokinin
CNQX	6-Cyano-7-nitroquinoxalin-2,3-dione
(s)EPSC	(spontaneous) excitatory postsynaptic current
GABA	$\gamma$ -aminobutyric acid
GABA <sub>A</sub> R	GABA-receptor, A-type
GABA <sub>B</sub> R	GABA-receptor, B-type
GAD	glutamic acid-decarboxylase
GAT	GABA transporter
HEPES	4-(2-Hydroxyethyl)piperazine-1-ethanesulfonic acid
(s)IPSC	(spontaneous) inhibitory postsynaptic current
NMDA	N-methyl-D-aspartic acid
p or P	postnatal day
PB	phosphate buffer
PBS	phosphate buffered saline
PFA	paraformaldehyde
RT	room temperature
THIP	gaboxadol
TTX	tetrodotoxin
(w/v)	weight per volume



# Introduction

## The hippocampal formation

### *Cellular architecture of the hippocampal formation*

The hippocampal formation is a paired C-shaped structure in the mammalian brain, processing signals from amygdala to the cortical layers. Hippocampal cellular architecture and fiber projections (Fig. 1) have already been described by Ramón y Cajal's using Golgi staining (1891) and by the work of Lorente de Nó (1933, 1934). The mammalian hippocampal formation consists of interconnected cellular nuclei of the hippocampus proper and the dentate gyrus (DG). The subiculum is the hippocampal output structure. The hippocampal formation receives strong excitatory input from the adjacent entorhinal cortex (EC) via perforant path fibers (PP).

The hippocampus proper and dentate gyrus are phylogenetically old structures of the archicortex and exhibit the typical archicortical three-layered structure: the principal cell layer in the middle is surrounded by two fibrous layers (Fig. 1). Hippocampal principal layers are the granule cell layer of dentate gyrus and the pyramidal cell layer of hippocampus proper. The hippocampus proper is divided into three regions (CA1, CA2 and CA3) according to pyramidal cell size, where the CA3 region with its large pyramidal cells lays adjacent to the hilar structure of the dentate gyrus.

### *Fiber projections of the hippocampal formation*

The hippocampus receives its main synaptic input via the perforant path (PP) from superficial layer II of entorhinal cortex across the hippocampal fissure. A major part of these afferent fibers projects on dentate gyrus granule cells. Another part of perforant path circumvents the dentate gyrus and projects directly to the dendritic layers of hippocampus proper, providing direct input from entorhinal cortex layer II to CA1.

Axons of dentate gyrus granule cells (mossy fibers, mf) reach proximal dendrites of CA3 pyramidal cells, sending collaterals to hilar interneurons. CA3 pyramidal cell axons in turn innervate apical and basal dendrites of CA1 pyramidal cells via the Schaffer collaterals (sc). Signals from CA1 pyramidal cell axons go directly and indirectly back to entorhinal cortex deeper layers V and VI. This describes the most important hippocampal excitatory loop, the trisynaptic circuit (Anderson *et al.*, 1971). There is also a recurrent feedback loop between the hippocampus and the neocortex. Deep entorhinal layers project to the same cortex areas from where the afferences towards superficial entorhinal layers emerge. An impulse coming from a defined cortical region is traveling through the whole hippocampal circuit and back to its origin, whereby information processing can take place.

### *Fiber projections of the dentate gyrus*

The densely packed granule cell layer is the principal cell layer of dentate gyrus. Compared to pyramidal cells, granule cells are relatively small neurons. Their axons are projecting towards CA3 and build the prominent hilar mossy fiber tract (hilus, H; mossy fiber, mf). The dendritic arbor of the granule cells is spanning the adjacent molecular layer (stratum moleculare, sm). Superficial layers of entorhinal cortex (EC) terminate at the outer two thirds of stratum moleculare and the inner third is innervated from commissural associative and septal fibers and receives inputs from deeper layers of the entorhinal cortex.

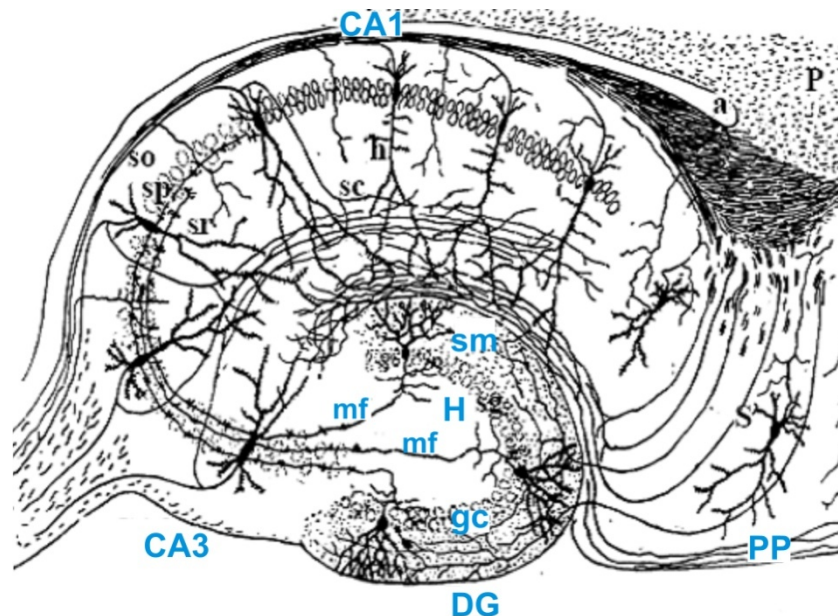


**Fig. 1 The hippocampus - areas, cell types, laminar layers and fiber projections.** *Areas:* dentate gyrus **DG**, hilus **H**, the hippocampus consisting of **CA1** and **CA3** region. subiculum **S**. *Principal cell types:* granule cells (**gc**) in the granule cell layer of dentate gyrus and pyramidal cells in the hippocampus (**h**: apical dendrite of a pyramidal cell). *Laminar layers:* granule cell layer/stratum granulosum (**sg**) and stratum moleculare (**sm**) of dentate gyrus; stratum oriens (**so**), pyramidal cell layer/stratum pyramidale (**sp**) and stratum radiatum (**sr**) of the hippocampus; *Fiber projections:* perforant path (**PP**), mossy fibers (**mf**), Schaffer collateral (**sc**) and alveus (**a**). Hippocampal areas, cell types, laminar layers and fiber projections were identified through Golgi studies by Ramón y Cajal (modified from Johnston and Amaral, 1998).

### **Physiological function of the hippocampal formation**

Because of the clearly laminated and therefore rather simple structure of the hippocampal network, the hippocampal formation has become an important model system. Here, information from various brain areas is integrated. The hippocampal formation is important for learning and memory related processes, especially for declarative and spatial memory formation. The mechanisms of transient information storage involve highly synchronized oscillations of hippocampal networks and hippocampal synaptic plasticity (see Fig. 2).

The dentate gyrus is regarded as the 'hippocampal gate' for afferent activity from entorhinal cortex. Granule cells receive neocortical information via the perforant path and each granule cell projects only onto approximately 10-15 CA3 pyramidal cells. Furthermore they make synaptic contacts to at

least an order of magnitude more interneurons (Acsady *et al.*, 1998; Heinemann *et al.*, 1992). This gating feature can also be applied to cognitive processes attributed to dentate gyrus. Hence, the dentate gyrus network is much more sensitive to differences, regarding, for example, small changes in spatial environment. In contrast, CA3 shows a relatively stable activity pattern, which switches into a different activity mode after coarse environmental changes (Leutgeb *et al.*, 2007; Leutgeb & Moser, 2007).

The dentate gyrus receives strong excitatory input from the entorhinal cortex. Inhibition in this region is therefore of particular importance to balance network activity at the hippocampal gate and to prevent overexcitation of the feedback loop between neocortex and hippocampus (Heinemann *et al.*, 1992; Stief *et al.*, 2007). In this context, the hippocampal formation, especially the dentate gyrus, is also associated with certain diseases. An example is temporal lobe epilepsy where excitation/inhibition balance of the neuronal network is disturbed.

It is therefore important to learn how inhibition of dentate gyrus network is organized, particularly during postnatal development, when main network patterns are formed from more immature stages.

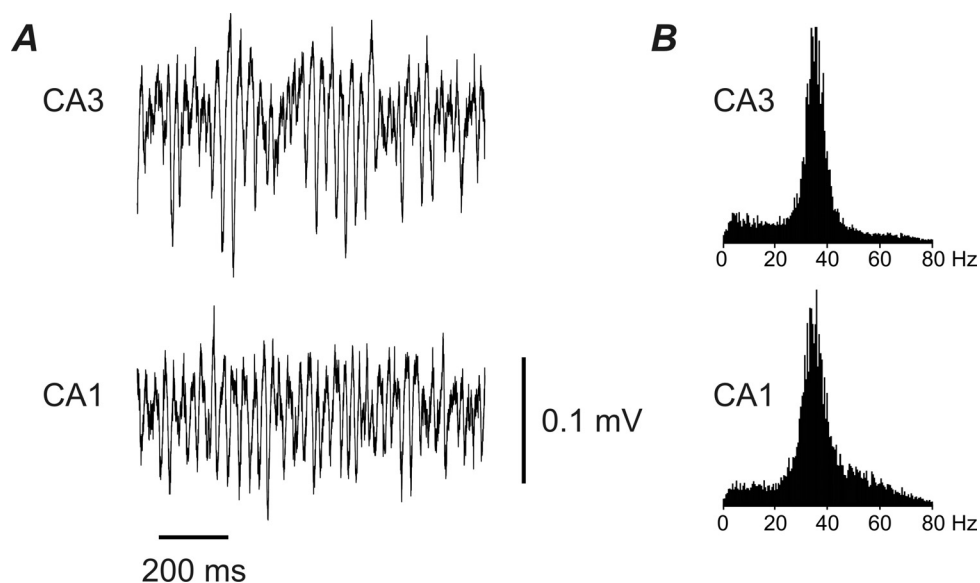


**Fig. 2 Example traces of hippocampal  $\gamma$  oscillations. (A)** Hippocampal  $\gamma$  oscillations of CA3 and CA1 region. **(B)** Frequency band of hippocampal  $\gamma$  oscillations peaks between 30 Hz and 40 Hz. *Example traces kindly provided by Dr. Martin Both.*

## The dentate gyrus – cell types and development

### *Dentate gyrus granule cells*

Dentate gyrus granule cells can be easily identified according to their location and morphology: their dendritic arbors span the molecular layer and their axons project towards the CA3 region. Furthermore, they express the excitatory neurotransmitter glutamate, but are as well capable to synthesize GABA (Mody, 2002).

Like other principal cells, granule cells arise relatively late during development (Altman & Bayer, 1990a). Most of the granule cells appear in the first postnatal week with a gradient from the suprapyramidal to the infrapyramidal blade (Soriano *et al.*, 1989a; Soriano *et al.*, 1989b; Soriano *et al.*, 1986). Granule cells are born in a specialized region of the subventricular zone (termed 'secondary matrix' by Altman and Bayer) and migrate radially along the primary radial glia scaffold to form the primordial granule cell layer. Migration takes place in such a way that older neurons are located at the tip of the upper blade and younger ones at the tip of the forming lower blade. Dividing precursor cells settle in the future hilus and continue to proliferate granule cells locally, these cells are called 'tertiary matrix' by Altman and Bayer (Li & Pleasure, 2005).

By the end of the first postnatal week, most of the dividing precursor cells are now located at the border between the granule cell layer and the hilus. In this specialized stem cell niche, granule cells continue to be born in decreasing number throughout the whole animal life (Kempermann *et al.*, 2004). These newborn granule cells migrate from the hilar border towards the outer border of granule cell layer, where they then exhibit mature morphology (Fig. 3). Adult neurogenesis in dentate gyrus is believed to be required for the normal function of the hippocampus (Leuner *et al.*, 2006) and may have a role in the formation of temporal association memory in the hippocampus (Ming & Song, 2005).

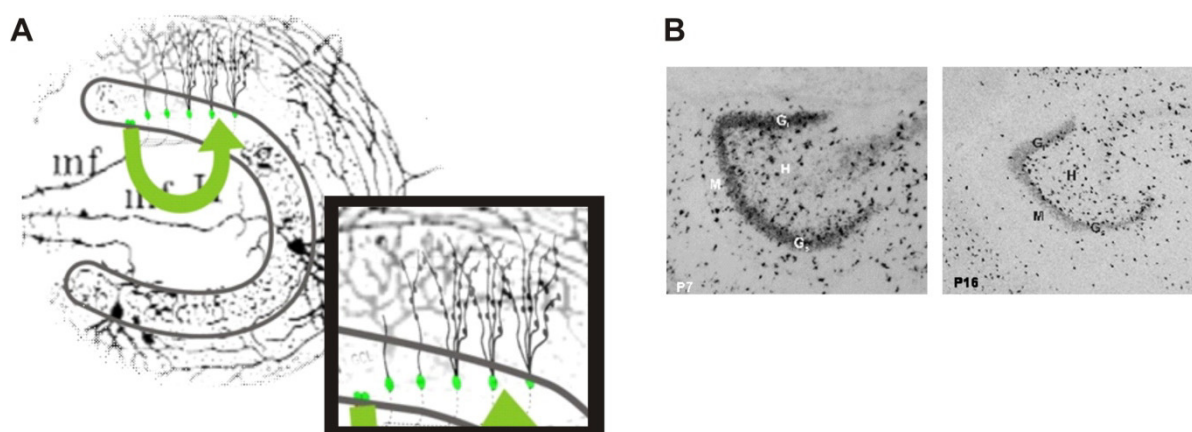


**Fig. 3 Dentate gyrus neuronal migration.** (A) Growth and maturation of adult newborn granule cells in dentate gyrus. Dividing precursor cells are located in subgranular zone of dentate gyrus, where the newborn granule cell appears. By about day 2 an apical process extends into the granule cell layer and the mossy fiber appears subsequently, growing into the mossy fiber pathway after the first week. The dendritic arborization develops and the cells migrate to their final location (Ming & Song, 2005; Shapiro & Ribak, 2005). (B) The distribution of GAT-1 and GAD67/65 positive interneurons at postnatal day 7 (p7) vs. postnatal day 16 (p 16). Note that GABAergic interneurons are redistributed during postnatal development in dentate gyrus. M molecular layer, G granule cell layer and H hilus (*modified from Frahm & Draguhn, 2001*).

## *Interneurons*

The neuronal network of dentate gyrus consists of glutamatergic principal neurons and GABAergic interneurons. These local circuit neurons provide only ~10% of the hippocampal cell population but are of crucial importance for the organization of network activity. They determine excitation/inhibition balance through feedback – or feedforward inhibition (Freund & Buzsaki, 1996; Somogyi & Klausberger, 2005; Soriano & Frotscher, 1989). In addition, they play a key role in synchronizing neuronal networks during oscillatory activity and thereby control information processing in large principal cell populations (Klausberger *et al.*, 2005; Somogyi & Klausberger, 2005; Whittington & Traub, 2003).

Interneurons are highly heterogeneous as compared to principal cells. Based on the Golgi-studies of Cajal, interneuron subtypes have been identified by morphological criteria, like soma localization and axonal projections. Furthermore, GABAergic interneurons are classified according to their expression pattern of histochemical marker proteins, like the neuropeptides somatostatin, vasoactive intestinal peptide (VIP) and cholecystokinin (CCK), or the calcium-binding proteins parvalbumin and calbindin. (Freund & Buzsaki, 1996; Matyas *et al.*, 2004; Somogyi & Klausberger, 2005).

In contrast to principal neurons, prospective interneurons are formed early during development of the hippocampal anlage of rodents (Soriano *et al.*, 1986) and continue to be generated during the first postnatal week (Navarro-Quiroga *et al.*, 2006). GABAergic interneurons of the dentate gyrus are formed in the subventricular zone and reach the dentate gyrus via the rostral migratory stream (Pleasure *et al.*, 2000). Many interneurons first appear in stratum moleculare of the suprapyramidal blade. During the first two postnatal weeks, a major portion of these cells migrate through the granule cell layer towards their final location in the hilus (Dupuy-Davies & Houser, 1999). These interneurons play a potential role in dentate gyrus development. They produce the transmitter GABA, which has rather neurotrophic than synaptic function in the immature brain (Dupuy-Davies & Houser, 1999; Schousboe & Redburn, 1995). While in adult animals most inhibitory interneurons are found in the hilus or at the hilar border of the granule cell band, some interneurons do persist in the molecular layer (Fig. 3B) (Dupuy & Houser, 1996; Dupuy & Houser, 1997; Dupuy-Davies & Houser, 1999; Frahm & Draguhn, 2001).

Hence, maturation of the dentate gyrus network is accomplished relatively late during ontogenesis. GABAergic signaling is believed to play a major role for neuronal differentiation (Ben-Ari *et al.*, 2004; Gozlan & Ben-Ari, 2003; Kriegstein, 2005). This suggests that the mature dentate gyrus network may result from the interplay between early appearing interneurons, the developing granule cell layer and increasing activity of input pathways, most notably the perforant path.

## *Network patterns and development of network patterns*

Immature network activity patterns of the dentate gyrus are characterized by massive spontaneous network events, called early network bursts. Single neurons show giant depolarizing potentials (GDPs) initiated by excitatory input to immature interneurons (Fig. 4; Leinekugel *et al.*, 1999). This immature activity is spontaneous and putatively non directional, however, it promotes neuronal survival and the formation of stable synaptic contacts (Katz & Shatz, 1996; Owens & Kriegstein,

2002). It has also been shown that early GABAergic potentials are sufficient to synchronize granule cells (Hollrigel *et al.*, 1998).

During the first and second postnatal week the network of dentate gyrus is changing. Mature network patterns like  $\theta$  oscillations and primitive sharp waves occur (Leinekugel *et al.*, 2002). This transition in network patterns goes along with the change of GABAergic neurotransmission from excitation to inhibition during early postnatal development (Ben-Ari *et al.*, 2007).

### *Chloride reversal potential and GABAergic postsynaptic potentials*

The  $\text{Cl}^-$  reversal potential determines whether a GABAergic synapse elicits a depolarization or a hyperpolarization at the postsynaptic membrane.  $\text{GABA}_A$ -receptors are ligand activated chloride channels and their chloride driving force is depending on the electrochemical chloride gradient.

Adult hippocampal neurons have low intracellular chloride, maintained by the outwardly directed  $\text{K}^+/\text{Cl}^-$  co-transporter (KCC2). Therefore,  $\text{Cl}^-$  influx leads to a membrane hyperpolarization, which in turn inhibits the neuron by driving the membrane potential further from the action potential threshold ( $E_{\text{Cl}} \sim -70 \text{ mV}$  vs. AP-threshold  $-40$  to  $-50 \text{ mV}$ ).

In contrast, in immature hippocampal neurons the inwardly directed  $\text{Na}^+/\text{K}^+/\text{Cl}^-$  co-transporter (NKCC1) maintains a high intracellular chloride concentration, and therefore GABAergic postsynaptic potentials are depolarizing, rather than hyperpolarizing (Ben-Ari, 2002; Leinekugel *et al.*, 1999). During the first postnatal week, neuronal intracellular chloride concentration decreases and the GABA reversal potential ( $E_{\text{GABA}}$ ) becomes more negative, leading to inhibitory postsynaptic events.

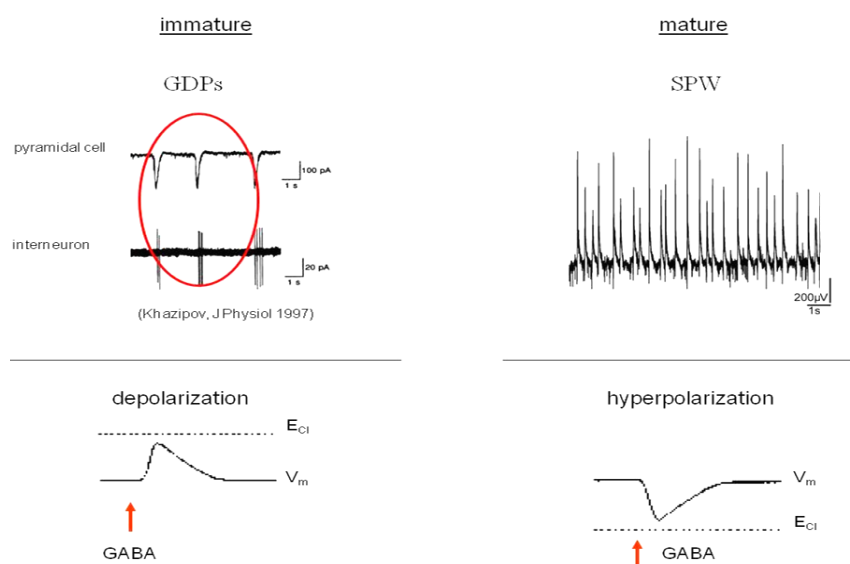


**Fig. 4 Immature and mature firing pattern.**

GDPs, Giant depolarizing potentials are characteristic for immature neurons.

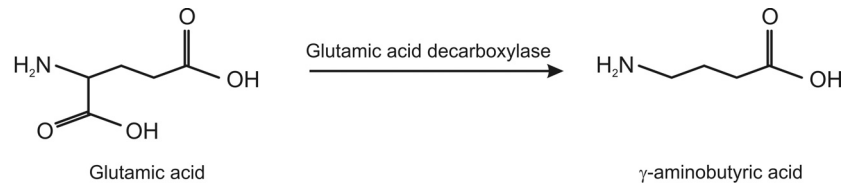
Mature hippocampal networks show sharp waves (SPW).

This transition in network patterns goes along with the change from depolarizing to hyperpolarizing chloride responses of the postsynaptic cells.

SPW CA1 raw data kindly provided by Elisa Weiss.

## The GABAergic synapse

A simplified scheme of the inhibitory synapse releasing the neurotransmitter GABA is depicted in figure 5. The neurotransmitter GABA ( $\gamma$ -aminobutyric acid) is produced at the presynaptic site of the GABAergic synapse by decarboxylating glutamic acid through the GAD-enzyme (GAD = Glutamic acid decarboxylase).



Then the vesicular GABA transporter (vGAT) transports GABA into synaptic vesicles. Upon the arrival of an action potential at the synapse, local  $\text{Ca}^{2+}$  influx triggers the fusion of the vesicular membrane with the synaptic membrane. Thereby, GABA is released into the synaptic cleft reaching millimolar concentrations (Mozrzymas *et al.*, 2003).

At the postsynaptic site, GABA binds to its receptors. The  $\text{GABA}_A$ -receptor is a ligand-gated chloride channel and its activation in mature neurons leads to chloride influx into the postsynaptic cell causing a membrane hyperpolarization. The  $\text{GABA}_B$ -receptor is a metabotropic G-protein coupled receptor. Binding of transmitter leads to an increased  $\text{K}^+$ -permeability by activation of inwardly rectifying potassium channels (GIRK or Kir3) underlying the late phase of inhibitory postsynaptic potentials. There are also  $\text{GABA}_B$ -receptors localized at the presynaptic site. Activation of presynaptic  $\text{GABA}_B$  receptors decreases neurotransmitter release probability by inhibiting voltage-activated  $\text{Ca}^{2+}$  channels of the N or P/Q type. Furthermore, activation of  $\text{GABA}_B$ -receptors interacts with cAMP production and various ion channels and proteins are targets of the cAMP-dependent kinase (protein kinase A, PKA).

At the presynaptic site neurotransmission is terminated by GABA-transporters clearing the synaptic cleft. They translocate the liberated transmitter back into the presynapse.

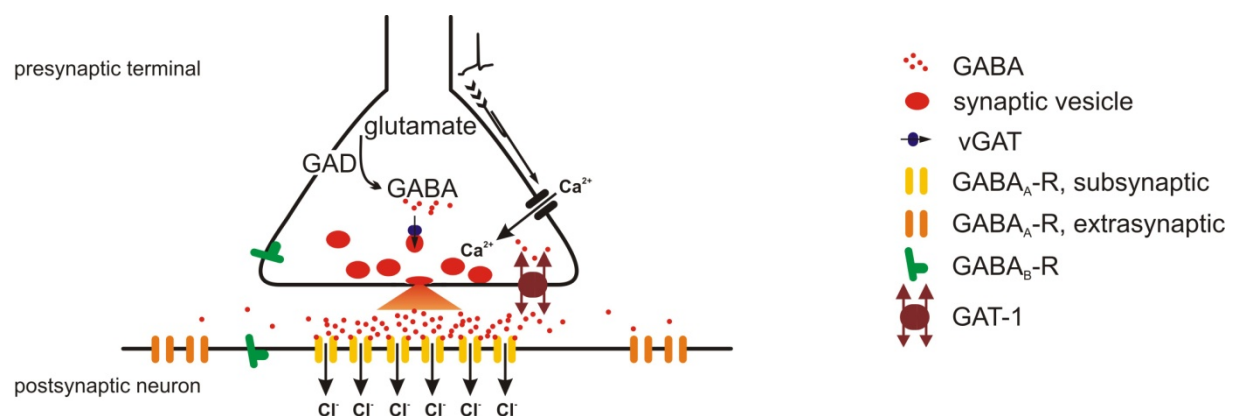


**Fig. 5 The GABAergic synapse.**

### GABA transporters

GABA transporters are high affinity membrane-bound translocators of GABA (Chen *et al.*, 2004). After action-potential mediated transmitter release, GABA transporters clear the synaptic cleft and thereby reduce the ambient GABA concentration in the extracellular space. The family of GABA transporters consists of glial and neuronal GABA transporter (GAT) 1, 2 and 3 (SLC6A1, SLC6A13, and SLC6A11), whereby rat GAT-3 is homologous to mouse GAT-4. Regarding the fact that only a few thousands of GABA molecules are released presynaptically, GAT-1, the most abundant neuronal GABA translocator, has a high density at the presynaptic membrane ( $\sim 1000$  GAT-1 molecules/ $\mu\text{m}^2$ ). Therefore, the uptake system probably binds a large fraction of the released GABA molecules. The GABA transporter cotransports the neurotransmitter with sodium and chloride in an electrogenic fashion (Kavanaugh *et al.*, 1992; Mager *et al.*, 1993; Malchow & Ripps, 1990). Usually, after synaptic GABA release the cotransporter translocates GABA along its concentration gradient from the synaptic cleft into the cell, the direction which is most thermodynamically favorable (Attwell *et al.*, 1993; Levi & Raiteri, 1993; Richerson & Wu, 2003).

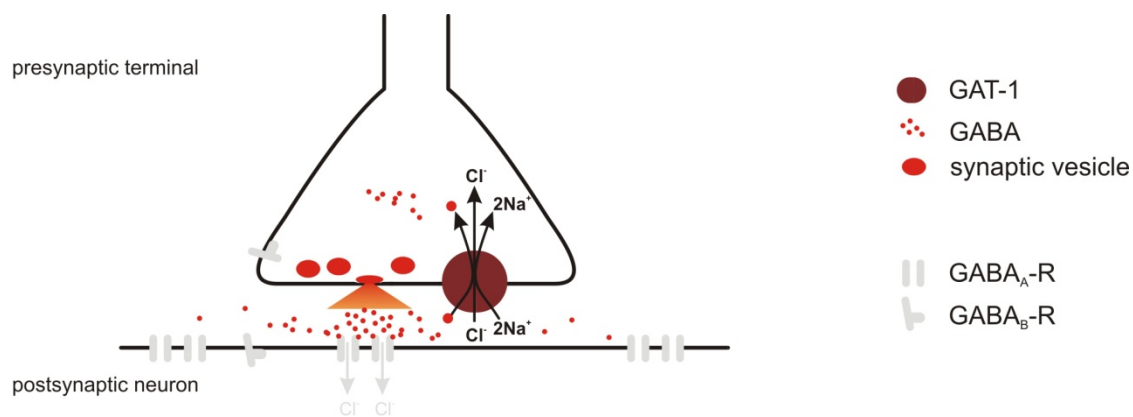


**Fig. 6 GABA transporter.** GABA transporters are Na<sup>+</sup>/Cl<sup>-</sup> dependent GABA translocators acting in the direction, which is most thermodynamically favorable. Together with the transmitter one chloride ion and two to three sodium ions are transported.

Under certain conditions the GABA uptake system may also function in reverse direction, resulting in nonvesicular GABA release. This has been shown biochemically for specific experimental conditions, when the transporter's driving force is inverted or when cells are strongly depolarized (Gaspary *et al.*, 1998; Schwartz, 1987). The reversal of GABA transport has also been discussed for early developmental time points. Prior to synapse formation, growth cones of neurons isolated from rat forebrain release GABA by reversal of GABA transport (Taylor & Gordon-Weeks, 1991).

Both, the removal of released transmitter and the possibility of inversed action make the uptake system an effective regulator of GABA concentrations in the extracellular space.

---

**Fig. 5 The GABAergic synapse.** At the presynaptic terminal glutamate is metabolized into GABA by the Glutamic acid decarboxylase (GAD). The vesicular GABA transporter (vGAT) transports GABA into synaptic vesicles. Local action-potential triggered calcium ion influx leads to transmitter release into the synaptic cleft. At the postsynapse ligand-bound GABA<sub>A</sub>-receptor (GABA<sub>A</sub>-R) opens and chloride influx caused membrane hyperpolarization. GABA is translocated back in the presynapse by neuronal GABA-transporter (GAT-1). GABA<sub>B</sub>-receptors are located at pre- and postsynaptic sites (GABA<sub>B</sub>-R).

## GABA<sub>A</sub>-receptors

The pentameric GABA<sub>A</sub>-receptors belong to the cysteine-loop ligand-gated ion channel families. Nineteen GABA<sub>A</sub>-receptor subunits ( $\alpha_1$ – $\alpha_6$ ,  $\beta_1$ – $\beta_3$ ,  $\gamma_1$ – $\gamma_3$ ,  $\delta$ ,  $\epsilon$ ,  $\tau$ ,  $\pi$  and  $\rho_1$ – $\rho_3$ ) and additional splice variants are expressed in different brain regions and neuronal populations (Laurie *et al.*, 1992). Of the various theoretically possible subunit combinations indeed only few exist. Five subunits form one receptor with a central ion channel, permeable to chloride, and to a lesser extent, to bicarbonate anions. The most abundant receptor subtype in the hippocampus consists of the subunits  $\gamma$ – $\beta$ – $\alpha$ – $\beta$ – $\alpha$ , arranged around the central receptor pore (Ben-Ari *et al.*, 2007; Stephenson, 1995).

Depending on their subunit composition, the heterogeneous receptor population shows functional differences. The different GABA<sub>A</sub>-receptor subunits control receptor distribution at the cell surface, receptor dynamics and pharmacological modulation of the native receptor. In addition to the receptor subunits, there are also other factors contributing to different GABA<sub>A</sub>-receptor functions in different cell types. For example intracellular calcium concentration (Mozrzymas & Cherubini, 1998), receptor phosphorylation (Moss & Smart, 1996) and associated cytoskeletal anchoring proteins (Chen *et al.*, 2000) have been shown to alter ligand affinity, peak current size and the rate of desensitization of GABA<sub>A</sub>-receptors.

In addition to the GABA binding site, GABA<sub>A</sub>-receptors have several different ligand binding sites. These are binding sites for benzodiazepines and barbiturates, both modulating receptor function (Mohler, 1992). Other ligand binding sites are occupied by allosteric inhibitors like bicuculline or gabazine (Ueno *et al.*, 1997).

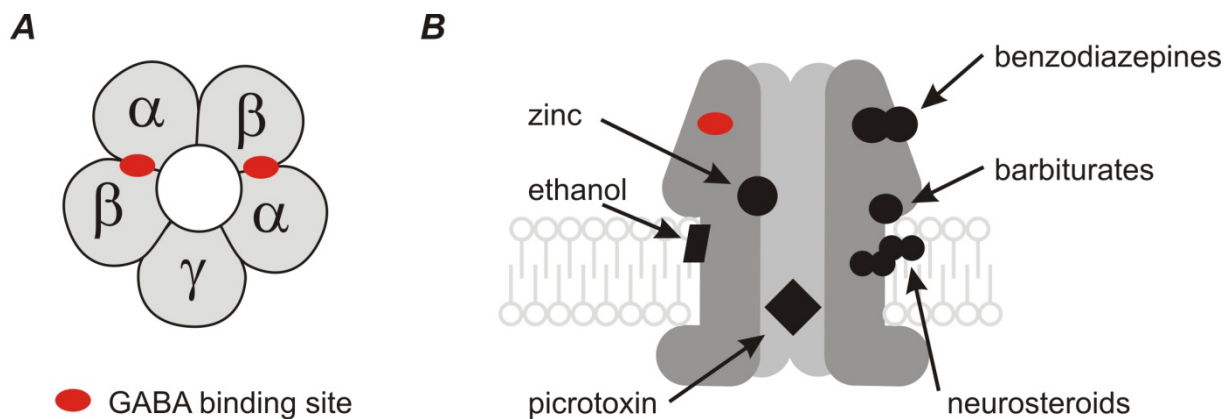


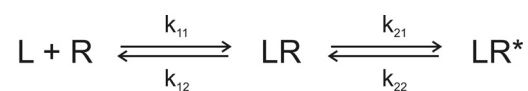
**Fig. 7 GABA<sub>A</sub>-receptor binding sites.** (A) The pentameric GABA<sub>A</sub>-receptor exhibits two transmitter binding sites. The binding pocket for GABA is located at the interface of  $\alpha$ - and  $\beta$ -subunit. (B) GABA<sub>A</sub>-receptors have additional ligand binding sites.

For efficient gating, the GABA<sub>A</sub>-receptor ion channel requires binding of two GABA molecules. The activation of postsynaptic GABA<sub>A</sub>-receptors leads to a membrane hyperpolarization and reduction of action potential firing by both, phasic and tonic GABAergic inhibitory currents.

## Phasic GABA<sub>A</sub>-receptor activation

Phasic inhibitory postsynaptic currents (IPSCs) are mediated by a small number of GABA<sub>A</sub>-receptors directly located at the synapse (Nusser *et al.*, 1997). After the rapid increase in GABA concentration by action-potential mediated vesicular release, the transmitter binds to the receptor at the postsynaptic site. The ligand gated ion channels open by conformational change and chloride flows into the cell along its electrochemical gradient. The increase in chloride conductance hyperpolarizes the postsynaptic cell ( $E_{Cl} < E_m$ ) and the generation of an action potential is impeded. Therefore, phasic activation of GABAergic postsynaptic receptors by rapid point-to-point communication is fundamental to information transfer in the brain.

Signals recorded from the postsynaptic neuron in this study are spontaneous inhibitory currents (sIPSC). These events show a rapid onset with rise times of a few hundred microseconds, reflecting a high speed of closed to open transition of the ion channel pores. The decay of the inhibitory postsynaptic current is determined by closure of the ion channel after ligand removal from the synaptic cleft (receptor deactivation). The fast sIPSC kinetics is also due to properties of subsynaptic GABA<sub>A</sub>-receptor subunits, reflecting the speed of transition between different receptor states (entry into and exit from agonist bound state). Different receptor conformations can be described by the following simplified activation scheme:



Whereby: ligand L; receptor R; closed receptor-ligand-complex LR; open ligand-bound channel LR\*; forward constants for the binding and the gating reactions  $k_{11}$  and  $k_{21}$ , respectively; backward constants for the binding and the gating reactions  $k_{12}$  and  $k_{22}$ , respectively.

These IPSCs decay kinetics may be varying during postnatal development and also between different cell types, which is probably due to the different subunits incorporated in GABA<sub>A</sub>-receptor subtypes.

### *The functional role of phasic inhibition*

Phasic inhibition mediated by GABA releasing interneurons and GABA<sub>A</sub>-receptors at the postsynaptic membrane prevents overexcitation of neurons and thereby avoids the development of pathological network activity. Moreover, GABAergic interneurons have an essential role in generating rhythmic activities in neuronal networks. Hippocampal basket cells are, for example, important for generating and maintaining theta and gamma frequency network oscillations. For the synchronization at high frequencies (gamma frequency) the rapid IPSC time course is essential. Also synchronous population spike activity is regulated by phasic GABA<sub>A</sub>-receptor activation (Huntsman *et al.*, 1999; Laurent, 2002).

Important for the impact of phasic inhibition on the cellular level is the spatial and temporal integration of GABAergic signals in the postsynaptic cells. Dendritic inhibitory signals are integrated over a long time period and prevent both, excitatory postsynaptic potentials (Tsubokawa & Ross, 1996) and dendritic Ca<sup>2+</sup> spikes (Miles *et al.*, 1996). In contrast, inhibitory synapses located directly at the soma lower action potential threshold of principal cells (Kempermann *et al.*, 2004; Miles *et al.*, 1996).

These examples show that point-to-point interactions by spatially restricted (subs synaptic) GABA<sub>A</sub>-receptors are important for both, regulating information transfer on the single cell and network level.

## Tonic GABA<sub>A</sub>-receptor activation

In addition to the subsynaptic GABA<sub>A</sub>-receptors there are also peri- and extrasynaptic GABA<sub>A</sub>-receptors. In contrast to the fast subsynaptic IPSCs (phasic inhibition), the activation of non-synaptic GABA<sub>A</sub>-receptors causes a long-lasting increase in chloride conductance (tonic inhibition, see Fig. 8). GABA is not only mediating rapid information transfer at the synapse, but also takes part in other forms of signaling. Ambient GABA in the extracellular space (Lerma *et al.*, 1986) can activate extrasynaptic GABA<sub>A</sub>-receptors since they exhibit a high GABA affinity.

Tonic inhibitory currents can be observed by blocking GABA<sub>A</sub>-receptor with specific antagonists like bicuculline, gabazine or picrotoxin. Perfusion of these drugs blocks sIPSCs and furthermore decreases the 'holding current' of the recorded neuron (Fig. 8C), which is voltage clamped to a selected membrane potential (see patch clamp technique, Material and Methods). This observed reduction in input conductance after block of GABA<sub>A</sub>-receptors is associated with a reduction in baseline noise (current variance), probably due to the reduced number of open GABA<sub>A</sub>-receptor channels (Nusser & Mody, 2002; Semyanov *et al.*, 2003).

Therefore, tonic GABA<sub>A</sub>-receptor activation causes a persistent increase in the neuron's input conductance, which reduces the size and duration of an excitatory postsynaptic potential to a given input current. The narrowed spatial and temporal window for signal integration interferes then with action potential generation.

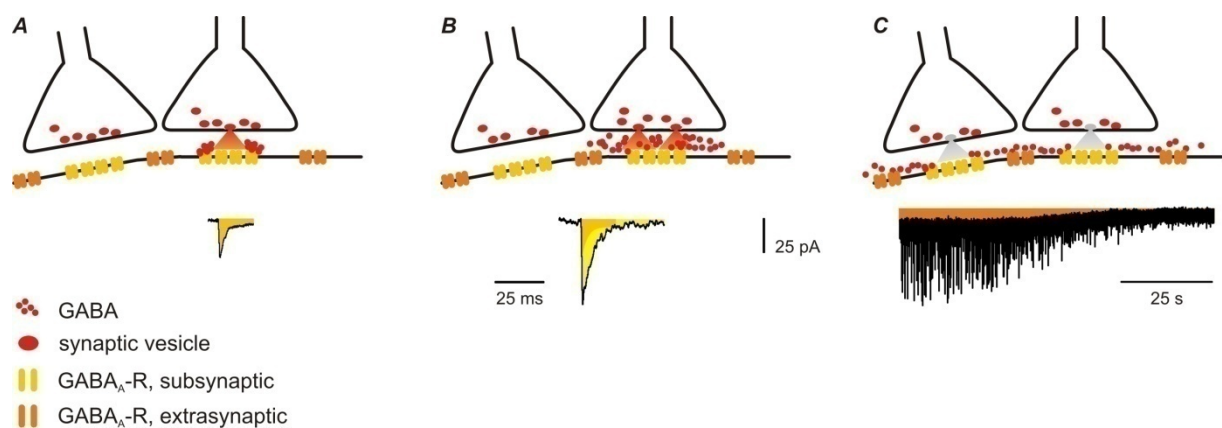


**Fig. 8 Phasic and tonic inhibitory currents.** (A) The release of a single vesicle (orange) from a synaptic terminal activates only subsynaptic GABA<sub>A</sub>-receptors (yellow). The example raw data trace shows a miniature inhibitory postsynaptic current recorded in the presence of TTX. (B) Action potential mediated release of multiple vesicles at the synaptic side activates GABA<sub>A</sub>-receptors at the synapse; the example trace shows the waveform of a postsynaptic IPSC. Note that released transmitter also diffuses away from the synaptic cleft. (C) The ambient transmitter in the extracellular space activates extrasynaptic GABA<sub>A</sub>-receptors (orange) exhibiting a high GABA affinity. Example trace shows block of phasic and tonic GABA<sub>A</sub>-receptors resulting in a shift in holding current. The charge carried by tonic inhibitory currents is marked with dark orange (modified from Farrant & Nusser, 2005).

Extrasynaptic GABA<sub>A</sub>-receptors are activated by ambient GABA in the extracellular space. In contrast to the GABA concentration at the synapse peaking around 1.5-3 mM, ambient GABA in the extracellular space reaches only concentration of about one micromolar (Lerma *et al.*, 1986). Various sources have been proposed for the normal amounts of GABA found in the extracellular space. GABA could be provided by astrocytic release, action-potential-mediated vesicular release (Fig. 8C) and non-vesicular release by either exocytosis or reversal of GABA transport. GABA uptake further controls the ambient transmitter concentrations in the extracellular space by limiting the spillover of released transmitter from the synapse into the extracellular space.

GABA<sub>A</sub>-receptors sensing these low ambient GABA concentrations in the extracellular space should exhibit a higher GABA affinity combined with less desensitization as compared to subsynaptic receptors. These different properties are due to differential subunit composition of subsynaptic versus extrasynaptic receptors. Subsynaptic GABA<sub>A</sub>-receptors usually contain the  $\gamma_2$ -subunit (Essrich *et al.*, 1998), whereas GABA<sub>A</sub>-receptors with preferential extrasynaptic localization contain  $\alpha_4$ ,  $\alpha_5$ ,  $\alpha_6$  and  $\delta$ -subunits (McKernan & Whiting, 1996). These receptors are not associated with synaptic anchoring proteins like gephyrin. The expression pattern of extrasynaptic subunits in dentate gyrus is as follows:  $\alpha_4$ -subunit shows a weak expression signal,  $\alpha_5$ - and  $\delta$ -subunits show a moderate to strong signal, whereas the  $\alpha_6$ -subunit is not expressed at all throughout development. Therefore,  $\alpha_5$ - and  $\delta$ -subunits are good candidates for mediating tonic inhibitory currents in dentate gyrus (Laurie *et al.*, 1992).

### *The delta-subunit*

Ultrastructural localization studies show that  $\delta$ -subunit containing GABA<sub>A</sub>-receptors are not associated with the synaptic GABA<sub>A</sub>-receptor anchoring protein gephyrin. They are not localized at GABAergic synapses, but are rather exclusively found at extrasynaptic somatic and dendritic membranes. The  $\delta$ -subunit is expressed in the neocortex, thalamus, striatum, cerebellar granule cells and dentate gyrus granule cells (Laurie *et al.*, 1992). In adult cerebellar granule cells and dentate gyrus granule cells, the  $\delta$ -subunit has been shown to mediate tonic inhibitory currents (Nusser *et al.*, 1998; Nusser & Mody, 2002). Specific properties of  $\delta$ -subunit containing receptors qualify them for long lasting activation by low GABA concentrations in the extracellular space. They indeed have a 50-fold higher GABA affinity than other GABA<sub>A</sub>-receptors, and they do not desensitize in the presence of the agonist (Saxena & MacDonald, 1994).

GABA<sub>A</sub>-receptors containing  $\delta$ -subunit show distinct pharmacological properties. These receptors are insensitive to benzodiazepines, showing that  $\delta$ -subunits are probably not associated with  $\gamma_2$ -subunits which exhibit high benzodiazepine sensitivity. Though, the  $\delta$ -subunit containing GABA<sub>A</sub>-receptors are sensitive to block by Zn<sup>2+</sup> (Saxena & MacDonald, 1994) and to potentiation by gaboxadol (THIP hydrochloride; Krosgaard-Larsen *et al.*, 2004). Furthermore, the tonically activated  $\delta$ -subunit is highly sensitive to stress related neurosteroids (Stell *et al.*, 2003) and to ethanol (Mody *et al.*, 2007).

### *The $\alpha_5$ -subunit*

GABA<sub>A</sub>-receptors containing the  $\alpha_5$ -subunit have been shown to be homogeneously distributed over the cell membrane (Sassoe-Pognetto *et al.*, 2000). Furthermore, they do not colocalize with gephyrin, despite of containing the  $\gamma_2$ -subunit, which is usually associated with the anchoring protein in subsynaptic GABA<sub>A</sub>-receptors. All together, this points to extrasynaptic localization of  $\alpha_5$ -subunit containing GABA<sub>A</sub>-receptors. The  $\alpha_5$ -subunit is expressed at high levels at birth and then expression declines during the postnatal period. In some areas like hippocampal CA1 pyramidal cells and dentate gyrus granule cells, expression level is still moderate to high in the adult (Laurie *et al.*, 1992). The  $\alpha_5$ -subunit is shown to contribute to tonic inhibitory currents in the hippocampus, as deletion of  $\alpha_5$ -subunit in cultured hippocampal neurons eliminates tonic conductance. The  $\alpha_5$ - and the  $\delta$ -subunit are mainly responsible for mediating tonic inhibition in adult hippocampal neurons, as shown in *Gabra5/Gabrd*<sup>-/-</sup> mice lacking both, the  $\alpha_5$ - and the  $\delta$ -subunit (Glykys *et al.*, 2008).

### *Functional role of tonic inhibition*

GABAergic neurotransmission participates not only in rapid point to point communication but also in slower forms of signaling. In contrast to phasic inhibition, the tonic inhibitory signals are defined by the ambient GABA concentration in the extracellular space. Fluctuations in tonic conductance do have profound effects on neuronal excitability, as the impact of tonic inhibition on the cells is quite large. Tonic inhibition is responsible for generating ~75% of the total inhibitory conductance received by hippocampal neurons (Mody & Pearce, 2004). In contrast to the timed action of phasic conductance, continuous tonic GABA conductance controls the gain of the neuronal input-output (Cavelier *et al.*, 2005; Chadderton *et al.*, 2004; Mitchell & Silver, 2003; Semyanov *et al.*, 2004).

There may also be clinical relevance, as enhancing function of tonically active GABA<sub>A</sub>-receptors by gaboxadol ( $\delta$ -subunit specific) has been proposed for the treatment of premenstrual dysphoric disorders (Maguire *et al.*, 2005). The  $\alpha_5$ -subunit containing GABA<sub>A</sub>-receptors have been shown to be critical for learning and memory in mouse knockout studies (Atack *et al.*, 2006; Caraiscos *et al.*, 2004).



# Aims of the study

As stated in the introduction, inhibitory control of the dentate gyrus is of particular importance. It is, however, unclear how this inhibitory control is achieved in dentate gyrus, especially during postnatal development. Therefore, different aspects of inhibitory currents in dentate gyrus were investigated in this study with a special focus on the postnatal period. To get a clear idea of synaptic inhibition in this region the main cell types were studied: inhibitory interneurons and dentate gyrus granule cells. Further, in dentate gyrus granule cells, the development of phasic and tonic inhibitory currents was analyzed.

- [1] GABAergic interneurons are of crucial importance for the organization of network activity. They determine the excitation/inhibition balance through feedback – or feedforward inhibition (Freund and Buzsaki, 1996; Somogyi and Klausberger, 2005; Soriano and Frotscher, 1989). In addition, they play a key role in synchronizing neuronal networks during oscillatory activity and thereby control information processing in large principal cell populations (Somogyi and Klausberger, 2005; Whittington and Traub, 2003). It was, therefore, crucial to understand the maturation and network integration of dentate gyrus interneurons in the course of postnatal development.
- [2] The dentate gyrus is regarded as the ‘hippocampal gate’ for afferent activity from entorhinal cortex. Granule cells receive neocortical information via perforant path and project only onto approximately 10-15 CA3 pyramidal cells. Overexcitation of the feedback loop between neocortex and hippocampus can lead to epileptic discharges (Heinemann *et al.*, 1992; Stief *et al.*, 2007). In this context it was important to characterize the maturation of dentate gyrus granule cells and their integration into the inhibitory network during postnatal development.
- [3] The inhibitory control to balance network activity of dentate gyrus can be mediated by GABAergic inhibition through two different mechanisms. By ‘phasic inhibition’ postsynaptic GABA<sub>A</sub>-receptors are briefly activated by pulse-like release of GABA-filled vesicles from presynaptic terminals. ‘Tonic inhibition’ is mediated by extrasynaptic GABA<sub>A</sub>-receptors. In contrast to phasic inhibition these receptors sense the ambient GABA concentration in the extracellular space and are due to a long-lasting increase in chloride conductance (Nusser and Mody, 2002; Semyanov *et al.*, 2004). Tonic inhibition is responsible for generating ~75% of the total inhibitory conductance received by hippocampal neurons (Mody & Pearce, 2004). Hence, it was important to ask whether tonic inhibition contributes to the excitability of the dentate gyrus granule cells. By focussing at postnatal development it was of further interest, if the contribution of tonic inhibitory currents changes with maturation of the dentate gyrus network.

# Experimental procedure

## Slice preparation

Brains of C57BL/6 mice (Charles River, Sulzfeld, Germany) were removed after decapitation and constantly kept under ice-cold sucrose-based artificial cerebrospinal fluid (aCSF) containing (mM): 87 NaCl, 2.5 KCl, 1.25 NaH<sub>2</sub>PO<sub>4</sub>, 7 MgCl<sub>2</sub>, 0.5 CaCl<sub>2</sub>, 25 glucose, 75 sucrose, 26 NaHCO<sub>3</sub> saturated with 95% O<sub>2</sub>- 5% CO<sub>2</sub>, pH 7.4 (Kuenzi *et al.*, 2000). Horizontal slices were cut with a vibrating blade microtome (Leica VT1000 S, Leica Microsystems, Nussloch, Germany) and incubated for 30 min in sucrose-based aCSF solution at 34°C. Subsequently, slices were stored up to 6 hours in pure artificial cerebrospinal fluid containing (mM): 124 NaCl, 3 KCl, 1.25 NaH<sub>2</sub>PO<sub>4</sub>, 1.8 MgCl<sub>2</sub>, 1.6 CaCl<sub>2</sub>, 10 Glucose, 26 NaHCO<sub>3</sub>, saturated with 95% O<sub>2</sub>- 5% CO<sub>2</sub>, pH 7.4.

All animal procedures were in accordance with the guidelines of the European Community Council and were announced to the local authorities.

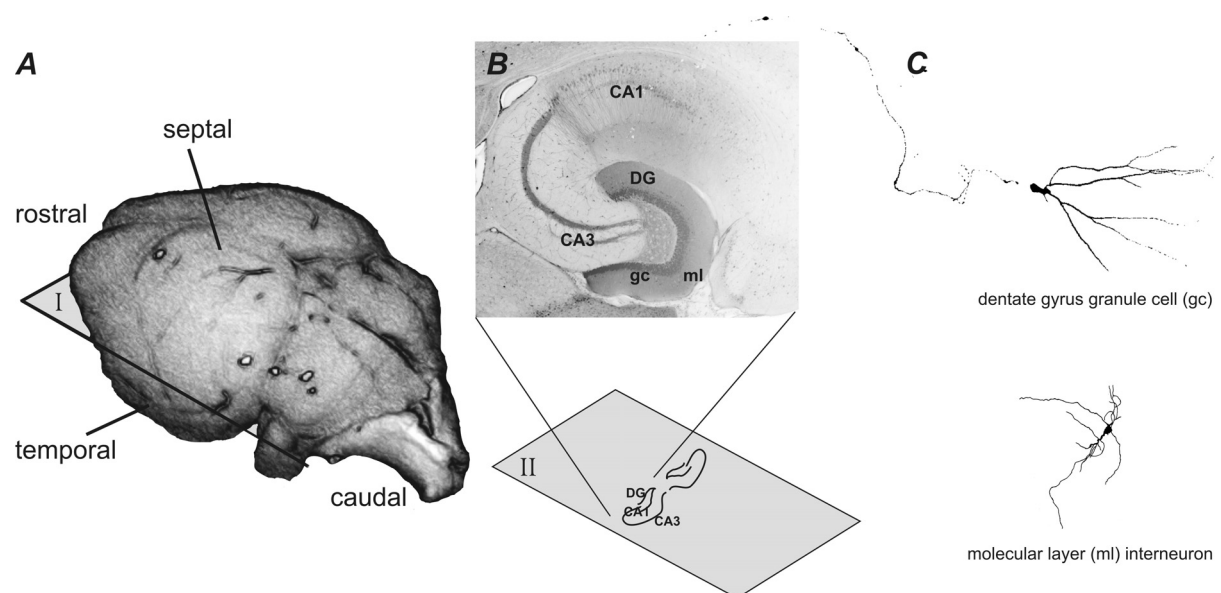


**Fig. 9 Horizontal hippocampal slice of a mouse brain.** (A) Processed picture of a mouse brain. The horizontal cutting plane is marked (I). Sketch of the hippocampal formation in the cutting plane (II). (B) Hippocampal regions CA1, CA3 and dentate gyrus (DG). Fibre projections of granule cells (gc) visualized by calbindin staining. (C) Example cells of mouse dentate gyrus: processed image of a granule cell, the principal cells in the dentate gyrus (gc) and an interneuron of the molecular layer (ml).

## Electrophysiological experiments

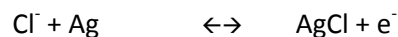
Electrophysiological experiments were carried out in a submerged type recording chamber. Slices were sealed on a cover slip coated with poly-L-lysine and subsequently placed in the recording chamber. Dentate gyrus molecular layer interneurons and granule cells were visually identified by contrast enhancing optics according to Dodt (Dodt & Zieglgansberger, 1990; Dodt & Zieglgansberger, 1998) combined with videomicroscopy (Olympus BX51 microscope; Olympus, Hamburg, Germany). Recordings were performed under constant perfusion (~ 2-3 ml/min) with aCSF.

## Whole cell patch clamp recordings

### *Recording electrodes and intracellular solutions*

The recording pipettes (borosilicate-glass; outer diameter 2.0 mm, inner diameter 0.80 mm; Science Products, Hofheim, Germany) were pulled at a Flaming/Brown Puller P-97 (Sutter Instruments, Novato, USA). Filled with intracellular solutions, the recording electrodes had a resistance of 2-4 MΩ.

For patch clamp recordings the glass pipette filled with intracellular solution was connected to a silver wire coated with silver-chloride. A second AgCl-coated silver wire placed in the extracellular solution served as reference electrode. At the surface of the electrode, the ionic current carried by chloride (Cl<sup>-</sup>) is converted into an electric current in the silver wire:



For the characterization of *molecular layer interneurons* a KCl-based intracellular solution was used containing (mM): 120 KCl, 5 NaCl, 0.5 CaCl<sub>2</sub>, 2 MgCl<sub>2</sub>, 10 HEPES, 10 EGTA, Mg-ATP 4, Na-GTP 0.1, pH adjusted to 7.2 with KOH.

The intracellular solution for recordings of *dentate granule cells* was CsCl-based (mM): 122 CsCl, 8 NaCl, 0.2 MgCl<sub>2</sub>, 10 HEPES, 2 EGTA, 2 Mg-ATP, 2 Na-GTP, pH adjusted to 7.2 with CsOH, if necessary QX314Bromide was added.

Osmolarity was adjusted to 280 mOsmol/l by adding glucose. Differences of 15-20 mOsmol/l between bath and pipette solutions were appropriate for stable recordings. Aliquots (1 ml) of the intracellular solutions were stored at -20°C. After thawing, the intracellular solution was kept at +4°C and discarded at the end of the day. To reconstruct recorded neurons 1% (w/v) neurobiotin (N (2 aminoethyl) biotinamid hydrochlorid; Vector Laboratories, Burlingame, UK) was added to the intracellular solution immediately before recording.

### *The 'Whole cell patch-clamp' technique*

The patch-clamp technique, a low noise recording technique, was developed by Neher and Sakmann (Hamill *et al.*, 1981; Neher & Sakmann, 1976; Neher & Sakmann, 1992). This technique allows recordings of small ionic currents across biological membranes. Here, postsynaptic currents of patched cells in mouse dentate gyrus were measured by means of the whole-cell patch-clamp technique using an EPC-7 amplifier (Heka electronics, Lambrecht/Pfalz, Germany).

To record from a single neuron a tight seal of the cell membrane and the glass recording pipette (filled with intracellular solution) was established. Thereby a small membrane patch was electrically isolated and the seal resistance typically exceeded several  $G\Omega$  ('Gigaseal'). This so called 'cell-attached configuration' allows separation of single channel currents from electrical background noise (Fig. 10B).

Then the so called 'whole-cell configuration' was established by applying a short pulse of suction through the patch pipette. The access resistance through this 'hole' in the cell membrane was in the range of  $20 M\Omega$ , depending on tip diameter of the pipette ( $2-4 M\Omega$ ). The tight giga seal connection of glass pipette and cell membrane prevents flow of leak currents between the pipette and the reference electrode in the extracellular solution. Hence, having access to the whole cell membrane it was possible to control the membrane potential of the cell body. In voltage clamp mode of the amplifier, cells were clamped at a negative holding potential ( $-70mV$  for molecular layer interneurons and  $-80 mV$  for dentate gyrus granule cells) and an averaged current response of all channels in the cell membrane could be recorded. Changes in membrane potential upon defined current injections were recorded in current clamp mode.

Furthermore, whole cell patch-clamp configuration gave the opportunity to control the composition of the intracellular solution precisely, since the cytoplasm was replaced by the intracellular pipette solution within approximately five minutes after the whole cell configuration was established. As soluble regulatory components of the cytoplasm, like ATP, were diluted, they have been added to the intracellular solution. It has to be noted, that the diffusion is limited in distal cell compartments and therefore the ionic composition of soma and dendrites may differ (*see: The space clamp problem*).

The process of sealing and breaking through the cell membrane was monitored by the current response to a  $5 mV$  square pulse of the command potential (see Fig. 10C).

### *Function of a patch-clamp amplifier*

To maintain the set holding potential ( $V_h$ ) of the recorded cell constant, differences between  $V_h$  and the membrane potential ( $V_m$ ) are measured. A current is injected to compensate for the measured difference. The current ( $I$ ) measured in voltage clamp mode of the patch clamp describes the ion movement across the cell membrane by changes in the membrane conductance at  $V_h$ .

The patch-clamp amplifier consists of an operational amplifier (OPA) and a feedback resistor ( $R_f$ , see simplified electrical circuit; Fig. 11). The operational amplifier determines the difference between  $V_h$  and  $V_m$  at its input terminals and exports the amplified potential difference at its output terminals. Due to the potential difference between circuit positions 1 and 2 (see Fig. 11) a current flows through  $R_f$  to the pipette. This current cannot flow through the OPA as its input resistance is very high. The current at the patch pipette is in opposite direction to the current altering the membrane potential  $V_m$  at a given holding potential  $V_h$  and therefore resets  $V_m$  to  $V_h$  (Sigworth, 1995).

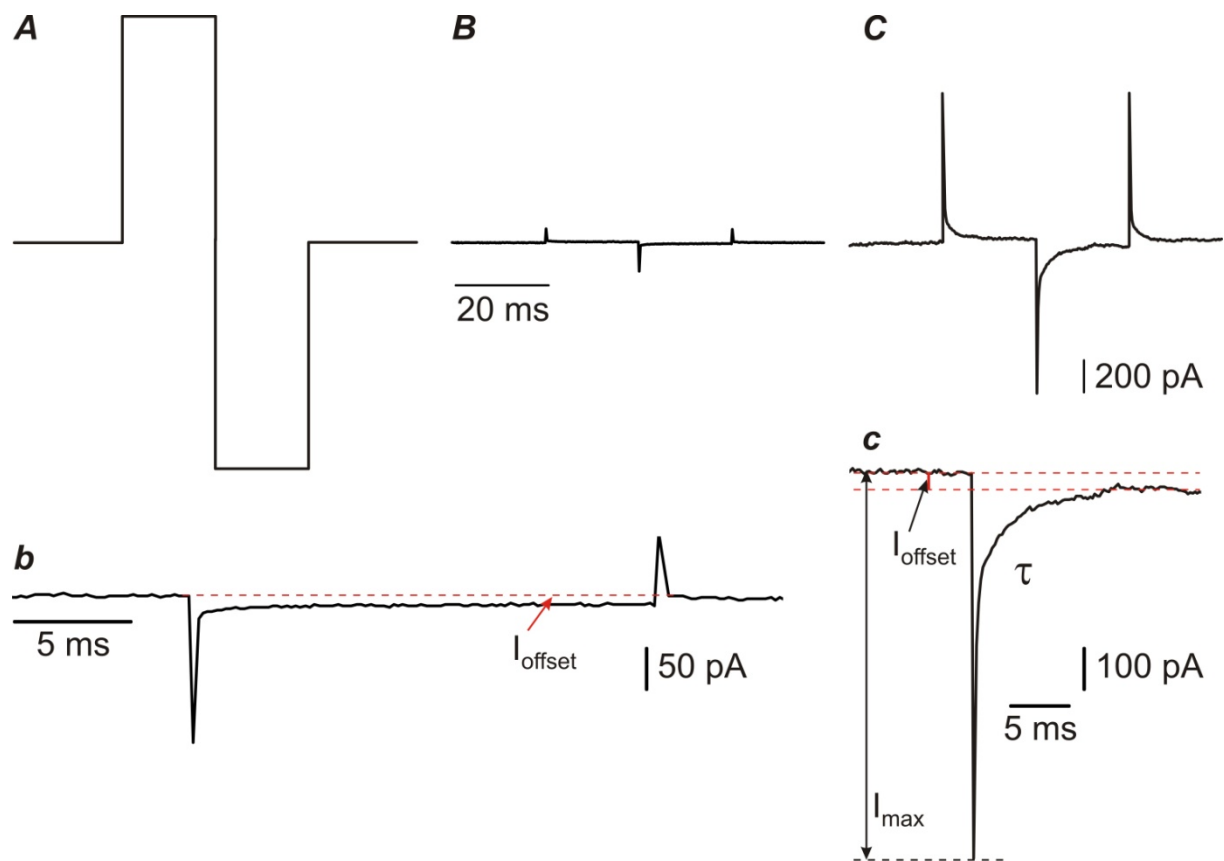


**Fig. 10** Current response to a 5 mV square pulse of the command potential in voltage clamp configuration. **(A)** The current response from an open pipette in extracellular solution is square shaped, the pipette behaves like an Ohm's resistor (here:  $R_{\text{pip}} = 3 \text{ M}\Omega$ ). **(B)** A 'Gigaseal' is formed in cell-attached configuration, showing two capacitive artifacts on a straight current trace. The magnification **(b)** shows the remaining leak current ( $I_{\text{offset}}$ ), which can be used to calculate membrane resistance ( $I_{\text{offset}} \sim 1/R_M$ ). **(C)** The current response in whole-cell configuration is characterized by capacitive artifacts. The '5 mV testpulse' can be used to control series resistance  $R_s$  during whole cell recordings ( $I_{\text{max}} \sim 1/R_s$ ). Membrane capacitance  $C$  can be determined by an exponential fit, whereby  $\tau = C \times R_s$ . Figure according to figure 3.3 and 3.7, Numberger and Draguhn, 'Patch-Clamp-Technik'.

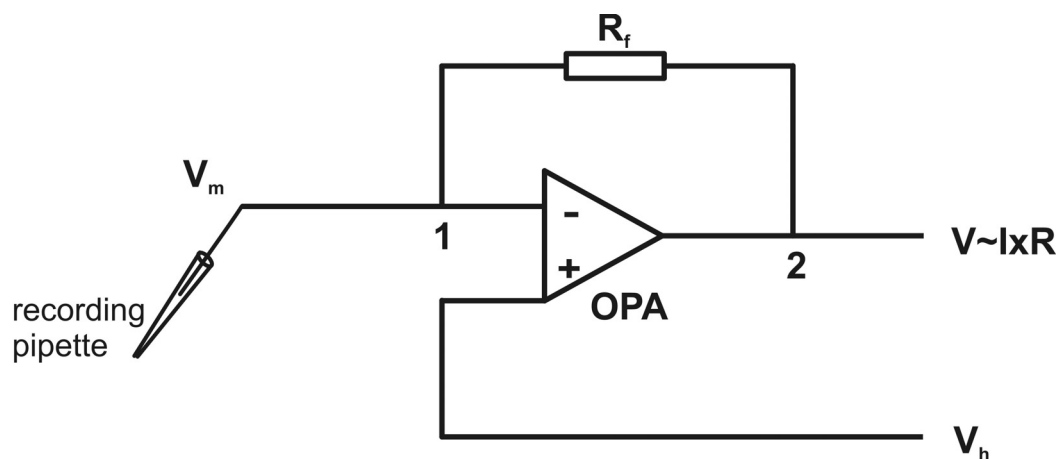


**Fig. 11** Simplified electrical circuit of a patch clamp amplifier (pre-amplifier, "headstage"). The operational amplifier (OPA) delivers the amplified potential difference of  $V_m$  and  $V_h$  to its output terminal (tip of the triangle). Note that the OPA has a very high input resistance at the input terminals. ( $R_f$  feedback resistor,  $V_m$  membrane potential,  $V_h$  holding potential). Figure according to figure 3.1, Numberger and Draguhn, 'Patch-Clamp-Technik'.

### Electrical properties of whole cell recording

The following equations are relevant for electrophysiological analysis of postsynaptic currents recorded in voltage clamp configuration:

As a first approximation, the membrane behaves like a simple resistor. The linear relation of membrane potential and the (ionic) current across the membrane can be described by Ohm's Law:

$$U = R \times I \quad (U \text{ in mV; } R \text{ in } M\Omega; I \text{ in pA})$$

The resistance  $R$  can be replaced by a term describing the conductance  $g$  ( $g = 1/R$ ):

$$U = I / g \quad \leftrightarrow \quad I = U \times g \quad (g \text{ in S})$$

In a whole cell patch-clamp experiment the voltage  $U$  equals the difference between membrane potential  $V_m$  and equilibrium potential  $E_m$  of the conducted ions.  $E_m$  is determined by the Nernst-Equation:

$$I = (V_h - E_m) \times g \quad (E_m \text{ in V})$$

The membrane conductance ( $g$ ) describing ion movements across the cell membrane at  $V_h$  can be calculated since the current ( $I$ ) is measured in voltage clamp mode of the patch amplifier. The amplitude of the recorded current is proportional to the potential difference ( $V_m - E_m$ ) and the membrane conductance.

Furthermore, the quality of the access to the patched cell via the pipette can be monitored by a 5 mV testpulse (see Fig. 10). The electrical circuit of a 'whole cell patch' (Fig. 12) describes the idealized spherical patched cell as a resistor ( $R_m$ ) in parallel with a capacitor ( $C_m$ ). The recording pipette is connected to the cell by a series resistor ( $R_s$ ). Hence, the potential between the extracellular reference electrode and the recording electrode drops across  $R_m$  and  $R_s$ . To measure accurate values for the membrane potential, it is essential that  $R_s$  is significantly smaller than  $R_m$ .

$$R_s \ll R_m$$

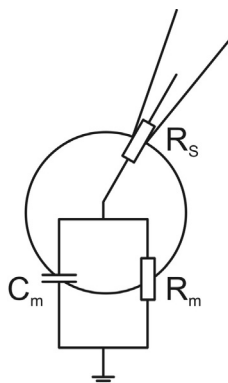


**Fig. 12 Electrical properties of whole cell patch-clamp recording**

Diagram shows the electrical circuit of an idealized spherical neuron. The cell is displayed as a parallel circuit of membrane resistance  $R_m$  and membrane capacitance  $C_m$ . The recording pipette is connected in series to the cell ( $R_s$ , series resistance). Figure according to figure 3.6, Numberger and Draguhn, 'Patch-Clamp-Technik'.

## Limitations of the patch clamp technique

Aforementioned assumptions are valid for recordings of an idealized spherical neuron with perfect access to the cell interior throughout the measurement. In contrast, real neurons in hippocampal slices are of different shape, they exhibit various branches. Furthermore, certain technical problems like offset potentials are not considered in the estimations mentioned above.

### *The space clamp problem*

In contrast to the idealized spherical neuron real hippocampal neurons display various branches. While the virtually spherical soma of the neuron can be voltage clamped, this cannot be assumed for the distal compartments. Distal compartments could be regarded as separated from the soma by a series of resistances with parallel capacitances. Therefore, the substantial voltage drop across these resistances is the reason for the insufficient control of membrane potential and for possible detection errors regarding the time course of postsynaptic currents in distal compartments.

However, this systematic error was less relevant, if data was compared from the same neuron obtained in different pharmacological conditions. These data underlies the same conditions regarding the space clamp. Nevertheless, one has to take in account that the data was obtained from dentate gyrus neurons of different ages. As an immature neuron is less branched than a more mature one, the electrophysiological control over the neuron may differ with ongoing development.

### *Series resistance*

For accurate control of the membrane potential, series resistance  $R_s$  has to be significantly smaller than the membrane resistance  $R_m$ . An adequate control of membrane potential is essential for qualitatively good recordings. Changes in  $V_m$  due to high  $R_s$  can lead to the uncontrolled activation of voltage-gated ion channels in the cell membrane. The postsynaptic currents recorded then do not reflect currents mediated by receptor-activated ion channels, but rather derive from voltage-gated ion channels, for example from voltage-gated  $\text{Na}^+$ -channels.

As the access to the patched cell could also change within the running experiment,  $R_s$  was monitored throughout the whole recording by means of a 5 mV square pulse. Whereby:

$$R_s \sim U/I_{\max} \quad (\text{if } R_s \ll R_m)$$

### *Offset potentials*

Another error source in whole cell patch clamp experiments are offset potentials occurring in the electrical circuit of chlorided silver wires and solutions containing unequal carrier ions. Offset potentials which are not compensated cause differences between holding potential  $V_h$  and membrane potential  $V_m$ .

The constant offset potential between electrode and recording solution was compensated in search-modus of the amplifier before the seal was formed. Further, the silver wire of the recording electrode and reference electrode were chlorided regularly to diminish offset potentials at the electrode surface.

Liquid junction potentials occur at the interface of solutions containing different carrier ions, for example extracellular solution, pipette solution and the cytosol (Neher, 1992). To minimize offset errors due to liquid junction potentials at the interface of extracellular and pipette solution, the pipette offset was corrected immediately before seal formation. For detailed information about offset potentials see *Neher, E (1995) Voltage offsets in patch-clamp experiments. In: Sakmann, B.; Neher, E.; Single Channel Recording, 2<sup>nd</sup> edition, Plenum New York, p 147-154.*

### Patch Clamp Setup

In the following, the main components of a patch-clamp setup are described: An upright microscope (BX51, Olympus, Hamburg, Germany) was placed on an active air suspension isolation table (Science Products, Hofheim, Germany) to dampen vibrations. To shield the setup from electrical noise, the patch-clamp setup was surrounded by a faraday-cage. 10x and 60x water-immersion objectives and the contrast-enhancing optics according to Dodt were used to visualize the cells in dentate gyrus. The recording chamber was perfused by gravity and the solution was removed by means of a pump. Three-axis piezo-crystal-driven micromanipulators (E-463; PI instruments, Karlsruhe, Germany) were used for positioning the electrodes. Electrophysiological data was recorded by means of a patch amplifier (EPC-7; HEKA, Lambrecht, Germany). Data was recorded and stored with a PC via an analogue/digital converter (CED 1401 micro; CED, Cambridge, UK).

For more information about the patch-clamp technique in general, the patch-clamp setup and the possible error sources see also 'Single-Channel Recording' (Sakmann and Neher, 1983) and 'Patch-Clamp-Technik' (Numberger and Draguhn, 1996).

## Recording protocols

### *Action potentials*

Action potentials were evoked by stepwise current injections in current clamp mode using a KCl based intracellular solution. For recordings of molecular layer interneurons the solution contained (mM): 130 KCl, 0.2 MgCl<sub>2</sub>, 10 HEPES, 2 Mg-ATP, 2 Na-GTP, pH adjusted to 7.2 with KOH. For recordings of dentate granule cells the intracellular solution contained: 122 KCl, 8 NaCl, 0.2 MgCl<sub>2</sub>, 10 HEPES, 2 EGTA, 2 Mg-ATP, 2 Na-GTP, pH adjusted to 7.2 with KOH.

### *Spontaneous inhibitory postsynaptic currents – dentate gyrus interneurons*

Spontaneous inhibitory postsynaptic currents (sIPSCs) were recorded at -70 mV holding potential in voltage clamp mode. For each data set, synaptic events were collected from 2 min of continuous recording. IPSCs were isolated by bath application of the glutamate receptor blockers APV (30 μM) and CNQX (20 μM), a NMDA and non-NMDA receptor blocker, respectively. Finally, the GABAergic nature of the currents was confirmed by addition of the GABA<sub>A</sub>-receptor blocker gabazine (2 μM). Amplitude and frequency of spontaneous inhibitory currents were analyzed (see section data recording and analysis). The time course of IPSCs was analyzed with a monoexponential fit of the decay time course. A biexponential fit of the IPSCs decay time course did not reveal any differences to the values obtained with the monoexponential fit.

### *Excitatory synaptic currents – dentate gyrus interneurons*

Excitatory postsynaptic currents (sEPSCs) were measured under block of GABAergic inhibition by GABA<sub>A</sub>- and GABA<sub>B</sub>-receptor blockers (1  $\mu$ M gabazine and 5  $\mu$ M CGP 5584A). Here, the intracellular solution contained (mM) 122 CsCl, 8 NaCl, 10 HEPES, 2 EGTA, 0.2 MgCl<sub>2</sub>, 2 ATP, 2 GTP, 5 QX314Br, the pH was adjusted to 7.2 with CsOH. Evoked EPSCs were measured by stimulating perforant path fibres. Therefore, a stimulation electrode (borosilicate glass electrode, 2-4 M $\Omega$ ) filled with extracellular solution was placed at the hippocampal fissure. At -70 mV, a NMDA receptor-mediated component was not clearly distinguishable. NMDA receptor-mediated events were isolated at +40 mV. Glutamatergic nature of the evoked EPSCs was confirmed by addition of 30  $\mu$ M APV and 20  $\mu$ M CNQX.

### *GABAergic inhibitory currents – dentate gyrus granule cells*

GABA<sub>A</sub>-receptor mediated inhibitory currents were recorded at -80 mV holding potential in voltage clamp mode. GABA<sub>A</sub>-receptor mediated inhibitory currents were isolated by bath application of the glutamate-receptor blockers APV (30  $\mu$ M) and CNQX (20  $\mu$ M) and by application of a GABA<sub>B</sub>-receptor antagonist (5  $\mu$ M CGP55845). To mimic an ambient GABA level in the extracellular space and to standardize conditions in mice of varying developmental stages, 2.5  $\mu$ M GABA was added to extracellular solutions. Slices were pre-incubated in GABA containing solution for ~5 min before starting the experiment. Phasic GABAergic IPSCs were blocked by addition of a low concentration of 200 nM gabazine. Total GABAergic currents consisting of both, phasic and tonic inhibitory currents, was blocked by application of 100  $\mu$ M picrotoxin. The analysis of tonic inhibitory currents is explained in part three of the results section.

## **Extracellular recordings (population spikes) - dentate gyrus granule cells**

For recording of granule cell population spikes, bath perfusion of extracellular solution (aCSF supplemented with 2.5  $\mu$ M GABA) was enhanced to ~4-5 ml/min. Extracellular recordings were performed in using a glass electrode filled with extracellular solution (~900 k $\Omega$ ) and an EXT 10-2F amplifier (npi electronic, Tamm, Germany). Population spikes were evoked by electrical stimulation of perforant path fibres at the hippocampal fissure with a bipolar platinum/iridium electrode (Science Products, Hofheim, Germany). Recording electrode was placed on the granule cell layer where a population spike could be recorded.

For the following 20 minutes the slice was allowed to recover from the mechanical stress of positioning and placing the electrodes. The maximal population spike amplitude was determined by subsequent increase of stimulation strength. This stimulation strength was then used for recording a row of ten population spikes (30 seconds intervals). Bath perfusion of drugs was monitored and again, population spikes were recorded at the same stimulus intensity used for baseline conditions.

## Drugs

DL-2-Amino-5-phosphonopentanoic acid (APV), 6-Cyano-7-nitroquinoxalin-2,3-dione (CNQX), SR 95531 hydrobromide (gabazine), CGP 55845A, picrotoxin, THIP hydrochloride (gaboxadol), TTX and NNC-711 as well as the intracellular applied substance QX314 bromide were purchased from Tocris Bioscience, Avonmouth, UK. L-655,708 was ordered from Sigma, Taufenkirchen, Germany. Strychnine (Sigma, Taufkrichen, Germany) was kindly provided by Prof. Misgeld, Heidelberg, Germany.

Drugs were perfused after obtaining a stable control recording period of at least 1 minute.

For more information about the drugs please see the Appendix.

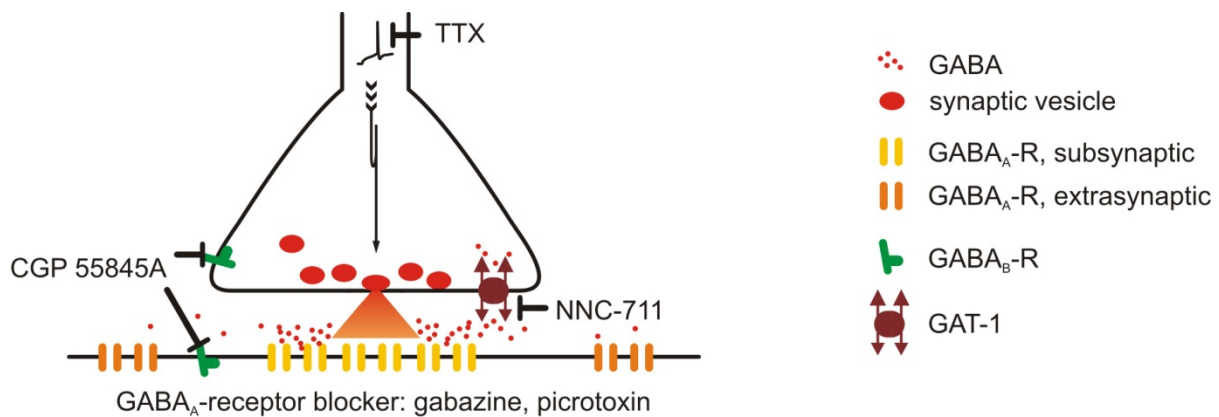


**Fig. 13 Targets for drugs used in the study.** Schematic drawing of the action of drugs targeted against the GABAergic system. CPG 55845A blocks GABA<sub>B</sub>-receptors, NNC-711 blocks GABA transport and the sodium channel blocker TTX prevents action potential mediated release of synaptic vesicles. GABA<sub>A</sub>-receptor blockers frequently used in the experiments were gabazine and picrotoxin.

## Temperature conditions

Experiments for interneuron characterization were carried out at room temperature and the experiments on dentate gyrus granule cells were performed at 32-34°C.

## Data recording and analysis

In patch clamp recordings, currents were low-pass filtered at 3 kHz and digitized at 20 kHz with a CED 1401 interface. All electrophysiological data were recorded, stored on a PC and subsequently analyzed offline with Spike5 and Signal3 software (Cambridge Electronic Design; Cambridge, UK) using custom-made routines. Data was further analyzed in Origin 7 (OriginLab Corp., Northampton, USA). Amplitude and frequency of spontaneous inhibitory postsynaptic currents were automatically identified with a custom-made detection algorithm by comparing measured events with a template, determined by 50 averaged synaptic events. Reliability of the algorithm was assessed by comparison with individual hand-evaluated traces.

Series resistance and membrane capacitance were monitored by a 5 mV depolarizing pulse throughout the experiment. Recordings were discarded if series resistance increased by more than 20% through an experiment or the resistance surpassed 20 M $\Omega$  at any time during the experiment. Series resistances were not compensated in the experiments.

In field potential recordings, currents were low-pass filtered at 2 kHz and digitized at 20 kHz with a CED 1401 interface. All electrophysiological data were recorded with Signal3 software, stored on a PC and subsequently analyzed offline with Excel software using custom-made routines. The population spike trace was tested for the number of minima at which the slope of the trace is zero and curve progression is turning from decreasing to increasing.

If not otherwise stated data represent mean  $\pm$  sem. Statistical significance of results was tested using GraphPad InStat Software (GraphPad Software, San Diego, USA). Data was tested for normality of distribution with Kolmogorov-Smirnov test. The statistical test used afterwards for each experimental condition is mentioned in the relevant results section. P values < 0.05 were considered statistically significant.

## Histochemical experiments

### Histological analysis

Visually identified cells of dentate gyrus were filled with neurobiotin-tracer during electrophysiological recordings. From each individual slice only one single neuron was recorded. After finishing data acquisition, the membrane of the recorded neuron was closed again by forming an outside-out patch.

Therefore the recording pipette was slowly removed from the cell and a thin membrane tube was formed between patched cell and recording pipette, which finally ruptured. Thereby, cell membrane is very likely closed and the membrane connected to the recording pipette establishes an outside-out-patch. Hence, the process of membrane closure could be monitored electrophysiologically. Cells were allowed to recover for about 10 minutes in the submerged type recording chamber, with time the neurobiotin-tracer was distributed across the cell body. Then slices were fixed in 4% paraformaldehyde (PFA) in phosphate buffer over night.

Neurobiotin- filled cells were visualised with avidin, Alexa Flour488 conjugate according to following protocols. Thereby, the fluorescent avidin-molecule binds to neurobiotin-tracer in the neuron, forming a very tight complex with a dissociation constant  $\sim 2 \times 10^{-8}$  (see Fig. 14).

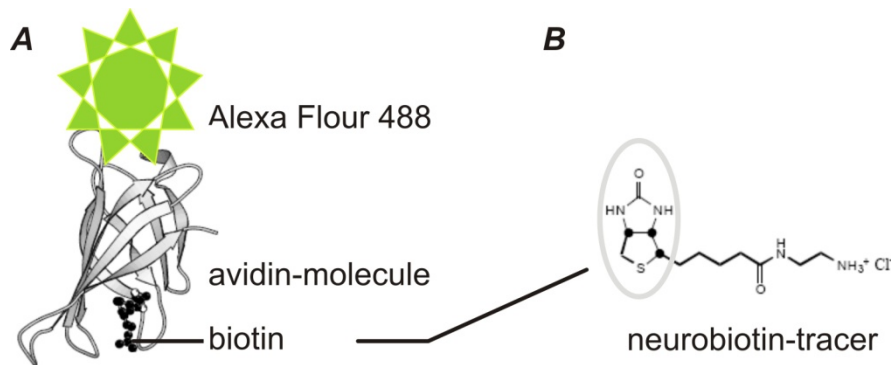


**Fig. 14 Visualization of neurobiotin by avidin conjugated to Alexa488 fluorophore. (A)** Schematic model of avidin protein conjugated to Alexa488 fluorophore (green), avidin is bound to biotin (black spheres). **(B)** Chemical structure of neurobiotin-tracer.

### *Molecular layer interneurons*

For histological reconstruction molecular layer interneurons were visualized with avidin, Alexa Fluor488 conjugate according to a protocol for mounted cyo-sectionend slices. After PFA- fixation slices were subsequently transferred to 15% sucrose and 30% sucrose in 4% PFA in phosphate buffer, each for at least 24 h (4 °C). The fixed slices were resectioned at 70  $\mu\text{m}$  either with a cryotome (Leica CM 3050S, Leica Microsystems, Wetzlar, Germany) or a vibrating blade microtome. Then slices were mounted on superfrost microscope slides (Menzel-Gläser, Braunschweig, Germany) and stored at -20°C. For the staining procedure slices were permeated in methanol (-20°C) for 10 min and then rehydrated in phosphate buffered saline (PBS) at room temperature. Background fluorescence was minimized by incubation in 0.3 M glycine in PBS for 30 min. After three washing steps nonspecific antibody binding sites were blocked with 1% BSA in PBS. Cells were stained with avidin, Alexa Fluor488 conjugate (Invitrogen, Karlsruhe, Germany) at 4 °C overnight. Samples were analyzed using an Olympus BX61 microscope (Olympus, Hamburg, Germany).

### *Dentate gyrus granule cells*

Dentate gyrus granule cells were visualized with avidin, Alexa Fluor488 conjugate according to a protocol for free-floating sections. In contrast to the protocol for mounted sections, the free-floating method could be readily combined with immunohistochemical staining using antibodies against certain antigens (see next section). Here, the fixed slices were embedded in 4% (w/v) agar in PBS and then sectioned with a vibrating blade microtome into 50-70  $\mu\text{m}$  slices. Free-floating sections were stained with avidin, Alexa Fluor488 conjugate (Invitrogen, Karlsruhe, Germany) at 4 °C overnight after permeation with PBS + 0.4% Triton X 100 for 30 min and block of unspecific staining with PBS + 0.2% Triton X 100 + 1% BSA for 30 min at room temperature. Processed sections were mounted on superfrost microscope slides (Menzel-Gläser, Braunschweig, Germany) and embedded in Mowiol. Samples were analyzed using an Olympus BX61 microscope (Olympus, Hamburg, Germany).

## Immunohistochemistry

### Protocol

Slices were instantly fixed in 4% PFA in phosphate buffer over night at 4 °C before embedding in 4% (w/v) agar in PBS. Finally, the material was re-sectioned at 30 µm with a vibrating blade microtome. Staining of free-floating sections started with three washing steps with PBS. Cell membranes were permeated with 0.4% of the non-ionic detergent Triton-X-100 in PBS (30 min, room temperature). Afterwards, unspecific staining was blocked by 1% BSA in PBS + 0.2% Triton X 100 (30 min, room temperature), BSA binds to unspecific binding sites reducing background staining. Subsequently, sections were incubated overnight at 4 °C with primary antibodies directed against the desired antigens. All antibodies were diluted to their final concentration in PBS + 0.5% BSA + 0.1% Triton-X-100. After three washing steps (10 min PBS + 0.5% BSA) labelled secondary antibodies (1:500; Dianova, Hamburg, Germany) were added for 2.5 h at room temperature. Secondary antibodies were labeled with fluorescent molecules of distinct color and therefore indirectly marked the antigen sites by binding to their correspondent primary antibodies (Fig. 15). For each antibody, 50 random samples were analyzed using an Olympus BX61 microscope and Analysis Five Software (Soft Imaging Systems, Münster, Germany).

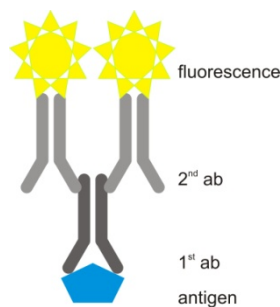


**Fig. 15 Model of 'labeled secondary antibody' immune reaction.** The antigen is detected by the first antibody raised in species A. The second antibody in turn recognizes the species A specific part of the 1<sup>st</sup> antibody. Finally, to visualize the antibodies bound to the antigen the 2<sup>nd</sup> antibody is coupled to a fluorophore.

### Molecular layer interneurons

In order to assess the expression pattern of typical marker proteins for interneurons, hippocampal sections of mice aged 7 and 15 days were stained. For each age and antibody, three animals from different litters were used. From each mouse, six horizontal hippocampal slices of 500 µm thickness were obtained. These slices were further processed separately as described above.

The following primary antibodies were used: rabbit monoclonal **anti-parvalbumin** (rb anti-PV 1:1000; swant swiss antibodies, Bellinzona, Switzerland), mouse monoclonal **anti-calbindin** (ms anti-CB 1:5000; swant swiss antibodies, Bellinzona, Switzerland), rabbit **anti-calretinin** (rb anti-CR 1:2000; swant swiss antibodies, Bellinzona, Switzerland) and rabbit polyclonal **anti-somatostatin** (rb anti-SS 1:1000; Chemicon International, Hampshire, UK).

To make antigen sites visible Cy3 labeled secondary antibodies directed against the primary rabbit or mouse derived antibody were used (1:500; Dianova, Hamburg, Germany).

Only cells within the stratum moleculare and with clear signal-to-background separation were counted. The total number of cells in stratum moleculare for each section was assessed and data from all sections within each age group (3 animals at both ages) was averaged. For each antibody, 50 random samples were analyzed using an Olympus BX61 microscope and Analysis Five Software (Soft Imaging Systems, Münster, Germany).

# Results

Results are divided in three parts: functional maturation of developing interneurons in dentate gyrus, the maturation of granule cells - the principal neurons of dentate gyrus and the effect of tonic inhibitory currents on dentate gyrus granule cells.

## Part 1

### Functional maturation of developing interneurons in the molecular layer of mouse dentate gyrus

In order to follow the functional maturation of interneurons in the dentate gyrus, visually identified cells in the middle portion of stratum moleculare were recorded. For comparison, cells were grouped into three different developmental periods (p 6-8, n=17; p 9-11, n= 13 and p 12-16, n=18).

All analyzed cells displayed action potentials upon depolarization in current clamp mode. Neurobiotin-stained cells showed typical neuronal morphology (6 cells recovered at p 6-8; 6 cells recovered at p 9-11; 10 cells recovered from p 12-16; see below). Most neurons were located in the middle portion of the molecular layer (Fig. 16). The position of an interneuron soma was analyzed as the relative location between the outer border of the granule cell band (0%) and the hippocampal fissure (100%) with the help of the measuring tool box of Analysis Five Software (Soft Imaging Systems, Münster, Germany).

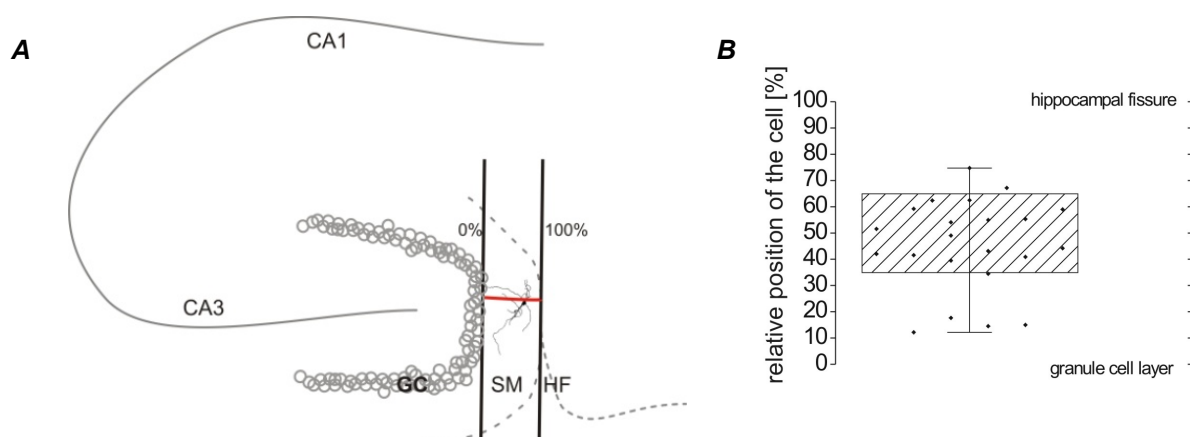


**Fig.16 Relative position of recorded neurons between the granule cell band and the hippocampal fissure. (A)** Schematic drawing of interneuron localization in stratum moleculare. The relative position of the neuron on the (red) axis between hippocampal fissure (HF) and granule cell layer (GC) in stratum moleculare (SM) was quantified. **(B)** Relative location of interneuron somata in stratum moleculare. Shaded area indicates the middle third of stratum moleculare, each dot represents a single reconstructed cell. Distribution of the cells within stratum moleculare is indicated by the bar.

## Passive intrinsic properties of molecular layer interneurons change with maturation

Passive membrane properties of a neuron are determined both through input resistance and membrane capacitance of the cell. The input resistance influences amplitude and propagation of electric signals. It depends on ion channel density and size of the neuron. By maturation density of e.g.  $\text{Na}^+$  channels increases, whereby input resistance decreases. Likewise, the size of neurons is usually increasing during development, membrane capacitance should therefore increase.

In order to assess changes in intrinsic passive properties, neurons were recorded in current clamp mode and voltage responses to hyperpolarizing current pulses were analyzed by a single exponential fit. Input resistance was calculated from the amplitude and membrane capacitance was determined by the time constant  $\tau$  (Fig. 17A). Input resistance decreased from  $\sim 400 \text{ M}\Omega$  at p 6-8 to  $\sim 300 \text{ M}\Omega$  at p 12-16. Correspondingly, and in accordance to the expected neuronal growth, mean membrane capacitance appeared to increase, although this parameter was not significantly different between the three age groups (Fig. 17B,C).

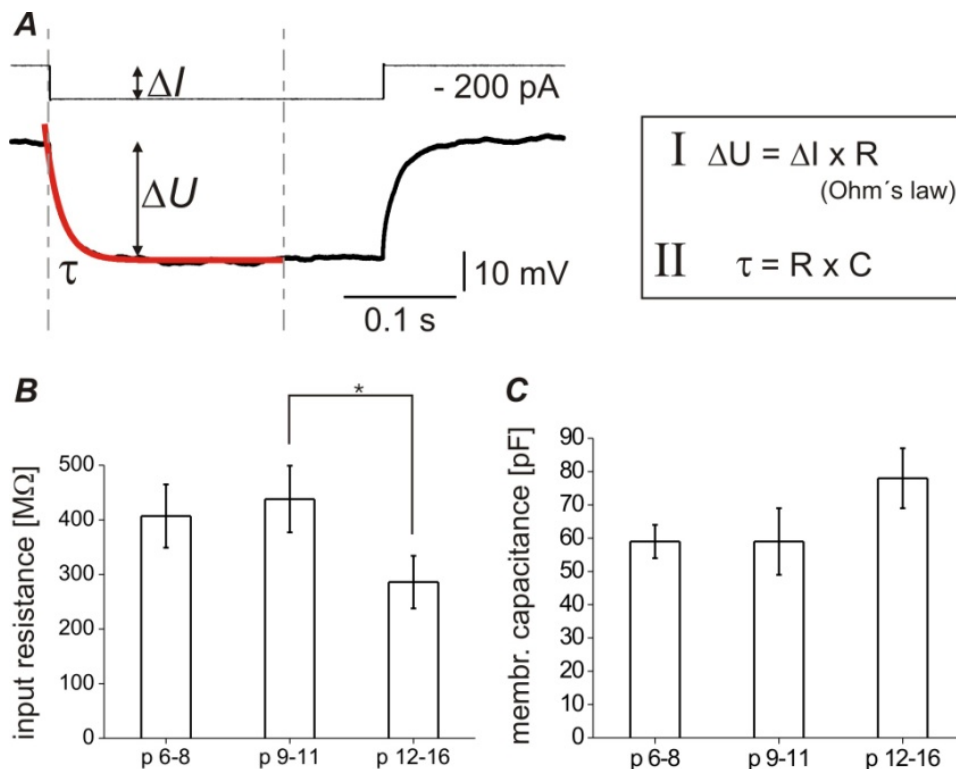


**Fig.17 Passive membrane properties change during postnatal development. (A)** Analysis of passive membrane properties by a single exponential fit of the voltage response to hyperpolarizing current pulse (amplitude of hyperpolarizing current pulse  $\Delta I$ , amplitude of voltage response  $\Delta U$ , time constant of single exponential fit  $\tau$ ). (I) Input resistance  $R$  is dependent on  $\Delta U$  and  $\Delta I$ . (II) Membrane capacitance  $C$  depends on  $R$  and  $\tau$ . Bar diagrams show the age-dependence of input resistance (**B**,  $p < 0.05$ ) and mean membrane capacitance (**C**). Modified figure 1 Holter et al., 2007.

## Active intrinsic properties of molecular layer interneurons change with maturation

As neurons of different age groups display a differential expression pattern of ion channels, not only passive intrinsic properties but also active properties can underlie changes with ongoing development. Therefore, both action potential waveform and frequency were investigated.

The action potential waveform is characterized by different parameters like its amplitude, threshold and velocity (see Fig. 18A,19A). Action potentials were elicited by depolarizing current injections (25 pA step increment, 300 ms duration) and the parameters of the first action potential, which could be triggered by the lowest possible current amplitude (mean:  $92 \pm 6$  pA), were quantified. With maturation, action potential parameters showed two main changes: spikes became faster and exhibited higher amplitudes.

Action potential threshold has an impact on cell excitability. Similar to action potential amplitude, this parameter may vary in different cell types. For example, mature neurons show generally larger action potential amplitudes than immature neurons. However, action potential amplitude increased by  $\sim 20\%$  during the observed time of development, while threshold ( $\sim -40$  mV) was not age-dependent (Fig. 18A,C). Action potential amplitudes of neurons from the intermediate age group (p 9-11) were significantly different from the immature group but similar to action potentials recorded at p 12-16.

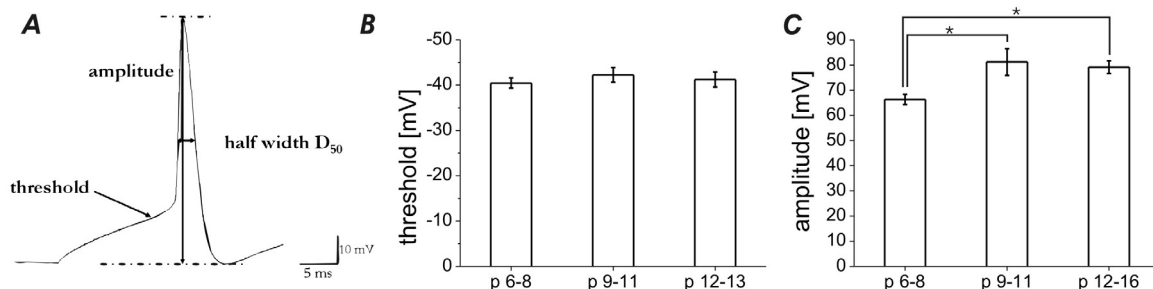


**Fig.18 Active intrinsic properties change during postnatal development.** (A) Analyzed action potential parameters exemplified at a molecular layer interneuron action potential raw data section. The turning point of the data trace marks the action potential firing threshold. Action potential amplitude is taken from baseline to peak. Action potential half width describes the full width at half maximum. Bar diagrams show the age-dependence of action potential firing threshold (B) and amplitude (C;  $p < 0.05$ ). Modified figure 1 Holter et al., 2007.

The velocity of an action potential can be described through the full width of half maximum and the slope of rise and decay (rate of de- and repolarization). Short and fast action potentials are characteristic for mature fast spiking interneurons. Here, action potentials of cells from immature animals (p 6-8) showed slow rates of rise and decay and, accordingly, had a longer duration as compared to older cells (action potential half width decreasing from  $\sim 5$  ms to about 3.5 ms; values at p 6-8 significantly different towards p 9-11 and p 12-16, each  $p < 0.01$ ; see Fig. 19 and Tab.1).

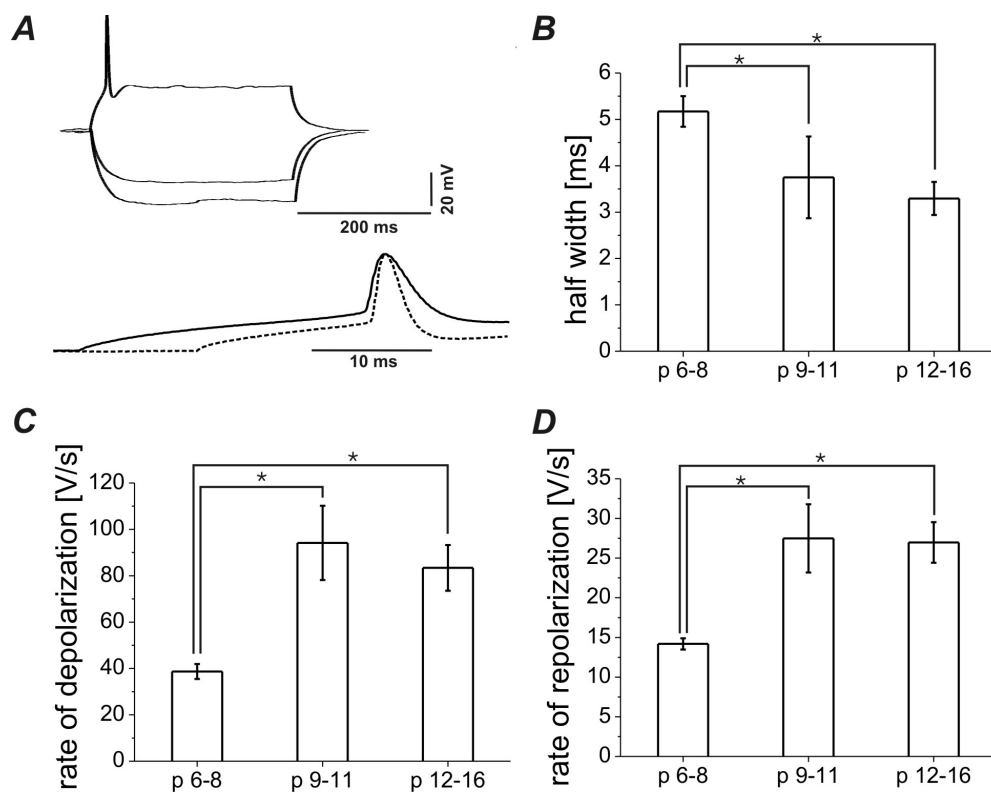


**Fig.19 Action potential velocity changes during postnatal development.** (A) Superimposed representative voltage traces in response to hyperpolarizing and depolarizing current injections in an interneuron from a mouse at p 7. Note the steep increase in voltage and absence of repetitive firing. Bottom: Superimposed and artificially scaled action potentials from a cell at p 7 (solid line) and at p 14 (dashed line). Note faster de- and repolarization in the more mature cell. Bar diagrams show age-dependence of action potential half-width (B) and the rates of voltage change during the depolarization (C) and repolarization (D). Asterisks mark significant differences  $p < 0.01$ . All kinetic parameters changed towards faster spiking with increasing age. *Modified figure 1 Holter et al., 2007.*

Besides action potential waveform, the discharge pattern is also characteristic for the degree of maturity. In most cells (7/9) from the first postnatal week, only one to three action potentials could be elicited by current steps of increasing amplitude. In the older groups of cells, regular trains of action potentials with no marked spike frequency adaptation were elicited (Fig.20). Spike frequency adaptation was calculated at maximum number of elicited action potentials. The values were obtained from trains of action potentials by dividing the averaged time intervals between the last three spikes through the time interval between the first two spikes.

In summary, discharge behavior of dentate interneurons matured after the first postnatal week and showed the typical fast waveform with little frequency adaptation at later states (Tab.1). These data indicate a fast change in intrinsic properties towards the end of the first postnatal week.

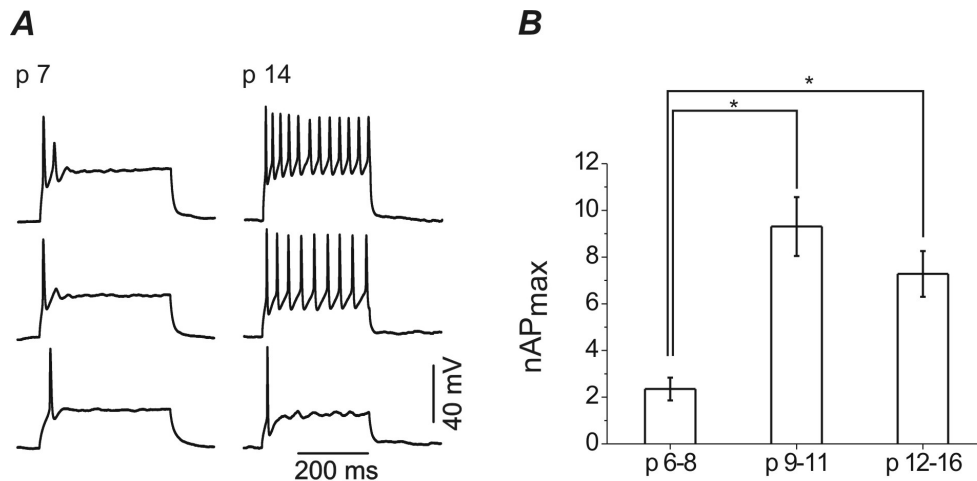


**Fig.20 Increase of repetitive firing during postnatal maturation.** The original traces in **(A)** show voltage responses to three current injections of increasing amplitude in a neuron at p 7 (left) and at p 14 (right). Note the fast repetitive firing pattern in the more mature cell, which shows little spike frequency adaptation. Bar diagram **(B)** shows the maximal number of spikes which could be elicited within 300 ms in neurons from the three different age groups;  $p < 0.01$ . *figure2 Holter et al., 2007.*

**Tab.1: Summary of intrinsic properties of interneurons in the molecular layer**

postnatal period	p 6-8	p 9-11	p 12-16
<b>intrinsic properties (n)</b>	17	13	18
input resistance [M $\Omega$ ]	407 $\pm$ 58; #	438 $\pm$ 61	286 $\pm$ 48
membrane capacitance [pF]	59 $\pm$ 5	59 $\pm$ 10	78 $\pm$ 9
<b>action potential parameters (n)</b>	17	13	18
threshold [mV]	-40.4 $\pm$ 1.1	-42.3 $\pm$ 1.6	-41.2 $\pm$ 1.7
amplitude [mV]	66.3 $\pm$ 2.0; * #	81.3 $\pm$ 5.3	79.2 $\pm$ 2.5
half width [ms]	5.2 $\pm$ 0.3; * #	3.7 $\pm$ 0.9	3.3 $\pm$ 0.4
rate of depolarisation [V/s]	39 $\pm$ 3; * #	94 $\pm$ 16	83 $\pm$ 10
rate of repolarisation [V/s]	14.2 $\pm$ 0.7; * #	27.5 $\pm$ 4.3	27.0 $\pm$ 2.6
maximal number of inducible action potentials	2.4 $\pm$ 0.5; * #	9.9 $\pm$ 0.3	7.3 $\pm$ 1.0
spike frequency adaptation	1.3 $\pm$ 0.01 (n=2)	1.4 $\pm$ 0.1 (n=10)	1.5 $\pm$ 0.1 (n=11)

**Tab.1:** Summary of intrinsic properties of interneurons in the molecular layer at three different ages. \*: Significantly different towards p 9-11; #: Significantly different towards p 12-16. All differences reached a significance level of  $p < 0.01$ , except the decrease in input resistance (#:  $p < 0.05$ ) and action potential amplitude (\*:  $p < 0.05$ ). No significant differences were encountered between cells from p 9-11 and cells from p 12-16.

## Spontaneous synaptic properties of molecular layer interneurons

In order to monitor network integration of the maturing interneurons, spontaneous synaptic currents were observed. Recordings were performed in voltage clamp mode at  $-70$  mV. First mixed (pharmacologically naive) postsynaptic currents were analyzed, which had a rather uniform appearance with slow, decaying phases. This waveform appearance points towards a dominance of inhibitory postsynaptic currents.

### *Excitatory synaptic currents were largely absent*

The contribution of excitatory synaptic events was analyzed by addition of  $1 \mu\text{M}$  gabazine in order to block inhibitory postsynaptic currents and isolate excitatory synaptic events. However, spontaneous excitatory events were not observed even though excitability was enhanced by elevating extracellular potassium concentration to  $8$  mM (Khazipov *et al.*, 2004; LeBeau *et al.*, 2002; Towers *et al.*, 2002). A detectable contribution of typical, fast excitatory synaptic currents (EPSCs) to the mixed spontaneous activity was lacking (Fig. 21).

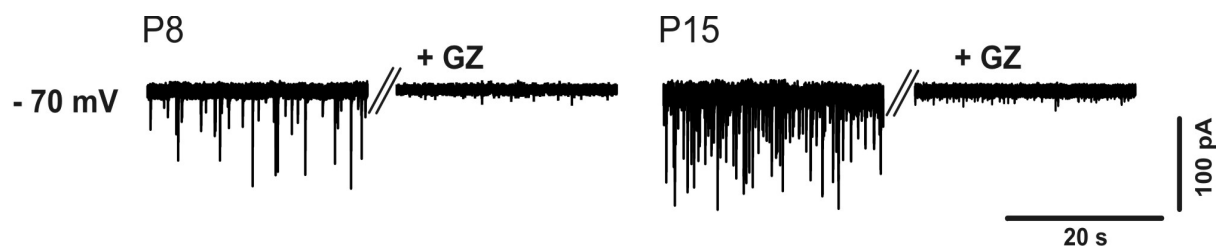


**Fig.21 Original current traces showing postsynaptic currents of a p8 (A) and p15 (B) stratum molecular interneuron, respectively.** Depicted is mixed spontaneous activity recorded in aCSF (left) and the absence of spontaneous EPSCs after application of  $1 \mu\text{M}$  gabazine (right). Taken from figure 3 Holter *et al.*, 2007.

In order to resolve whether interneurons in molecular layer of dentate gyrus show excitatory events at all, pharmacologically isolated excitatory events were elicited by electrical stimulation in the hippocampal fissure, where the perforant path enters the molecular layer. At  $-70$  mV responses appeared as typical fast inward currents or as bursts of multiple superimposed EPSCs (Fig. 22). The latter, complex type of response was more frequent in the youngest age group (5/6 cells at p7/8) as compared to the more mature group (p 14/15: 2 cells show monosynaptic responses, 3 complex bursts and 1 cell with mixed responses). Bursts of synaptic currents did already occur upon stimulation at the lowest possible intensity (response threshold). At positive membrane potentials ( $+40$  mV), the same stimulation elicited outward currents with slower decay kinetics, indicative of an NMDA receptor-mediated component (Fig. 22). Currents were completely blocked by CNQX ( $20 \mu\text{M}$ ) and  $\pm$ -APV ( $30 \mu\text{M}$ ), indicating their excitatory nature.

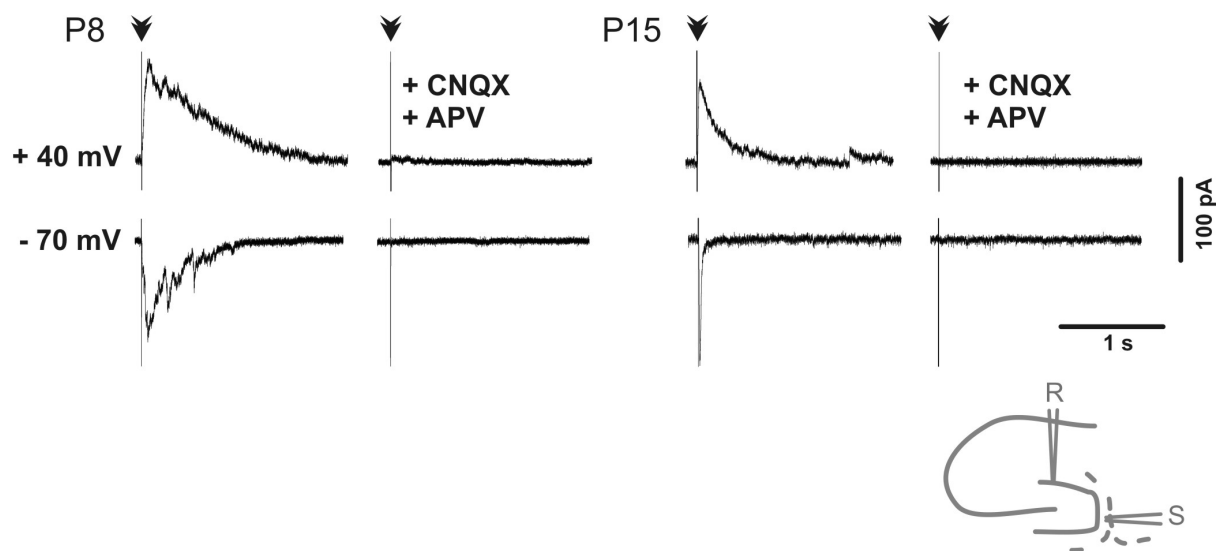


**Fig.22** Original current traces showing stimulus-evoked excitatory postsynaptic currents recorded in the presence of gabazine (GZ, 1  $\mu$ M). Stimulus-evoked excitatory postsynaptic currents (in 1  $\mu$ M GZ) at -70 mV and +40 mV in cells from an animal at p 8 (left) and p 15 (right), respectively. Currents were completely blocked by CNQX (20  $\mu$ M) and APV (30  $\mu$ M). Stimuli indicated by arrowheads. Drawing shows the position of recording electrode (R) and stimulation electrode (S). Taken from figure 3 Holter *et al.*, 2007.

#### *Inhibitory synaptic activity of molecular layer interneurons increased with maturation*

As spontaneous excitatory postsynaptic currents were largely absent in the present preparation, further analysis was restricted to pharmacologically isolated spontaneous inhibitory currents in the presence of CNQX (20  $\mu$ M) and APV (30  $\mu$ M). Block of glutamatergic excitation increased, rather than decreased, the frequency of spontaneous synaptic events by  $\sim$ 50%, similar to previous observations (Maccaferri & Dingledine, 2002; McBain *et al.*, 1992).

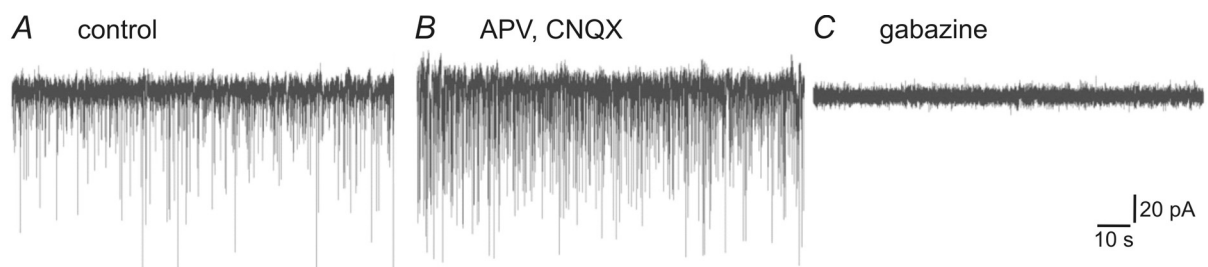


**Fig.23** Original traces showing the effect of CNQX and GZ on spontaneous synaptic events. **(A)** Control conditions spontaneous synaptic currents in aSCF. **(B)** Block of glutamatergic excitation by CNQX and APV; CNQX increased the frequency of spontaneous synaptic events. **(C)** Currents were completely blocked by application of gabazine (GZ 2  $\mu$ M).

All recorded cells (p 6-8, n=9; p 9-11, n=12; p12-16, n=11) displayed spontaneous inhibitory synaptic currents (sIPSCs). However, the frequency of sIPSCs in the youngest group (p 6-8) was markedly lower than in more mature tissue (p 9-11 and p 12-16, respectively), increasing from ~80 events/min to > 300 events/min. Waveform of synaptic currents did not change: mean rise time constant  $\tau_{on}$  was about 2.8 ms, the mean decay time constant  $\tau_{off}$  about 18 ms. Both time constants were not significantly different between age groups ( $\tau_{on}$ :  $2.0 \pm 0.8$  ms at p 6-8,  $2.4 \pm 0.1$  ms at p 9-11,  $3.1 \pm 0.9$  at p 12-16; decay time constant  $\tau_{off}$ :  $15.3 \pm 2.2$  ms at p 6-8;  $14.8 \pm 1.1$  ms at p 9-11,  $22.1 \pm 5.8$  ms at p 12-16). Likewise, median amplitude of sIPSCs did not show any significant change during development (Fig. 24), although the relative amount of very large events seemed to decrease.

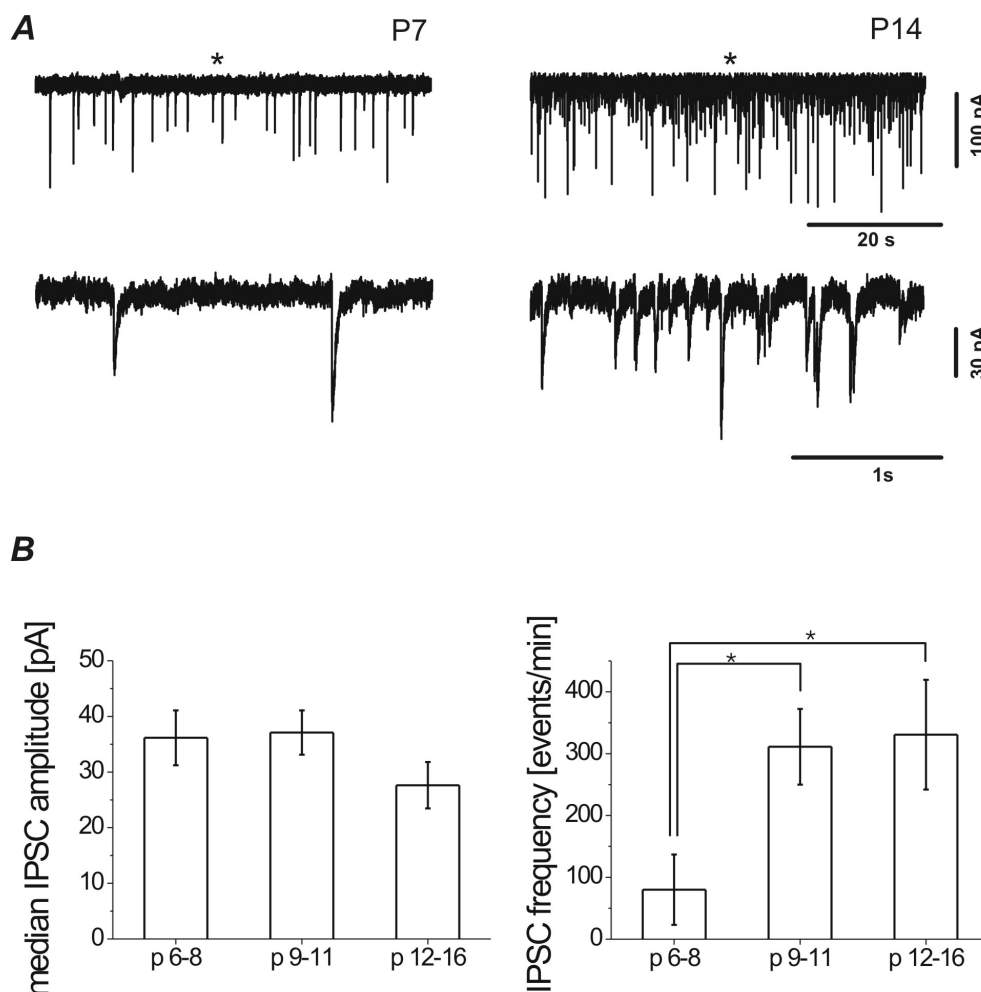


**Fig.24 Inhibitory synaptic activity increased in maturing neurons in the molecular layer. (A)** Original current traces showing spontaneous inhibitory synaptic activity in the cells depicted in (D). Bottom traces taken from the section indicated by \* at higher time resolution. **(B)** Group comparison of the median IPSC amplitude (which does not change with age:  $36.2 \pm 4.9$  pA at p 6-8,  $37.1 \pm 3.8$  pA at p 9-11 and  $27.6 \pm 4.2$  pA at p 12-16) and the average frequency of synaptic events which shows a clear increase between p 6-8 and p 9-11 (IPSC frequency in events per minute:  $80 \pm 57$  at p 6-8,  $311 \pm 61$  at p 9-11 and  $331 \pm 89$  at p 12-16;  $p < 0.01$ ). Taken from figure 3 Holter et al., 2007.

In summary, the maturation of interneurons in the molecular layer goes along with faster and larger action potentials, increased repetitive firing, and increased frequency of spontaneous postsynaptic inhibitory currents.

### Morphology of recorded stratum molecular interneurons

During electrophysiological recordings, cells were filled with neurobiotin for subsequent morphological analysis. Altogether, 22 out of 48 interneurons could be recovered for histological analysis (6 immature cells at p 6-8, 6 intermediate cells at p 9-11 and 10 juvenile cells at p 12-16). Most of the recorded neurons were located in the middle portion of the molecular layer (see Fig. 16). All analyzed cells showed a multipolar dendritic branching pattern (Fig. 25). Cells with deviating morphology were excluded from the analysis, including one ectopic granule cell (Marti-Subirana *et al.*, 1986) and one outer molecular layer cell projecting across the hippocampal fissure (Ceranik *et al.*, 1997).

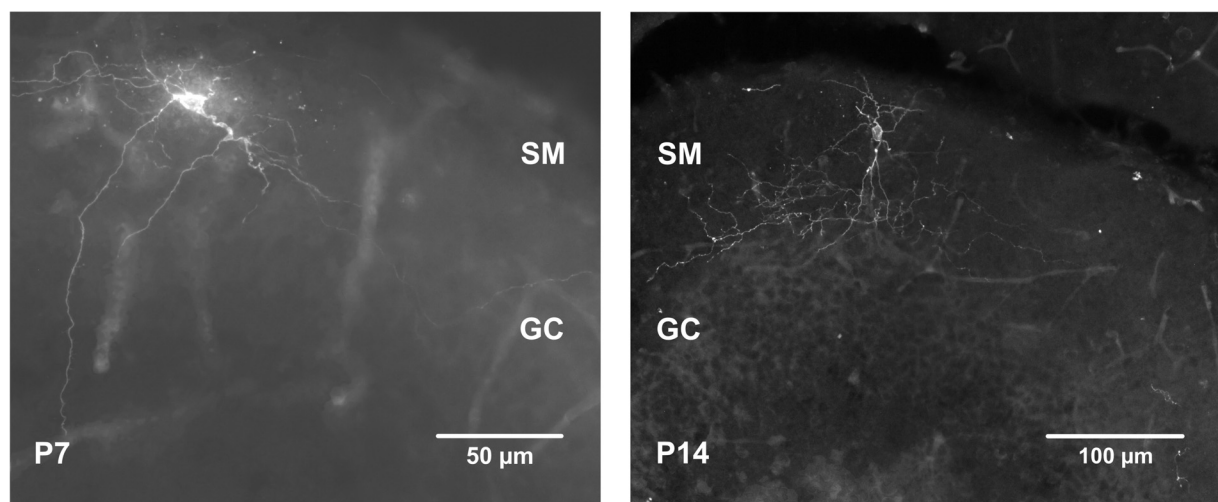


**Fig.25** Photomicrographs of neurobiotin-filled and reconstructed cells from p 7 and p 14, respectively. Cells were located in stratum molecular (SM) of dentate gyrus. Granule cell layer (GC). Taken from figure 3 Holter *et al.*, 2007.

### Classification of interneurons in developing stratum molculare

Hippocampal interneurons are heterogeneous and can be classified by different morphological, histochemical or functional properties (Freund & Buzsaki, 1996). In order to gain information about the expression of interneuron subtypes throughout the first postnatal weeks, immunohistochemical staining was performed in slices taken from animals aged 7 days and 15 days, respectively. The expression of the typical marker proteins parvalbumin (PV), calbindin (CB), calretinin (CR) and somatostatin (SS) was quantified.

The majority of cells expressed the calcium-binding protein calretinin (CR; cells/ 30  $\mu$ m section in stratum moleculare:  $88 \pm 1$  at p 7;  $60 \pm 1$  at p 15;  $p < 0.0001$ ). Many of these cells were located in the outer portion of the molecular layer and displayed horizontal morphology, usually with one thick (main) dendrite (Fig. 26A). Cells with this location and morphology were not included in the functional analysis. CR-positive neurons in the middle molecular layer showed a multipolar branching pattern. The calcium-binding protein parvalbumin (PV) exhibited the typical age-dependence of expression (Nitsch *et al.*, 1990), being absent at p 7 but strongly expressed in several interneurons at p 15 (Fig. 26C). These cells were mostly located at the inner border of the granule cell layer towards the hilus. Their morphology was compatible with the shape of PV-positive basket cells. The molecular layer contained no (p 7) or very few (p 15;  $1.3 \pm 0.1$  cells per 30  $\mu$ m slice) PV-positive neurons ( $p < 0.0001$ , see Fig. 26E). Calbindin, another calcium-binding protein, is highly expressed in granule cells and -slightly less pronounced- in CA1 pyramidal cells (Sloviter, 1989). This pattern was also apparent in sections of both age-groups analyzed in the present study (Fig. 26B). Some CB-positive somata were found in the inner molecular layer, close to the granule cell band which was not always clearly demarcated. Therefore, it is possible that these cells represent ectopic granule cells. Their total number in the molecular layer, however, was low as compared to the number of cells expressing the predominant marker CR. The neuromodulatory protein somatostatin (SS) was exclusively expressed in hilar neurons and absent from cells in the molecular layer in both age groups (Fig. 26D).

Altogether, typical markers of interneurons revealed a clear prevalence of calretinin-positive cells in the molecular layer, reducing the heterogeneity of neurons recorded in the middle portion of the molecular layer of the developing dentate gyrus.

**Fig. 26 Expression patterns of interneuron markers. (A)** Expression of interneuron marker calretinin in the mouse dentate gyrus. Multiple neurons were stained within the molecular layer at p 7 (left), at p 15 (middle) and in an adult control staining (right). Cells positioned close to the fissure revealed bipolar morphology. The number of cells in stratum moleculare decreased during early postnatal development. At p 15 adult expression pattern was reached. **(B)** Comparison of the expression pattern of calbindin at p 7 (left) and p 15 (right). Note strong staining of granule cells and large number of CB-positive cells in close vicinity to the granule cell band. **(C)** Parvalbumin was absent at p 7 (left) and strongly expressed in few neurons at p 15 (right). Most of these cells were located towards the hilar border of the granule cell layer, indicative of basket cells. **(D)** Absence of somatostatin (SS) from neurons in the molecular layer. Note widespread expression in hilar neurons at both ages. **(E)** Summary of cell numbers for CR (decreasing with age) and PV (absent at p 7, expressed in few neurons at p 15). *Modified figure 4 Holter et al., 2007.*

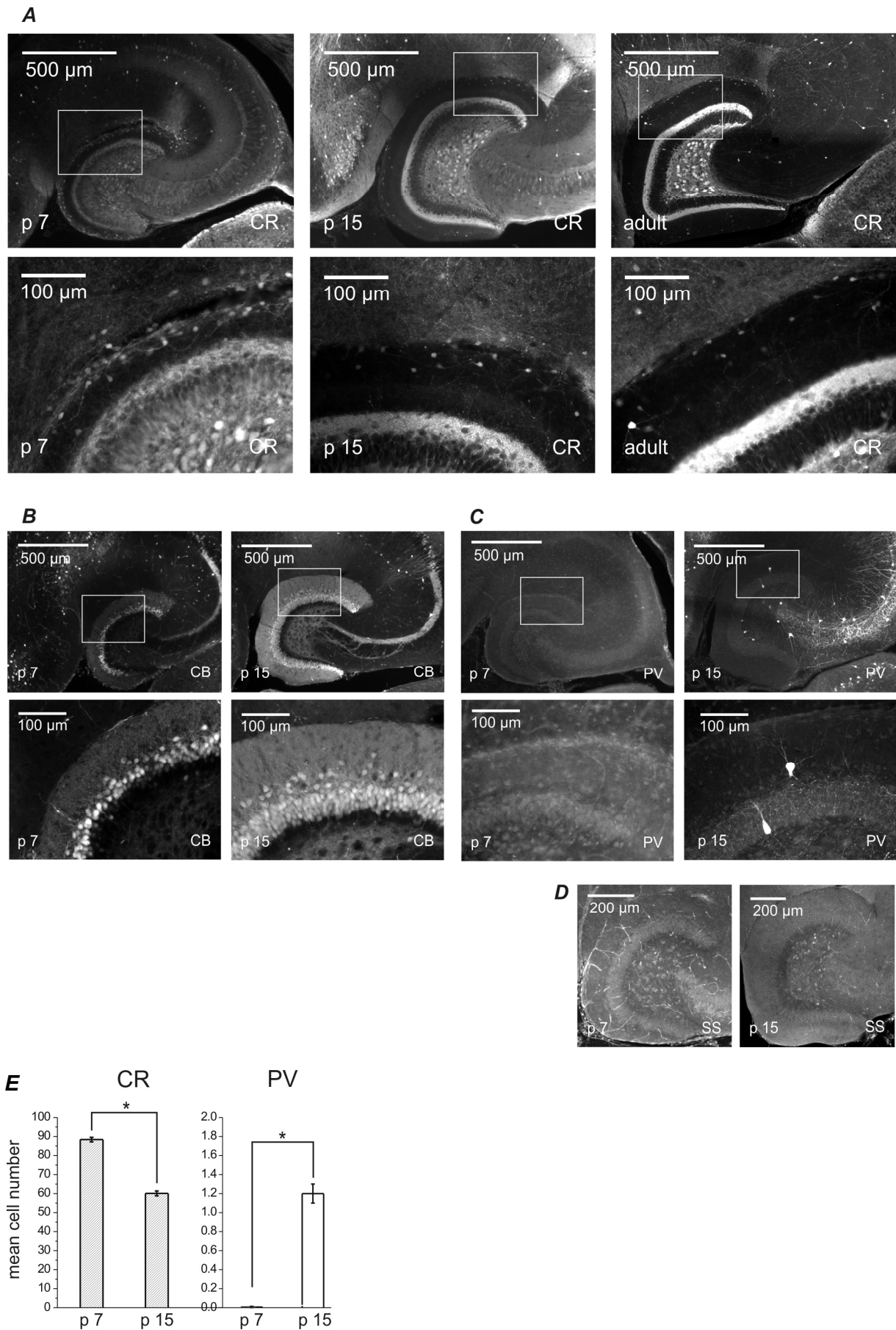


**Fig. 26** Expression patterns of interneuron markers.

## Part 2

### Maturation of dentate gyrus granule cells during early postnatal development

Besides characterizing the functional maturation of interneurons in the dentate gyrus I also studied the electrophysiological properties of dentate gyrus granule cells during early postnatal development. Therefore, visually identified cells in the granule cell layer of dentate gyrus were recorded with the patch-clamp technique. Similar to the data obtained from the molecular layer interneuron, recordings from dentate gyrus granule cells at different postnatal time points were performed (p 7/8, n=21 and p 14/15, n=29). In addition an adult control group of more than 45 days was analyzed (n=33); at this age most of the receptors (e.g. GABA<sub>A</sub>-receptors) show a stable expression pattern (Laurie *et al.*, 1992). A potential complication of studying dentate gyrus granule cells is that in dentate gyrus adult neurogenesis takes place. Newborn granule cells appear first at the hilar border of the granule cell layer and then migrate towards the outer granule cell layer (Shapiro & Ribak, 2005). Therefore only cells from the outer granule cell layer were recorded.

Putative granule cells were filled with neurobiotin during the recording through the patch pipette and were visualized with streptavidin-Alexa488 complex after PFA-fixation. Neurobiotin filled cells displayed typical granule cell morphology with cell bodies located in the granule cell layer, the principal cell layer of dentate gyrus (Fig. 27 and 28A,B). They showed a branched dendritic tree in molecular layer of dentate gyrus and the axon was projecting to CA3 region, both typical for granule cells of dentate gyrus.

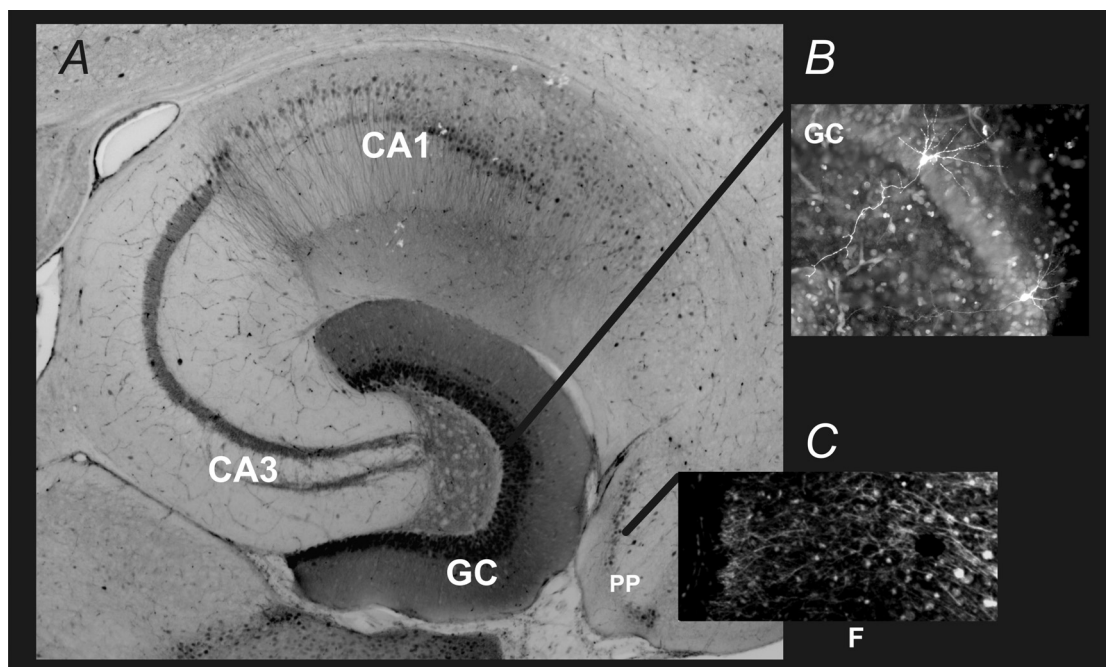


**Fig.27 Cellular localization, projections and inputs of granule cells in hippocampus.** (A) Cells were located in the granule cell layer (GC) and their fibres (mossy fibres) were projecting towards CA3 region of hippocampus. Cells stained for calcium binding protein calbindin. (B) Example cells: neurobiotin filled granule cells at postnatal day 7. (C) Cells with somata located in entorhinal cortex (EC) project to dentate gyrus (projecting fibres, F). Cells were labeled with neurobiotin and visualized with streptavidin-Alexa488 complex.

## Passive intrinsic properties of granule cells change with maturation

The passive intrinsic properties of the cell input resistance and membrane capacitance are both dependent on the size of the neuronal membrane. As neurons grow postnatal, these passive intrinsic properties should be modified with maturation. Hence, voltage responses to hyperpolarizing current pulses in dentate gyrus granule cells were analyzed. Input resistance was calculated from the amplitude and membrane capacitance was determined from the time constant  $\tau$  of the voltage response measured by a monoexponential fit (see Fig. 17, part 1). Input resistance decreased from  $\sim 800\text{ M}\Omega$  at p 7/8 to  $\sim 300\text{ M}\Omega$  at p >45 ( $p < 0.05$ ) as the size of the granule cells increased during development (Fig. 28C). Accordingly, mean membrane capacitance increased significantly with ongoing maturation ( $\sim 40\text{ pF}$  at p 7/8 to  $\sim 90\text{ pF}$  at p > 45,  $p < 0.05$ ; Fig. 28D).

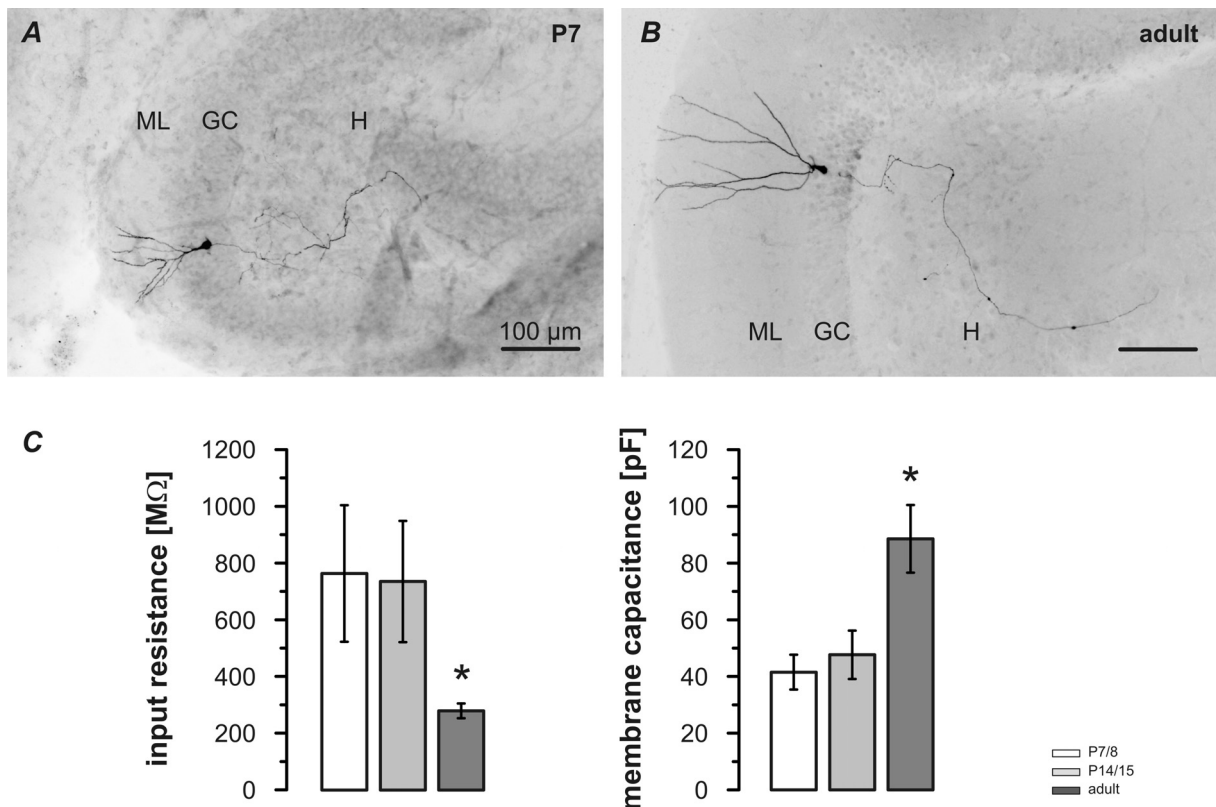


**Fig.28** Passive membrane properties of granule cells change during postnatal development. Photomicrographs of neurobiotin-filled granule cells at the immature stage of postnatal day 7 (A) compared to an adult granule cell. Note the larger size of the adult granule cells, which goes along with the general increase of hippocampal size. Olympus BX61 microscope, 10x magnification; colors inverted. (B). Bar diagrams show the age-dependence of input resistance and mean membrane capacitance (C,  $p < 0.05$ ).

## Active intrinsic properties of dentate granule cells change with maturation

Active intrinsic properties were investigated by eliciting action potentials in current clamp mode of the amplifier by depolarizing current injections (10 pA step increment, 800 ms duration) and adjacent analysis of action potential waveform. The following parameters were derived from the first action potential, which could be triggered by the lowest possible current amplitude, action potential amplitude, threshold and velocity.

In contrast to the development of molecular layer interneurons, action potential threshold of dentate granule cells became significantly more negative from p 7/8 to p > 45 ( $p < 0.05$ ). Granule cells were more excitable with development, which was in line with the observation that at very immature stages not all granule cells showed an action potential (2 out of 7). Likewise action potential amplitude was increased by ~60% with ongoing maturation. Action potential amplitudes of neurons of the end of the first postnatal week (p 7/8) were significantly different from the adult group ( $p < 0.05$ ) but similar to values recorded at p 14/15 (Fig. 29).

Action potential velocity is described by the three parameters full width of half maximum (AP  $D_{50}$ ), rate of depolarization and rate of repolarization. Action potential shape of granule cells was shown to mature during postnatal development in the characteristic way already described for molecular layer interneurons. Action potentials of mature animals (> p45) showed significantly faster rates of rise and decay and had a longer duration as compared to immature cells ( $p > 0.05$ ; Fig. 29).

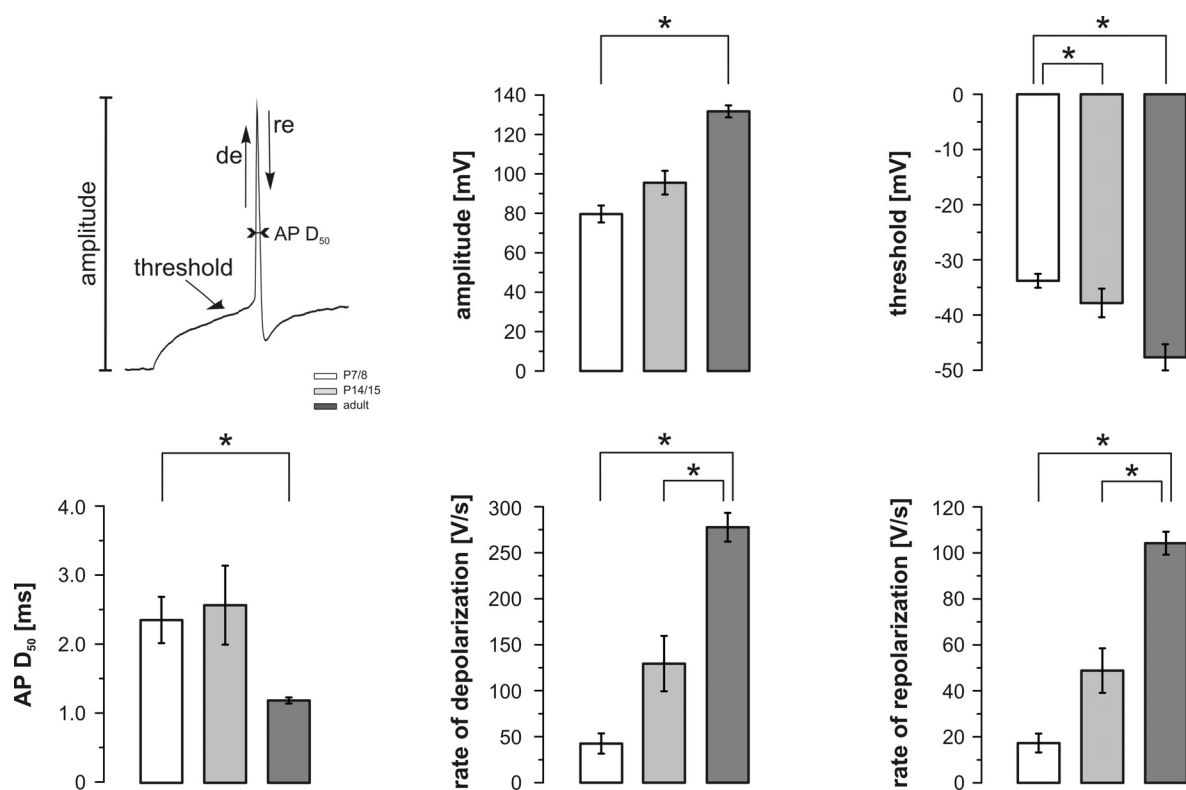


**Fig.29 Active intrinsic properties change during postnatal development. (A)** Analyzed action potential parameters exemplified at a dentate gyrus granule cell action potential raw data section. The turning point of the data trace marks the action potential firing threshold. Action potential amplitude is taken from baseline to peak. AP  $D_{50}$  describes the full width at half maximum. Bar diagrams show age-dependence of action potential parameters ( $p < 0.05$ ).

Discharge behavior of dentate gyrus granule cells was shown to mature after the second postnatal week. The waveform of immature action potentials was smaller and slower compared to the action potentials recorded from the adult control group. Also, granule cells exhibited lower thresholds with ongoing postnatal development.

**Tab.2: Summary of intrinsic properties of granule cells in the dentate gyrus**

postnatal period	p 7/8	p 14/15	p > 45
<b>intrinsic properties (n)</b>	7	12	8
input resistance [M $\Omega$ ]	764 $\pm$ 240; #	736 $\pm$ 214	307 $\pm$ 38
membrane capacitance [pF]	42 $\pm$ 6; #	48 $\pm$ 9	85 $\pm$ 12
<b>action potential parameters (n)</b>	7	12	8
threshold [mV]	-33.8 $\pm$ 1.3; *#	-37.8 $\pm$ 2.6	-47.7 $\pm$ 2.4
amplitude [mV]	79.7 $\pm$ 4.3; #	95.5 $\pm$ 6.0	131.7 $\pm$ 3.0
half width [ms]	2.4 $\pm$ 0.3; #	2.6 $\pm$ 0.6	1.2 $\pm$ 0.04
rate of depolarisation [V/s]	42 $\pm$ 11; * #	129 $\pm$ 30	278 $\pm$ 16
rate of repolarisation [V/s]	17.3 $\pm$ 0.4; * #	48.8 $\pm$ 9.7	104.2 $\pm$ 4.9

**Tab.2: Summary of intrinsic properties of granule cells in the dentate gyrus at different developmental ages.**

\*: significantly different towards p 14/15; #: significantly different towards p >45. Differences were considered statistically significant by reaching P- values < 0.05.

## Postnatal development of Inhibitory Postsynaptic Currents (IPSCs)

Since I was primarily interested in inhibition, I also monitored the network integration of developing granule cells in the inhibitory GABAergic network of dentate gyrus. Recordings were performed in voltage clamp mode at -80 mV with a CsCl<sup>-</sup> based intracellular solution. Inhibitory currents were pharmacologically isolated blocking glutamatergic excitation by adding CNQX (20  $\mu$ M) and APV (30  $\mu$ M) to the extracellular solution.

All recorded cells (p 7/8, n=14; p14/15, n=17; adult, n=25) displayed spontaneous inhibitory synaptic currents (sIPSCs). The median amplitude of IPSCs did not change significantly throughout postnatal development. However, the relative amount of very large events seemed to decrease, similar to stratum molecular interneurons (Fig. 30, Tab.3). IPSC frequency again changed with development, increasing from about 170 events/minute to > 300 events/minute ( $p < 0.05$ ; Fig. 30, Tab.3). Similar, the IPSC waveform became faster in the adult. The mean decay time constant  $\tau_{off}$  was changing significantly from about 15 ms during the first two postnatal weeks to about 10 ms in the adult ( $p < 0.05$ ; see Tab. 3), while the mean rise time stayed constant ( $t_{on} \sim 1$ ms) throughout development.

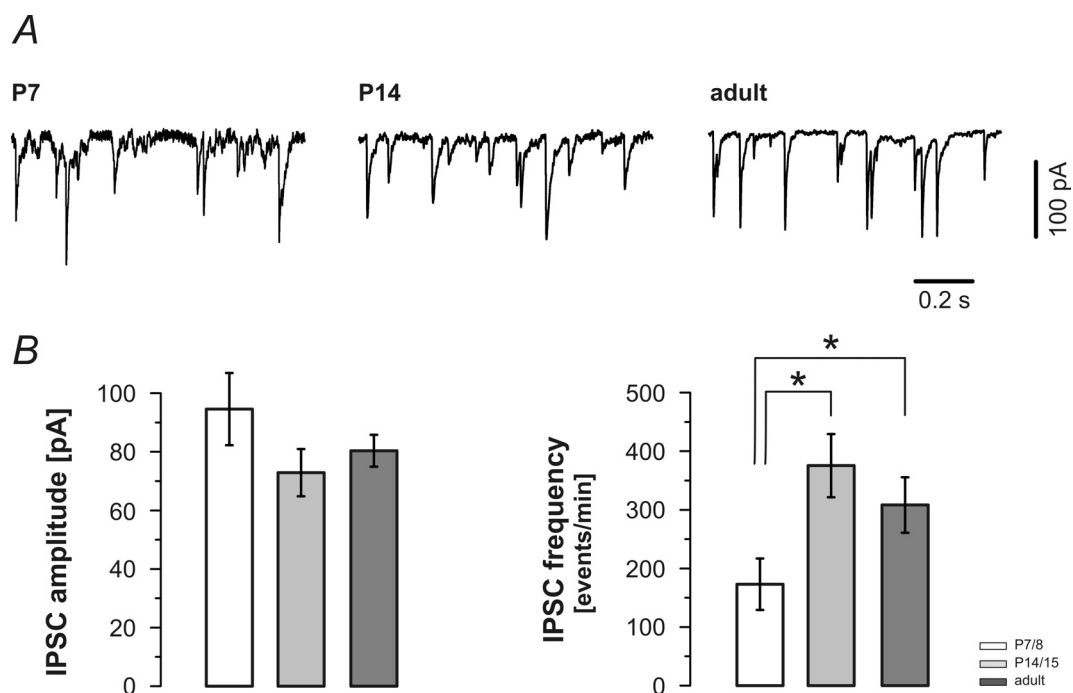


**Fig.30 Inhibitory synaptic activity increases in maturing granule cells of dentate gyrus. (A)** Original current traces showing IPSCs from dentate granule cell of p7, p14 and adult (p >45). **(B)** Group comparison of the median amplitude (which does not significantly change throughout development) and the mean IPSC frequency, which shows a clear increase between p 7/8 and p 14/15 (p < 0.05).

In summary, the maturation of granule cells of dentate gyrus went along with both faster and larger action potentials. Similarly, mature dentate gyrus granule cells showed an increased frequency of spontaneous postsynaptic inhibitory currents, indicating the ongoing integration of granule cells in the synaptic network of dentate gyrus.

**Tab.3: Summary of IPSC properties of granule cells in the dentate gyrus**

postnatal period	p 7/8	p 14/15	p > 45
synaptic properties (n)	14	17	25
tau on [ms]	1.07 ± 0.1	1.05 ± 0.1	1.0 ± 0.1
tau off [ms]	15.7 ± 1.2; #	15.0 ± 0.6; #	10.8 ± 0.5
IPSC amplitude [pA]	-94 ± 12	-70 ± 8	-80 ± 5
IPSC frequency [events per minute]	172 ± 44; *#	375 ± 54	308 ± 47

**Tab.3: Summary of IPSC properties of granule cells in the dentate gyrus at different developmental stages.**

\*: significantly different towards p 14/15; #: significantly different towards p >45. Differences were considered statistically significant by reaching P- values < 0.05.

## Maturation of dentate granule cells recorded at physiological conditions

The experiments in this thesis have been performed under different experimental conditions. The recordings from molecular layer interneurons were done in pure aCSF solution, while recordings from dentate gyrus granule cells were performed in aCSF solution with supplemented GABA (2.5  $\mu$ M). The ambient transmitter GABA in the extracellular space is probably washed out by regular bath perfusion, especially in the superficial cell layers used for patch experiments. To achieve more physiological recording conditions 2.5  $\mu$ M GABA was added to the extracellular solution. This transmitter concentration is assumed to be physiological in the extracellular space (Lerma *et al.*, 1986; Tossman & Ungerstedt, 1986).

The recording conditions used in the second and third part of the thesis were further optimized by integrating a heating element in the recording chamber and performing experiments at 34°C. Increasing recording temperature to physiological levels is likely not only to increase GABA uptake but also to increase synaptic GABA release and to affect GABA receptor kinetics (Asztely *et al.*, 1997, Otis and Mody, 1992).

### *Effect of temperature on IPSCs in dentate granule cell layer*

Therefore, sIPSCs recorded from dentate gyrus granule cells at room temperature were analyzed ( $n = 19$ ) and compared to sIPSCs recorded at the more physiological temperature of 34°C ( $n = 19$ ). Note that both datasets were recorded in aCSF without additional GABA. Median sIPSC amplitude stayed the same at raised temperature levels ( $50.5 \pm 4.6$  pA at RT vs.  $56.5 \pm 6.7$  pA at 34°C), while sIPSC frequency was significantly increased ( $74 \pm 25$  events/minute;  $225 \pm 49$  events/minute;  $p < 0.05$ ; non-parametric Mann-Whitney-test, pooled data tested). Figure 31 shows pooled data for simplicity reasons; statistics resemble the same when performed on the data of the single age groups.

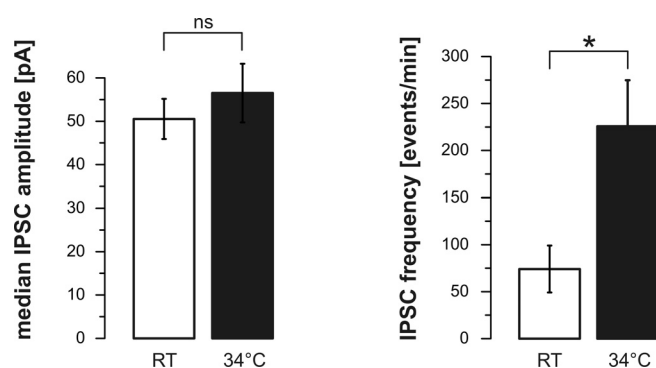


**Fig. 31 Effect of temperature on sIPSC parameters.** Bar diagrams show mean values of pooled age groups. Spontaneous IPSCs recorded in slices with more physiological temperature show the same median amplitude as sIPSCs recorded at RT. However, sIPSC frequency is significantly increased at elevated temperature ( $p < 0.05$ ).

The sIPSC waveform was not affected by the increased temperature in the first two postnatal weeks, but became significantly faster in the adult. The mean decay time constant  $\tau_{off}$  was changing significantly from about 15 ms at room temperature to about 10 ms at more physiological temperatures ( $p < 0.05$ ; unpaired Student's t-test). The mean rise time constant was stable in both experimental conditions ( $t_{on} \sim 1$ ms).

### Effect of GABA on IPSCs in dentate granule cell layer

The addition of 2.5  $\mu\text{M}$  GABA to the extracellular solution could have affected spontaneous inhibitory postsynaptic currents. Therefore, sIPSCs recorded from dentate gyrus granule cells were analyzed under both conditions; aCSF supplemented with 2.5  $\mu\text{M}$  GABA ( $n = 65$ ) and pure aCSF ( $n = 19$ ), respectively. Both, median sIPSC amplitude and mean sIPSC frequency tended towards higher values in dentate gyrus granule cells recorded in aCSF supplemented with 2.5  $\mu\text{M}$  GABA. The two experimental conditions were not significantly different (Fig. 32) and also no significant difference could be observed among the different age groups investigated.

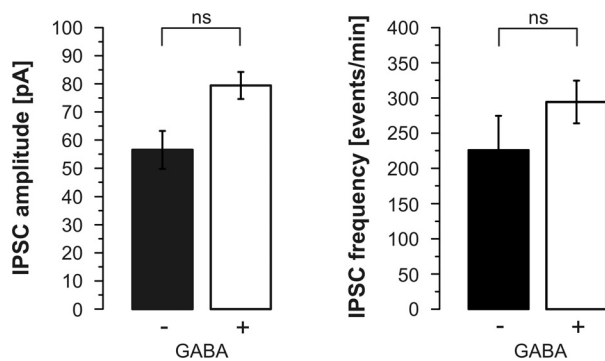


**Fig. 32 Effect of 2.5  $\mu\text{M}$  GABA in extracellular solution on sIPSC parameters.** Bar diagrams show mean values of pooled age groups. Spontaneous IPSCs recorded in slices perfused with 2.5  $\mu\text{M}$  GABA tended towards higher sIPSC amplitudes and frequencies (not significant).

The sIPSC waveform was not affected by the increased GABA level in the extracellular solution. The mean decay time constant  $\tau_{\text{off}}$  was  $16 \pm 4$  ms in aCSF compared to  $10 \pm 1$  ms in aCSF supplemented with GABA (not significant; unpaired Student's t-test). The mean rise time constant was similar in both conditions, with and without GABA supplementation ( $t_{\text{on}} \sim 1\text{ms}$ ).

To summarize the effects of recording conditions, GABA supplementation had no significant effect on dentate gyrus granule cell sIPSCs. Median sIPSC amplitude, IPSC mean frequency and IPSC kinetics were similar in pure aCSF and aCSF with added transmitter. However, raising the recording temperature to physiological levels significantly increased mean sIPSC frequency and also fastened sIPSC waveform, while median sIPSC amplitude was not altered throughout development.

## *Part 3*

### Tonic inhibitory currents in mouse dentate gyrus granule cells during postnatal development

The dentate gyrus receives strong excitatory input from entorhinal cortex. Therefore, inhibition in this region is of particular importance to balance network activity at the hippocampal gate. However, the inhibitory control of the dentate gyrus is not solely mediated by subsynaptic GABA<sub>A</sub>-receptors producing a fast inhibitory postsynaptic current (see above: IPSCs Fig. 24,30). Continuous activation of non-synaptic GABA<sub>A</sub>-receptors mediates in fact a different type of GABAergic inhibition, tonic inhibitory currents. The non-synaptic GABA<sub>A</sub>-receptors exhibit a high affinity to the ambient transmitter GABA in the extracellular space. In contrast to the fast subsynaptic IPSCs the activation of non-synaptic GABA<sub>A</sub>-receptors causes a long-lasting increase in chloride conductance.

In the first two parts of the thesis both, the postnatal maturation of postsynaptic inhibitory currents and the integration of cells into the synaptic network of dentate gyrus have been described. Not only synaptic inhibition but also tonic inhibition may be crucial for excitation-inhibition balance of dentate gyrus network. Therefore, it was of interest, whether early postnatal dentate gyrus granule cells display tonic inhibitory currents, as they have been previously described for adult dentate gyrus granule cells (Nusser & Mody, 2002). Further, the effect of tonic inhibitory currents on excitation inhibition balance of dentate gyrus network was investigated, especially in the critical period of the first two postnatal weeks of development.

## Detection and analysis of tonic inhibition

Tonic inhibitory currents increase the 'holding current' that is required to clamp the cells at a given membrane potential (see introduction Fig. 8). Therefore, blocking GABAergic inhibitory currents by a high concentration of the GABA<sub>A</sub>-receptor blocker picrotoxin (100 μM) decreased the 'holding current' of the recorded cell (Fig. 33A). This was associated with a reduced baseline noise, consistent with the decrease in the number of open GABA<sub>A</sub>-receptor channels.

The size of tonic inhibitory current (Δ holding current) was determined by subtracting the holding current under baseline conditions from the holding current in presence of the GABA<sub>A</sub>-receptor blocker picrotoxin (100 μM). For analyzing the holding current of the recorded neuron a method according to Glykys and Mody, 2007 was used.

A twenty seconds period of raw data was analyzed by plotting an all-point histogram (Fig. 33B). The resulting histogram curve (black curve, Fig. 33C and E) was smoothed by Savitzky-Golay algorithm (green curve, Fig. 33C) and a Gaussian was fitted to the right part of the smoothed curve (red curve, Fig. 33E).

The Gaussian equation:

$$y = y_0 + \frac{A}{w\sqrt{\pi/2}} e^{-2\frac{(x-x_c)^2}{w^2}}$$

For initializing the Gaussian Fit the maximum of the smoothed curve (green) - obtained through simple differentiation (Fig. 33D) - was used as  $x_c$  (x-value of the Gaussian's peak). The other parameters of the Gaussian Fit were initialized as following:  $y_0 = 0$ , half width (w) was initialized with 10 and the area under the curve (A) was initially set to 100000. The resulting Gaussian was not deformed by synaptic events compared to both, the resulting histogram curve and the smoothed curve (see arrow Fig. 33E). The mean of the fitted Gaussian was considered to be the mean holding current.

The measured holding current was analyzed with the help of Origin-Software (7G SR2; OriginLab Corporation, Northampton, USA). The software provided the tools for histogram analysis, Savitzky-Golay algorithm and for doing a Gaussian Fit.

**Fig. 33 Analysis of tonic inhibitory currents according to the method published by Mody et al., J. Physiol. 2007. (A)** Raw data traces of the same cell recorded in aCSF under block of glutamatergic excitation (right) and application of 100 μM picrotoxin (left). The wash in of picrotoxin is depicted in the middle. Note the shift in holding current after block of tonic inhibitory currents. **(B)** All-point histograms of the aCSF baseline condition and of the block of tonic inhibitory currents. **(C)** Resulting histogram curve (black) and the smoothed curve (green, Savitzky-Golay algorithm). **(D)** Differentiated smoothed curve. **(E)** Gaussian Fit (red) of the right part of the histogram curve. Note that the Gaussian was not deformed by synaptic events (arrow).

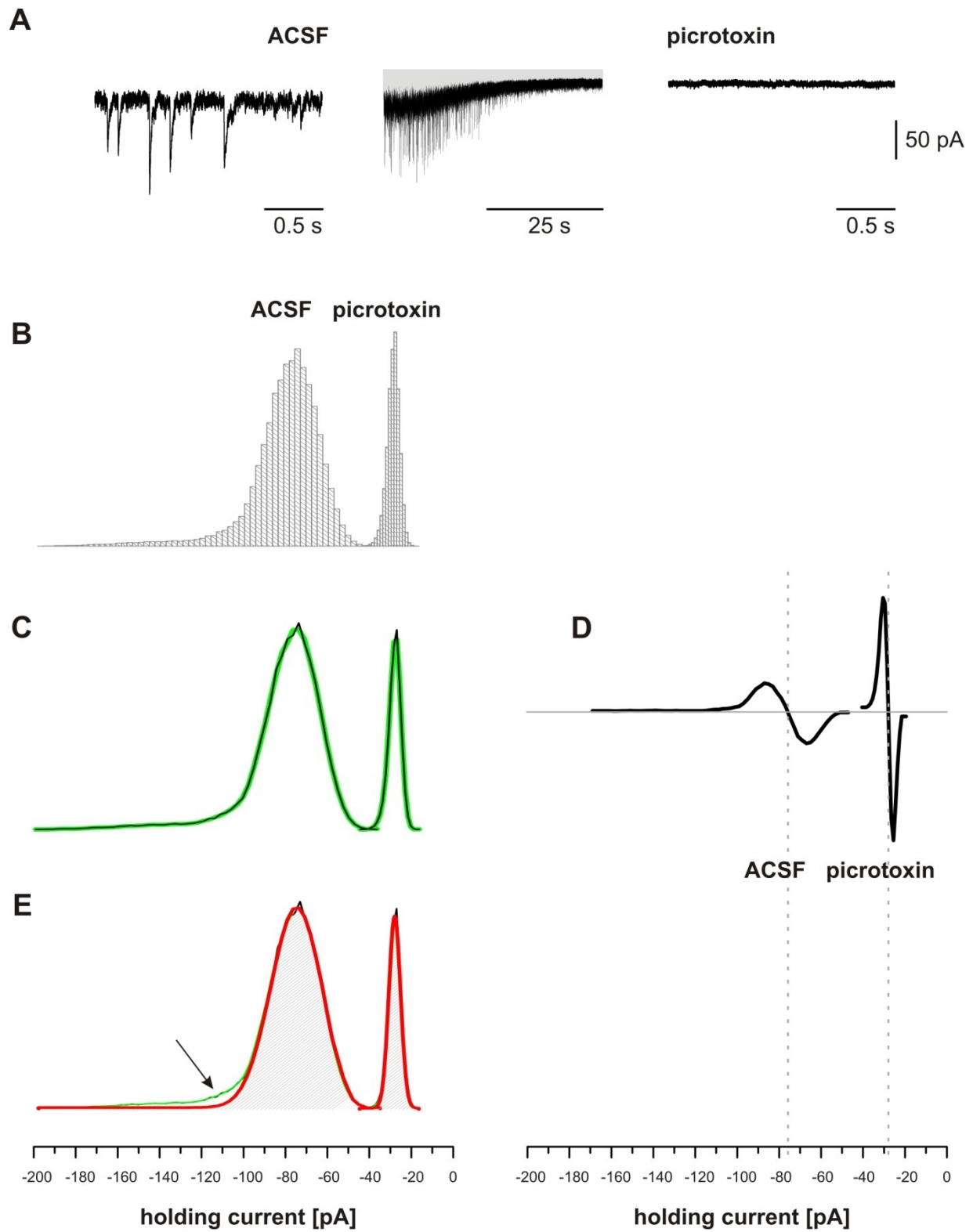


Fig. 33 Analysis of tonic inhibitory currents according to the method published by Glykys and Mody, 2007.

## Tonic inhibitory currents at “physiological” recording conditions

Tonic inhibitory currents are mediated by high-affinity GABA<sub>A</sub>- receptors sensing the ambient GABA in the extracellular space. The transmitter is found in the extracellular space at micromolar levels (Lerma *et al.*, 1986) but might easily be washed out just by regular bath perfusion. Therefore, recordings of tonic inhibitory currents in dentate gyrus granule cells were performed in aCSF supplemented with 2.5  $\mu$ M GABA. Also the recording temperature ( $\sim 20^{\circ}\text{C}$ ) was elevated to more physiological levels (Glykys & Mody, 2007). Most of the earlier performed experiments on tonic inhibitory currents in adult dentate granule cells were performed at room temperature without additional transmitter. Therefore, control recordings were performed to test if the chosen experimental conditions significantly affected the tonic inhibitory currents recorded in dentate gyrus granule cells.

### *Effect of temperature on tonic inhibitory currents of dentate gyrus granule cells*

It has been shown by Kullmann and coworkers that tonic signaling in stratum radiatum interneurons and CA1 pyramidal cells persists at physiological temperature, whereby increased temperature results in no significant change of tonic inhibitory currents (Scimemi *et al.*, 2005). In the present study, raising temperature to physiological levels yielded similar results. The magnitude of tonic inhibitory currents was not significantly affected, nevertheless there was a strong tendency towards higher values (not significant, non-parametric Mann Whitney test; RT: n = 13; 34°C: n = 19; Fig. 34).

### *Effect of the GABA-supplementation on tonic inhibitory currents of dentate gyrus granule cells*

Also the addition of 2.5  $\mu$ M GABA to the extracellular solution could have affected the magnitude of tonic inhibitory currents. Therefore, tonic inhibitory currents recorded in dentate gyrus granule cells were analyzed under both conditions; aCSF supplemented with 2.5  $\mu$ M GABA (n = 65) and pure aCSF (n = 19), respectively. The magnitude of tonic inhibitory currents, analyzed as described above, was apparently enhanced by the presence of 2.5  $\mu$ M GABA, though not significantly. Also no significant difference could be observed between the two experimental conditions within the different age groups (non parametric Man Whitney test; see Fig. 34, age groups pooled for simplicity reasons).

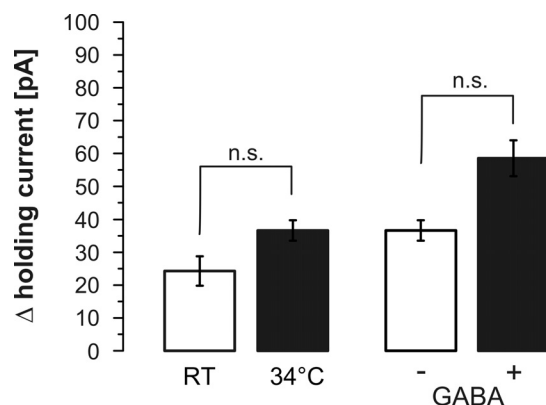


**Fig. 34** Effect of different recording conditions on tonic inhibitory currents in dentate gyrus granule cells. Raising temperature and elevating GABA levels enhanced tonic inhibitory currents in dentate gyrus granule cells, though not in a significant way (non parametric Mann Whitney test). Bar diagrams show pooled data (age groups) for simplicity reasons.

## Tonic inhibitory currents of dentate gyrus granule cells

To determine whether tonic inhibitory currents are present throughout development, visually identified mouse dentate gyrus granule cells were recorded at different postnatal stages (p7/8 and p14/15). The adult control measurements were performed in granule cells of mice aged more than 45 days (p>45), where most of the receptors, e.g. GABA<sub>A</sub>- receptors show a stable expression pattern (Laurie *et al.*, 1992). Adult neurogenesis in dentate gyrus had to be taken into consideration and therefore, only inhibitory currents from cells of the outer granule cell layer were recorded (see also introduction and part2).

Whole cell recordings were performed at -80 mV in voltage clamp mode of the amplifier. Inhibitory currents were isolated by block of glutamatergic excitation (30  $\mu$ M APV and 20  $\mu$ M CNQX), furthermore GABA<sub>B</sub>-receptor mediated events were blocked (CGP 55845; 5  $\mu$ M). To mimic the physiological ambient GABA level and to standardize conditions in mice of varying developmental stages 2.5  $\mu$ M GABA was added to extracellular solutions. This extracellular solution was referred to as 'aCSF<sup>+</sup>' in the following experiments on tonic inhibitory currents.

### *Pharmacological separation of tonic and phasic inhibitory currents in dentate gyrus granule cells*

GABA<sub>A</sub>-receptors of different cell types and localizations (subsynaptic, perisynaptic and extrasynaptic) exhibit diverse receptor properties. These can be used for their pharmacological separation. For guinea pig stratum radiatum interneurons it has been shown that it is possible to separate phasic and tonic inhibitory currents by application of the GABA<sub>A</sub>-receptor blocker gabazine at a low concentration of 0.5  $\mu$ M (Scimemi *et al.*, 2005). Furthermore, in guinea pig stratum radiatum interneurons separation of tonic from phasic inhibitory currents was realized by application of a low concentration of GABA<sub>A</sub>-receptor blocker picrotoxin (1  $\mu$ M).

In contrast to the reported effects in guinea pig interneurons, application of 1  $\mu$ M picrotoxin in mouse dentate gyrus granule cells caused a reduction of phasic inhibitory currents as well as tonic inhibitory currents. Furthermore after application of 100  $\mu$ M picrotoxin there was still an additional shift in holding current detectable (tested for 2 cells each developmental time point; Fig. 35B).

In the present study synaptic GABAergic currents of dentate gyrus granule cells should be separated from tonic inhibitory currents by application of a low concentration of the GABA<sub>A</sub>-receptor blocker gabazine (200 nM; Fig. 35A). The remaining inhibitory current (tonic component) should be blocked by application of a high concentration of the GABA<sub>A</sub>- receptor blocker picrotoxin (100  $\mu$ M; Fig. 35A).

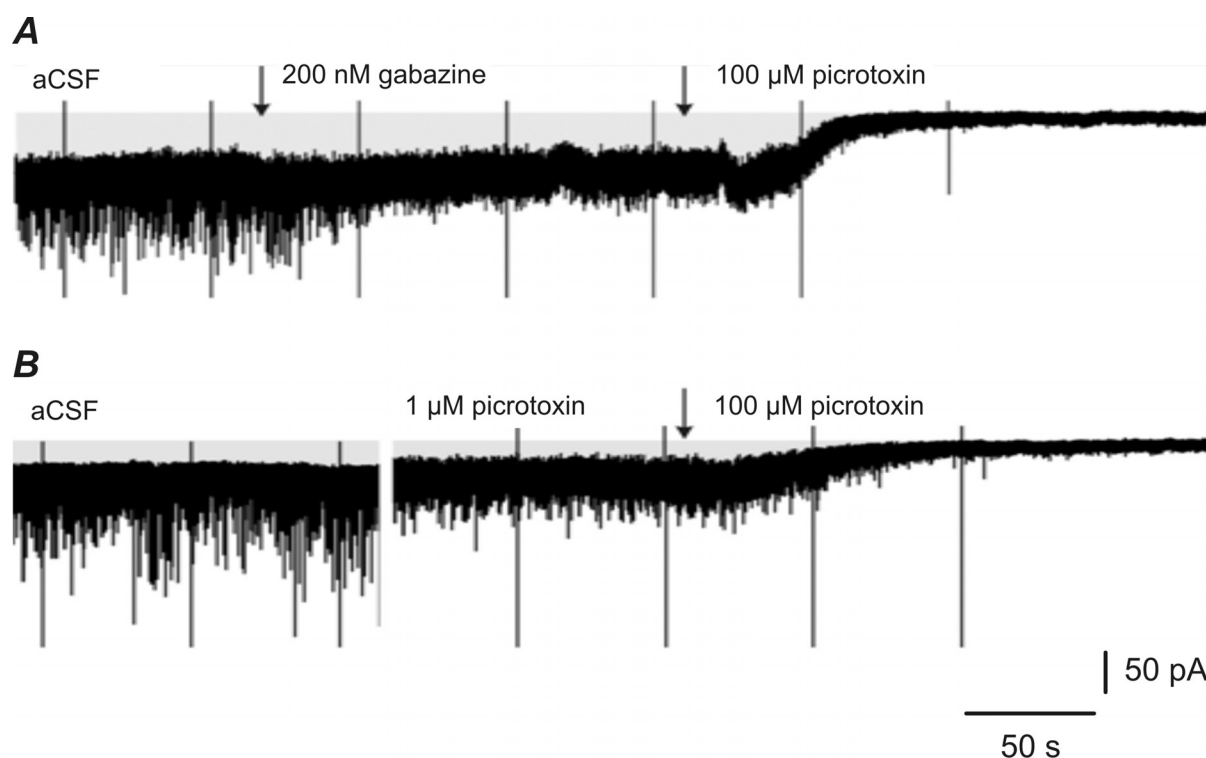


**Fig. 35 Original data traces: Separation of phasic and tonic GABAergic currents of dentate gyrus granule cells. (A)** Inhibitory currents recorded in aCSF + 2.5 μM GABA. Gabazine (200 nM) perfusion blocked postsynaptic inhibitory currents, further application of picrotoxin (100 μM) reduced holding current. **(B)** Inhibitory currents recorded in aCSF + 2.5 μM GABA. Perfusion of 1 μM picrotoxin blocked tonic inhibitory currents only partially, as they were reduced further by application of 100 μM picrotoxin (100 μM). Note that sIPSC amplitude was also reduced by 1 μM picrotoxin.

### Tonic inhibitory currents of dentate gyrus granule cells could be detected throughout postnatal development

After achieving stable recordings of at least three minutes under control conditions ('aCSF<sup>+</sup>'), phasic GABAergic current was blocked by applying a low concentration of gabazine (200 nM). The distinct spontaneous inhibitory postsynaptic currents (sIPSCs) disappeared. The application of this low concentration of 200 nM gabazine already caused a decrease in holding current, and therefore also affected tonic inhibitory currents (Fig. 36A).

The remaining tonic GABAergic currents were then blocked by application of 100 μM picrotoxin, which binds to the GABA<sub>A</sub>-receptors. Picrotoxin binds to any GABA<sub>A</sub>-receptor and the general effect on tonic inhibitory currents mediated by any GABA<sub>A</sub>-receptor subunit could be investigated. However, the wash in of the GABA<sub>A</sub>-receptor antagonist resulted in a clearly visible shift of the holding current of the recorded cell (Fig. 36 A).

The size of tonic inhibitory currents was then determined by subtracting the holding current under baseline conditions (aCSF<sup>+</sup>) from the holding current in the presence of picrotoxin (100 μM + 200 nM GZ). Tonic inhibitory currents could be detected at all investigated age groups throughout postnatal development (83.8 ± 23.2 pA at p7/8, n = 7; 81.7 ± 23.4 pA at p14/15, n = 6 and 51.0 ± 8.5 pA at p>45, n = 6). Tonic inhibitory currents decreased during development from ~50 pA in adult granule

cells to  $\sim 80$  pA during the first two postnatal weeks (Fig. 36), though the difference appeared not to be significant (unpaired Student's t-test).

Tonic inhibition also affected the intrinsic properties of the cells. The membrane resistance was significantly increased after picrotoxin application ( $\sim 90\%$ ), while the membrane capacitance was not affected. The reduction of the ion flux across the neurons membrane probably also affects the general excitability of the cell.

Interestingly, tonic inhibitory currents in dentate gyrus correlated with the maturational stage of the animal and not with the cell size (membrane capacitance) characterizing the developmental stage of the granule cell.

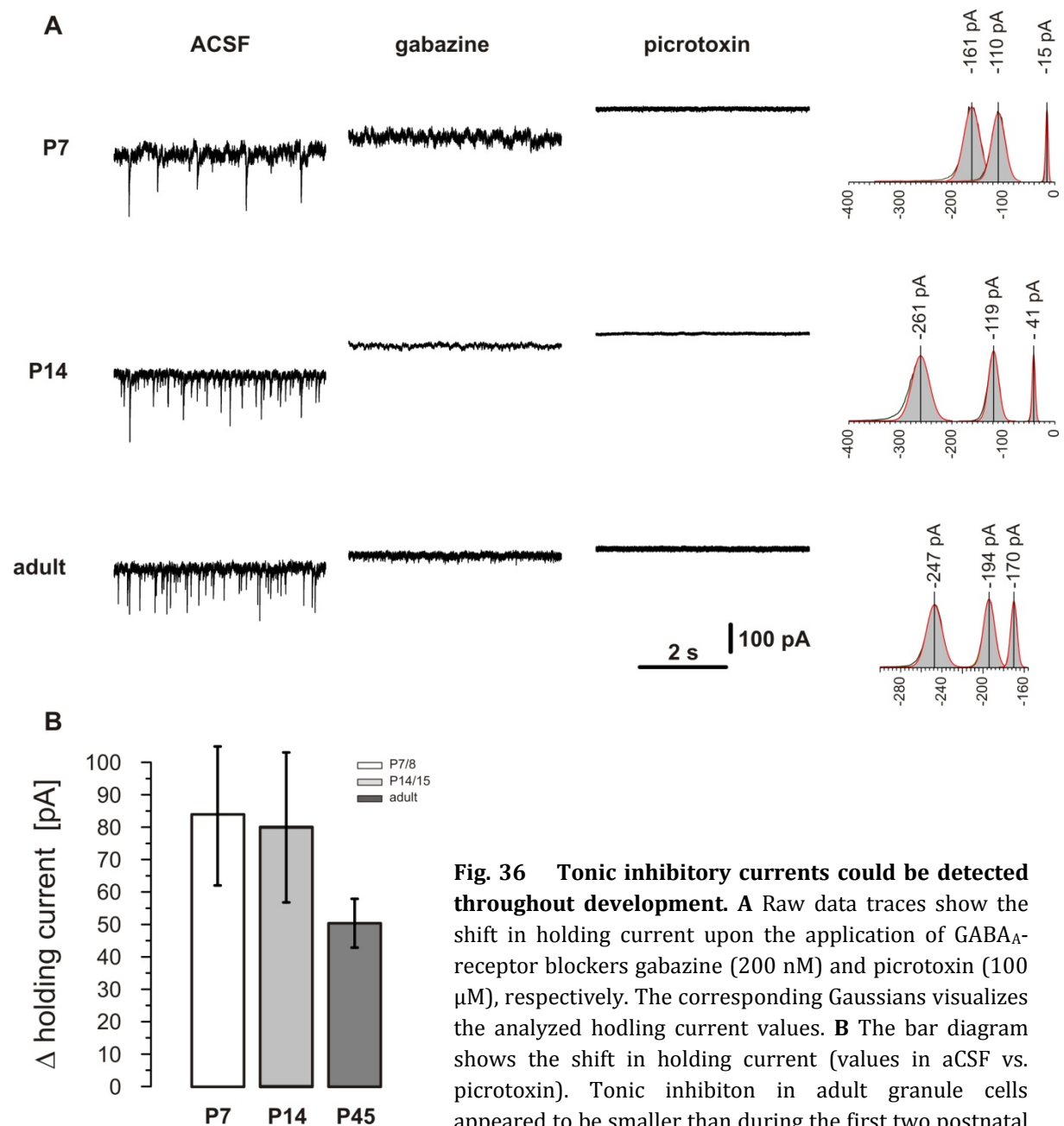


**Fig. 36 Tonic inhibitory currents could be detected throughout development.** **A** Raw data traces show the shift in holding current upon the application of GABA<sub>A</sub>-receptor blockers gabazine (200 nM) and picrotoxin (100  $\mu$ M), respectively. The corresponding Gaussians visualize the analyzed holding current values. **B** The bar diagram shows the shift in holding current (values in aCSF vs. picrotoxin). Tonic inhibition in adult granule cells appeared to be smaller than during the first two postnatal weeks (not significant)

## Receptors contributing to tonic inhibitory currents of dentate gyrus granule cells during postnatal development

Inhibitory transmission in the hippocampus is predominantly GABAergic, but recently there is also morphological and electrophysiological evidence for glycine receptor mediated inhibition (Danglot *et al.*, 2004; Ito & Cherubini, 1991). Similar to GABA<sub>A</sub>-receptors, glycine receptors containing the  $\alpha_2$ -subunit are found at synaptic and extrasynaptic locations. These extrasynaptic glycine receptors may therefore contribute to tonic inhibitory currents.

So, to block tonic inhibitory currents the specific GABA<sub>A</sub>-receptor blocker picrotoxin (PTX = picrotin and picrotoxinin) was used in a high concentration (100  $\mu$ M). However, this substance potentially blocks glycine receptors, though in a use dependent manner (Yang *et al.*, 2007).

### *GABA<sub>A</sub>-receptors and not glycine receptors are contributing to tonic inhibitory currents in dentate gyrus granule cells*

Therefore, the contribution of extracellular glycine receptors to tonic inhibitory currents of dentate gyrus granule cells during postnatal development was tested. Potential glycinergic tonic inhibitory currents of recorded dentate gyrus granule cells were blocked by application of the specific glycine receptor blocker strychnine (1  $\mu$ M). Residual GABA<sub>A</sub>-receptor mediated tonic inhibitory currents were then blocked by addition of picrotoxin (100  $\mu$ M and 200 nM gabazine). Changes in holding current after strychnine and picrotoxin application were analyzed. Perfusion of the glycine receptor specific blocker strychnine (1  $\mu$ M) did not significantly change the holding current throughout the investigated period of development (Fig. 37A,B). Calculated mean values were: 3.28 pA  $\pm$  1.64 pA at p 7/8 (n = 3); 8.11 pA  $\pm$  5.36 pA at p14/15 (n = 4); 1.98 pA  $\pm$  1.3 pA at p>45 (n = 5). By subsequent wash in of the GABA<sub>A</sub>-receptor blocker picrotoxin (100  $\mu$ M + 200 nM gabazine) holding current was significantly shifted towards more positive values: 52.5 pA  $\pm$  21.6 pA at p7/8, 30.9 pA  $\pm$  10.9 pA at p14/15; 27.3 pA  $\pm$  3.4 pA at p>45 (p < 0.05; paired Student's t-test;). Likewise, amplitude and frequency of sIPSCs were not significantly affected by application of 500 nM strychnine (Fig. 37C).

In summary, throughout postnatal development of dentate gyrus granule cells both the phasic inhibitory currents (sIPSCs) and the tonic inhibitory currents are not mediated by glycine receptors, but by GABA<sub>A</sub>-receptors.

### *GABA<sub>A</sub>-receptor $\alpha_5$ - and $\delta$ -subunits are mediating tonic inhibitory currents in dentate gyrus granule cells during development*

Tonic inhibitory currents are mediated by peri- and extrasynaptic GABA<sub>A</sub>-receptors sensing the ambient GABA in the synaptic cleft. For the present study it was of interest, which GABA<sub>A</sub>-receptor subunits contributed to the tonic inhibitory currents of dentate gyrus granule cells throughout postnatal development. The most promising candidates were GABA<sub>A</sub>-receptor  $\alpha_5$ - and  $\delta$ -subunits, as tonic inhibitory currents of adult dentate granule cells have been shown to be mediated by  $\alpha_5$ - and  $\delta$ -subunits (Glykys *et al.*, 2008).

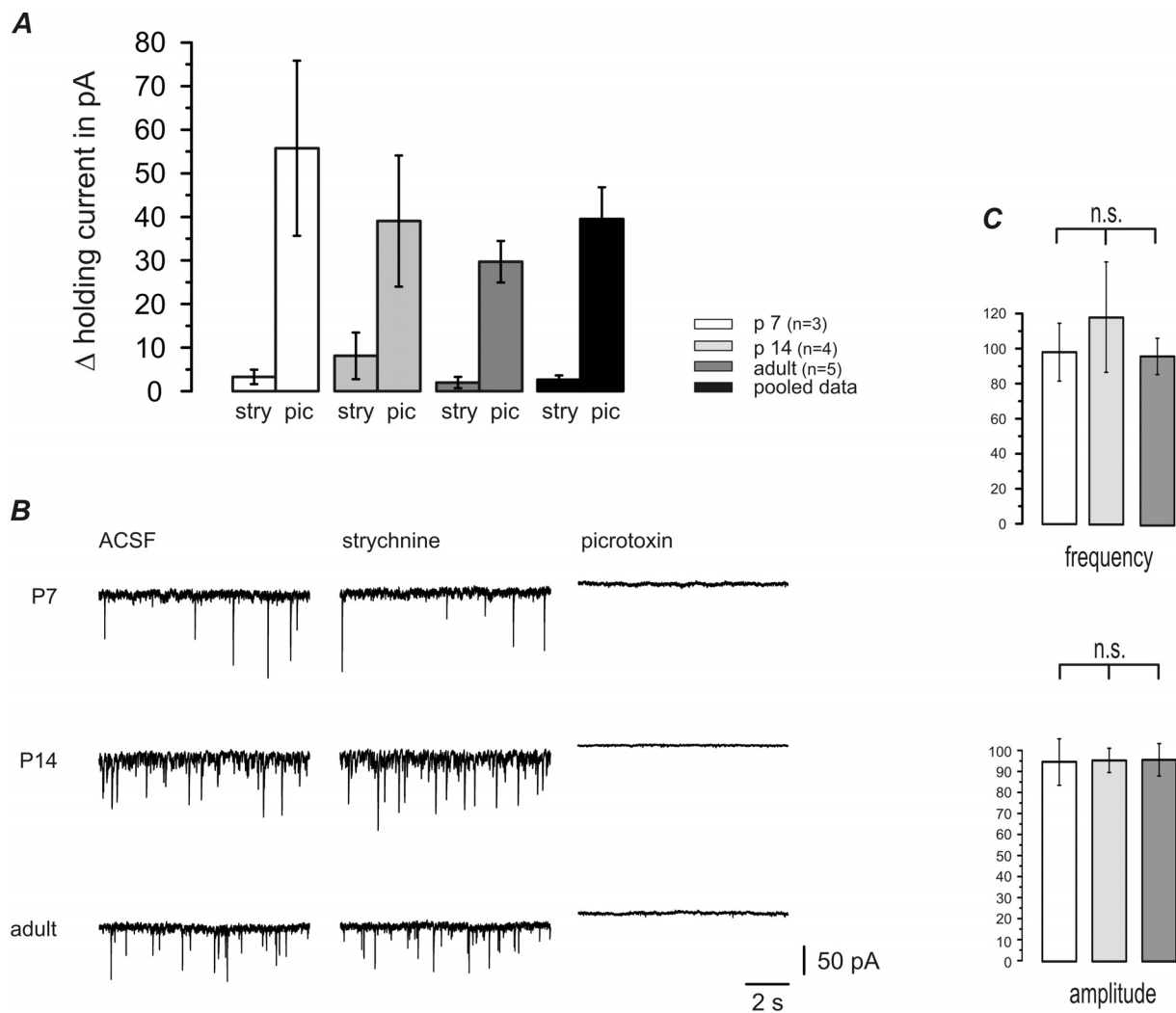
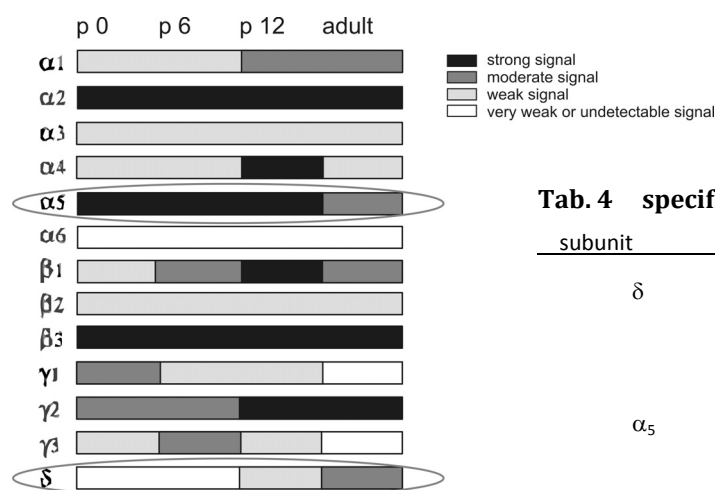


**Fig. 37 Glycine receptors do not contribute to tonic inhibitory currents of dentate gyrus granule cells.** (A) Block of glycine receptors by 1  $\mu$ M strychnine did not affect tonic inhibitory currents of the cells. Block of GABA<sub>A</sub>-receptors currents by application of picrotoxin (100  $\mu$ M + 200 nM gabazine) changes holding current significantly. (B) Note the stable holding current in presence of strychnine and holding current decrease after picrotoxin application. (C) Bar diagrams show normalized sIPSC frequency and amplitude.

It has also been shown that GABA<sub>A</sub>-receptors containing  $\alpha_5$ -subunit are of extrasynaptic localization and that  $\delta$ -subunit containing receptors are preferentially localized close to the synapse (perisynaptic localization) (Wei *et al.*, 2003). These receptors have a high GABA affinity and are therefore ideal to sense the low concentration of ambient GABA in the extracellular space.

As these GABAergic receptor subunits are also expressed in the dentate gyrus throughout postnatal development (Laurie *et al.*, 1992), their functional contribution to tonic inhibitory currents was tested in different postnatal age groups. Therefore, we made use of the specific pharmacology of GABA<sub>A</sub>-receptor subunits (Mody, 2001).



**Tab. 4 specific subunit pharmacology**

subunit	pharmacology
$\delta$	high Zn <sup>2+</sup> sensitivity high affinity for GABA little or no desensitization sensitivity to THIP
$\alpha_5$	low sensitivity to zolpidem and alpidem high sensitivity to L655,708 high sensitivity to Ro 15-4513 & B-CCM

**Fig. 38 Schematic representation of the expression of GABA<sub>A</sub>-receptor subunit mRNAs in rat dentate gyrus.** Modified after (Laurie *et al.*, 1992). Note development of  $\alpha_5$ - and  $\delta$ -subunit, which mediate tonic inhibition.

**Tab. 4 specific subunit pharmacology of GABA<sub>A</sub>-receptor  $\alpha_5$ - and  $\delta$ -subunit.** Modified after (Mody, 2001).

First the magnitude of the **GABA<sub>A</sub>-receptor  $\alpha_5$ -subunit** mediated fraction of tonic inhibitory currents was analyzed during postnatal development of dentate gyrus granule cells. Here, the GABA<sub>A</sub>R  $\alpha_5$ -subunit specific blocker L-655,708 was used. L-655,708 is an imidazo[1,5-*a*]benzodiazepine that is a selective and high affinity ( $K_d \sim 2.5$  nM) ligand for GABA<sub>A</sub>R $\alpha_5$  (Quirk *et al.*, 1996). After recording a stable baseline current, active perfusion with L-655,708 (500 nM) reduced the  $\alpha_5$ -subunit specific tonic current and the holding current was shifted towards more positive values (21 pA  $\pm$  6.3 pA at p 7/8, n = 7; 26.9 pA  $\pm$  4.5 pA at p14/15, n = 7; 12.6 pA  $\pm$  2.2 pA at p>45, n = 7; Fig. 39A,B). Subsequent application of picrotoxin (100  $\mu$ M and 200 nM gabazine) blocked residual phasic and tonic GABAergic currents (50.4 pA  $\pm$  13.4 pA at p 7/8, n = 7; 40 pA  $\pm$  7.5 pA at p14/15, n = 6; 35.7 pA  $\pm$  7.5 pA at p>45, n = 6; Fig. 39A,B). Application of L-655,708 did not affect the amplitude and frequency of spontaneous inhibitory postsynaptic currents, indicating that  $\alpha_5$ -subunits were not present in subsynaptic GABA<sub>A</sub>-receptors mediating sIPSCs (Fig. 39A). Hence, a major fraction of GABA<sub>A</sub>R  $\alpha_5$ -subunits seemed indeed to be located extrasynaptically.

To summarize, tonic inhibitory currents were significantly affected by application of the  $\alpha_5$ -subunit specific blocker and about 50% of the tonic inhibitory currents were mediated by GABA<sub>A</sub>R  $\alpha_5$ -subunits (Fig. 39A).

Second the contribution of **GABA<sub>A</sub>-receptor  $\delta$ -subunit** to tonic inhibitory currents during postnatal development of dentate gyrus granule cells was analyzed. It has been shown, that the GABA<sub>A</sub>-receptor  $\delta$ -subunit is necessary for tonic inhibition in dentate gyrus granule cells (Glykys *et al.*, 2008). In the present study the  $\delta$ -subunit specific agonist THIP hydrochloride (THIP, 1  $\mu$ M) was used (Krogsgaard-Larsen *et al.*, 2004). Application of the agonist indeed shifted the holding current to more negative values compared to baseline conditions, indicating that the GABA<sub>A</sub>-receptor  $\delta$ -subunit is involved in mediating tonic inhibitory currents. These experiments were restricted to cells from the end of the first and the end of the second postnatal week (p7/8, n = 4 and p14/15, n = 4; Fig. 39C).

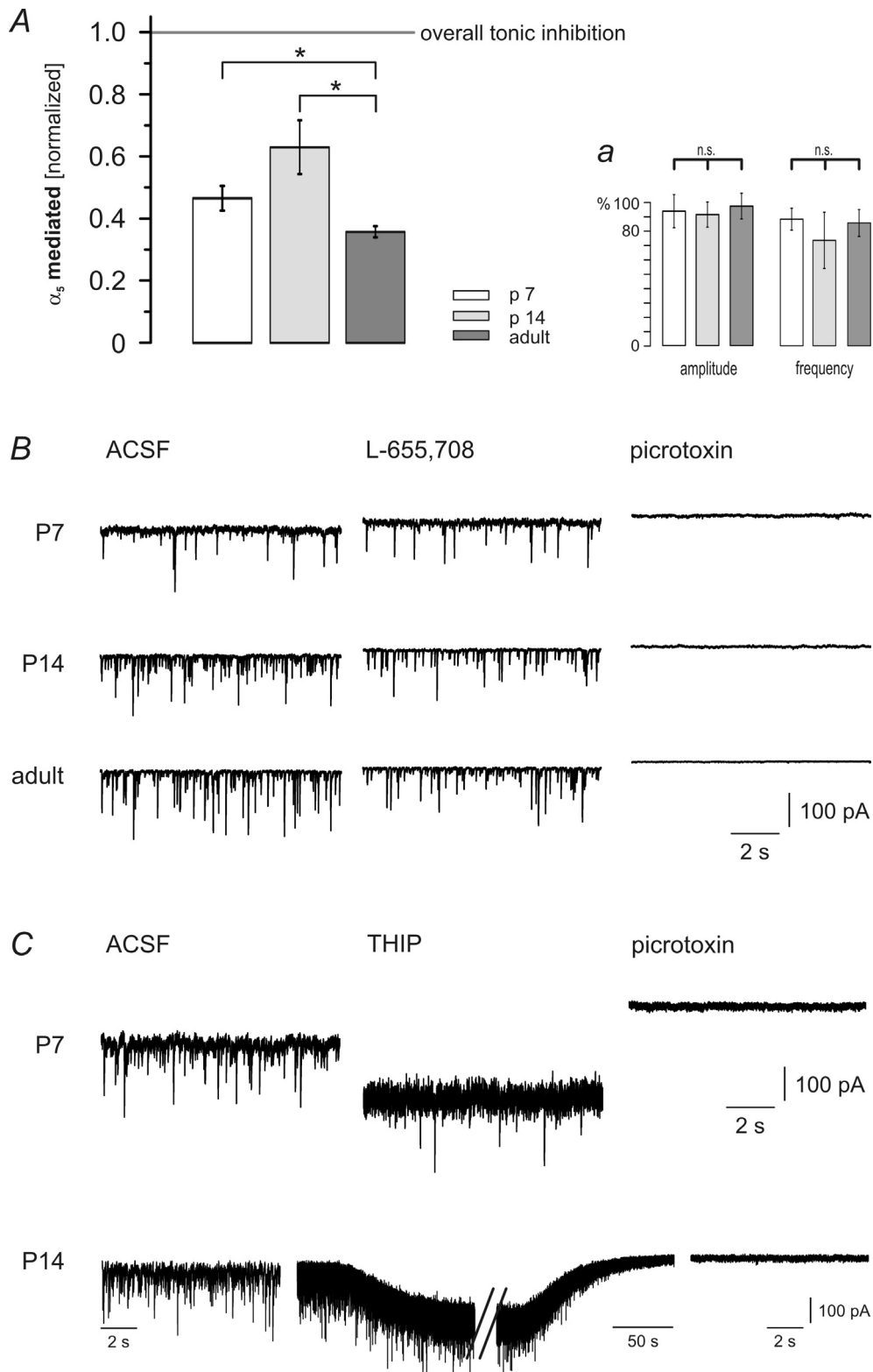


**Fig. 39 Contribution of GABA<sub>A</sub>-receptor  $\alpha_5$ -subunit and  $\delta$ -subunit to tonic inhibitory currents. (A)** Bar diagram shows the shift in holding current after application of  $\alpha_5$ -subunit blocker (500 nM L-655,708) normalized to the holding current shift caused by picrotoxin (100  $\mu$ M + 200 nM gabazine). **(a)** Amplitude and frequency of sIPSCs were not affected **(B)** Raw data traces showing contribution of GABA<sub>A</sub>-R  $\alpha_5$ -subunit to tonic inhibitory currents. **(C)** Raw data traces showing contribution of GABA<sub>A</sub>-R  $\delta$ -subunit to tonic inhibitory currents. The  $\delta$ -subunit specific agonist augmented tonic inhibitory currents. Tonic inhibition was blocked by application of picrotoxin (100  $\mu$ M + 200 nM gabazine).

## Sources of ambient GABA for tonic inhibitory currents of dentate gyrus granule cells

Extrasynaptic  $\alpha_5$ -subunit containing GABA<sub>A</sub>-receptors and  $\delta$ -subunit containing receptors were contributing to the tonic inhibitory currents throughout postnatal development. These receptors have a high GABA affinity and are also in preferred position to be activated by the low concentration of ambient GABA in the extracellular space. Ambient GABA is found in the extracellular space at concentrations from 0.2 to 5  $\mu$ M (Lerma *et al.*, 1986), but its origin is rather unclear. One possible source for GABA in the extracellular space could be the synaptic release of GABA by action potential-dependent mechanisms. Subsequently, the transmitter 'spills over' the synaptic cleft into the extracellular space and diffuses into the extracellular space. It is also feasible that GABA transport, usually acting as a GABA sink, works in inverted way as a GABA source, particular during postnatal development (Demarque *et al.*, 2002; Taylor & Gordon-Weeks, 1991).

### *Synaptically released transmitter GABA acts as a source for the ambient GABA in the extracellular space throughout postnatal development*

In adult dentate gyrus molecular interneurons and CA1 pyramidal cells synaptically released GABA is the main source of ambient GABA in the adult mouse. Immature granule cells were less integrated in the synaptic network of the dentate gyrus and possibly receive less synaptic input (see results part 2). It was therefore interesting to observe how action potential-dependent vesicular release contributes to tonic inhibitory currents, especially during postnatal development.

A stable baseline recording of inhibitory GABAergic currents was achieved in aCSF (+ 30  $\mu$ M APV, 20  $\mu$ M CNQX, 5  $\mu$ M CGP55845), whereby the aCSF was not supplemented with GABA. Action potential-dependent vesicular release was blocked by TTX application (0.5  $\mu$ M). The block of synaptic transmission led to a significant reduction in sIPSC frequency compared to baseline recording of the same cell (reduction to: 67.8 %  $\pm$  13.9 % at p 7/8, n = 6; 24.9 %  $\pm$  8.5 % at p14/15, n = 9; 43.9%  $\pm$  9.9 % at p>45, n = 8; frequency in aCSF was set to 100 %; paired Student's t-test; p < 0.5; Fig. 40C). Astonishingly, sIPSCs amplitude was not significantly affected (Fig. 40C). In addition, perfusion of TTX significantly shifted the holding current of the cell to more positive values (22.5 pA  $\pm$  3.7 pA at p 7/8, n = 10; 25.2 pA  $\pm$  3.3 pA at p14/15, n = 11; 16.0 pA  $\pm$  4.7 pA at p>45, n = 8; p < 0.05, paired Student's t-test; Fig. 40A,B). Residual sIPSCs and remaining tonic inhibitory currents were blocked by addition of picrotoxin (100  $\mu$ M + 200 nM gabazine). Picrotoxin caused an additional significant shift in holding current (15.1 pA  $\pm$  2.3 pA at p 7/8, n = 7; 17.2 pA  $\pm$  1.7 pA at p14/15, n = 6; 18.4 pA  $\pm$  4.0 pA at p>45, n = 6; p < 0.05 paired Student's t-test; Fig. 40A,B). The changes in holding current after TTX and picrotoxin application were detectable in all three age groups investigated during postnatal development of mouse dentate gyrus. The block of action potential-dependent GABA release significantly reduced tonic inhibitory currents by approximately 50%. This reduction was not different among the age groups tested, though the contribution in the adult seemed to be reduced.

To summarize, synaptic spillover acts as a main transmitter source (~50%) for ambient GABA in dentate gyrus extracellular space throughout development. The contribution of synaptically released GABA to tonic inhibition stayed surprisingly stable during postnatal development.

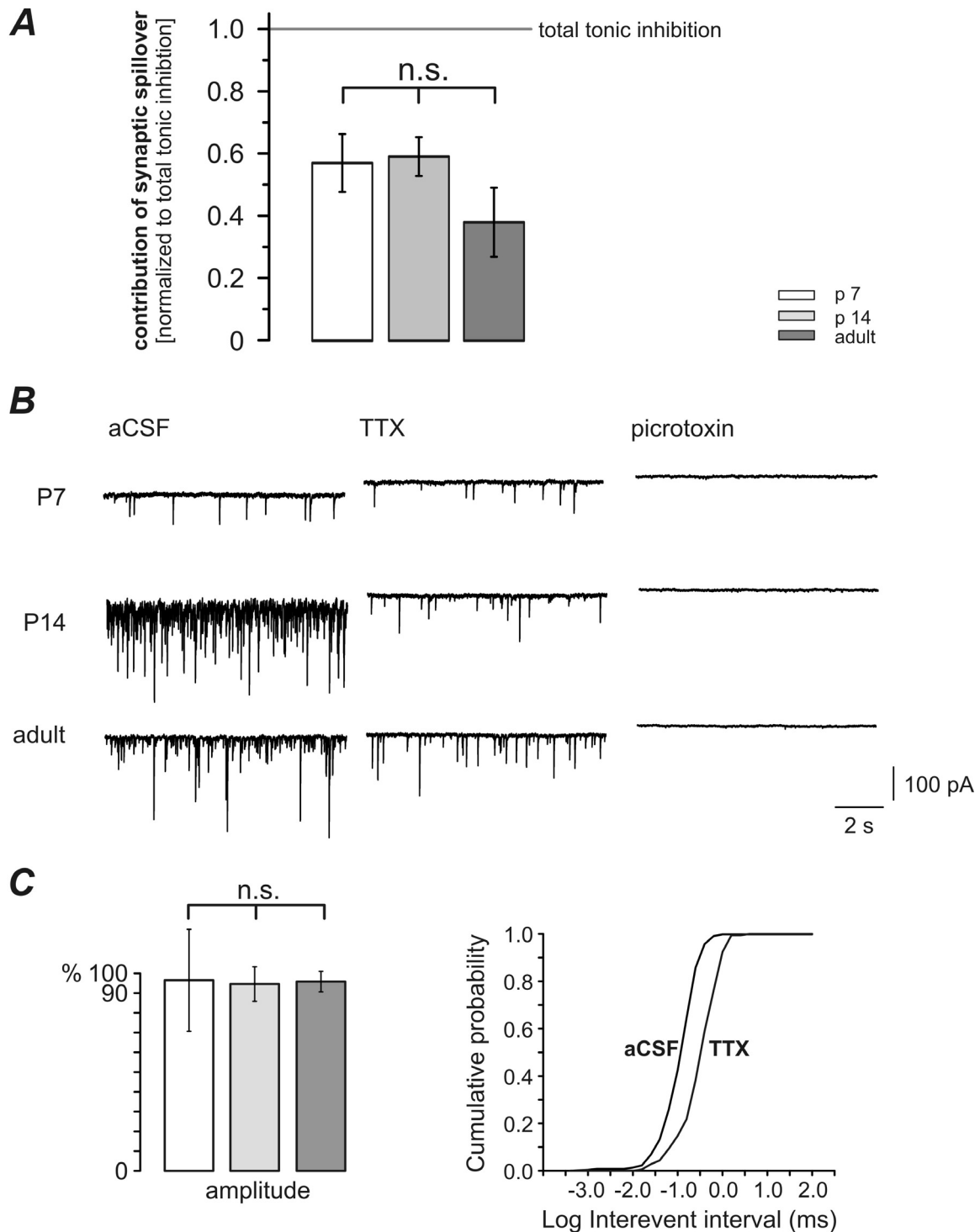


**Fig. 40 Contribution of GABA released by an action potential dependent mechanism to tonic inhibitory currents.** (A) Bar diagram showing the contribution of synaptic spillover to tonic inhibitory currents (shift in holding current after TTX application) normalized to total tonic inhibition (holding current after picrotoxin application subtracted from aCSF baseline values) (B) Raw data traces showing block of action potential dependent transmitter release ( $0.5 \mu\text{M}$  TTX) and subsequent block of GABAergic inhibition ( $100 \mu\text{M}$  picrotoxin +  $200 \text{ nM}$  gabazine). (C) Effect of TTX application on sIPSC amplitude and frequency. Amplitude of sIPSCs obtained in TTX proportional to amplitudes in aCSF. Cumulative probability of the Log scaled interevent intervals of the adult example cell in B. Interevent intervals in TTX were shifted to higher values, sIPSC frequency in TTX decreased.

### *Contribution of GABA transporter GAT-1 to tonic inhibition during postnatal development*

Also during the first two weeks of postnatal development, one identified source of ambient GABA found in the extracellular space was the transmitter release by action potential-dependent mechanism (Glykys & Mody, 2007). By clearing the synaptic cleft, also GABA transport takes part in this mechanism. Subsequent to action-potential transmitter release the largest fraction of released GABA is indeed bound by the transporters. The most abundant GABA transporter, GAT-1 is a high affinity  $\text{Na}^+/\text{Cl}^-$ -dependent membrane translocator of GABA (Chen *et al.*, 2004), usually acting as a GABA sink. For cerebellar granule cells it is shown, that early on in development, tonic inhibition depends on firing of action potentials (Brickley *et al.*, 1996; Kaneda *et al.*, 1995), but in adult granule cells this source of GABA is replaced by action-potential independent mechanism (Rossi *et al.*, 2003; Wall & Usowicz, 1997).

Under certain conditions the GABA uptake system may also function in reverse, then becoming a source of GABA (Richerson & Wu, 2003). This is true for specific experimental conditions, when the transporters driving force is inversed by changed ionic concentrations ( $\text{Na}^+$ , see introduction) or when cells are overly depolarized. In cell culture systems it has been shown, that carrier mediated GABA release activates GABA receptors in hippocampal neurons, indicating that this release of GABA results from the reversal of GABA transport (Gaspary *et al.*, 1998). The reversal of GABA transport has also been discussed for early developmental time points prior to synapse formation (Demarque *et al.*, 2002).

The GABA removal and the possibility of inversed action make the uptake system an effective regulator of GABA concentrations in the extracellular space. Therefore, it was important to analyze the contribution of GABA transport to tonic inhibition, especially during postnatal development.

The influence of neuronal GABA transporter GAT-1 on the ambient GABA concentration in the dentate gyrus extracellular space was investigated by application of the specific GAT-1 blocker NNC-711 (Suzdak *et al.*, 1992) after recording a stable baseline in 'aCSF'. Following NNC-711 perfusion (10  $\mu\text{M}$ ), the holding current of the cell shifted towards more negative values (Fig. 41Aa,B). Subsequent wash in of gabazine (200 nM) and picrotoxin (100  $\mu\text{M}$ ) shifted the cells holding current again to more positive values, exceeding baseline value (Fig. 41Ab). This was true for all developmental age groups investigated (see raw data traces Fig. 41B). Then the shift in holding current obtained after pharmaceuticals application was analyzed. Surprisingly, the contribution of GAT-1 to tonic inhibitory currents stayed the same throughout postnatal development (Fig. 41Ac). GABA transport acted always as a GABA sink and increased tonic inhibitory currents by ~65% ( $p < 0.05$ ; Fig.41Aa,c). Also, the differences in holding current obtained after gabazine and picrotoxin application did not change with ongoing maturation of dentate gyrus.

Under the present experimental conditions GABA transport in dentate gyrus granule cells rather acted as a GABA sink than as a GABA source. Here, action potential mediated release was identified as the GABA source for ambient GABA in the extracellular space.

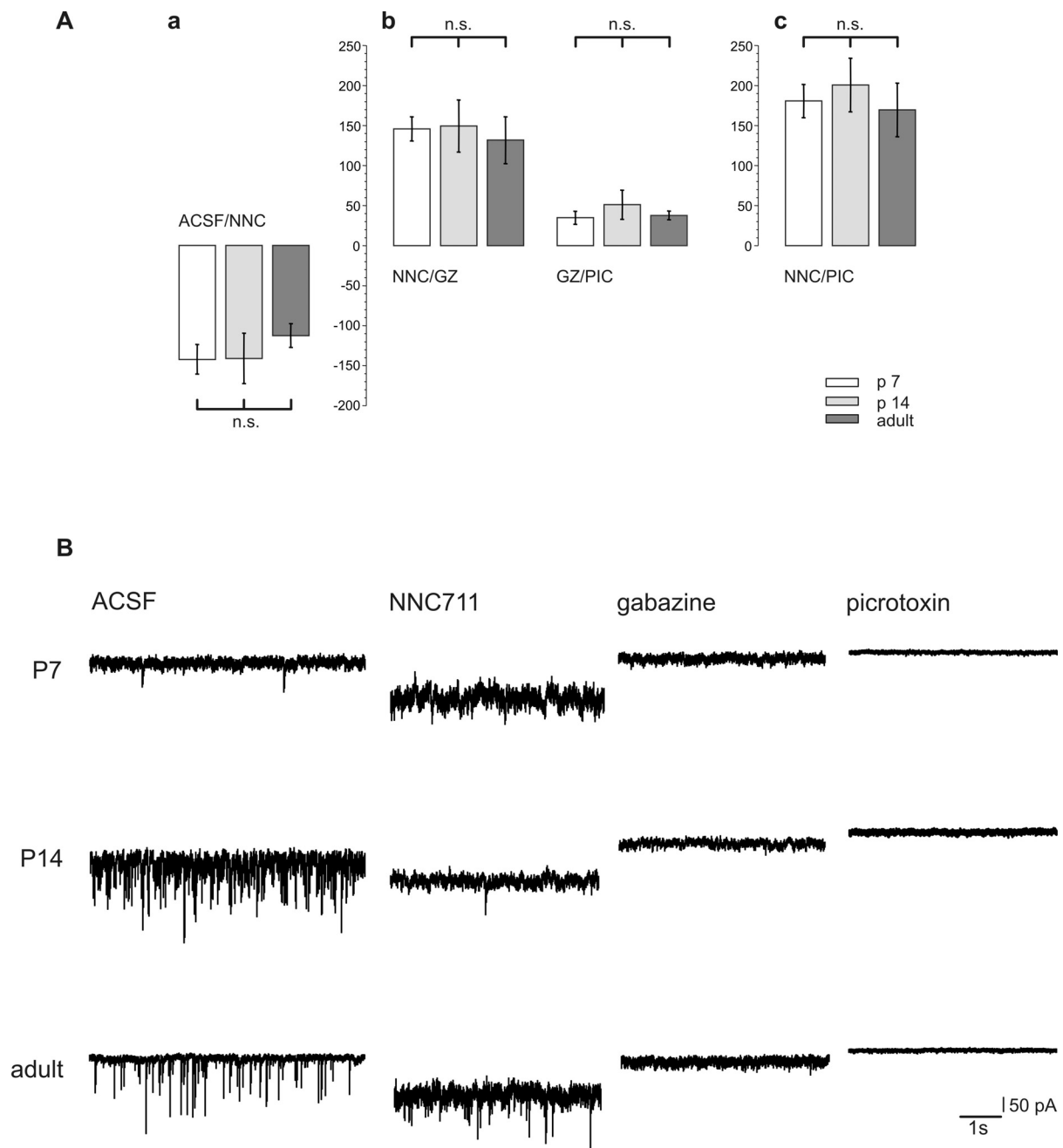


**Fig. 41 GABA transport acted as a GABA sink throughout development. (Aa)** Following NNC-711 perfusion (10  $\mu$ M), the holding current of the cell shifted significantly towards more negative values (the magnitude of the shift was not significantly altered among the investigated age groups). **(Ab)** Subsequent wash in of gabazine (200 nM) and picrotoxin (100  $\mu$ M) shifted the cells holding current again to more positive values, exceeding baseline value (aCSF). This was true for all developmental age groups investigated, see raw data traces in B. **(Ac)** The shift in holding current obtained after pharmaceuticals application stayed the same throughout postnatal development. **(B)** Raw data traces corresponding to bar diagrams in A.

## Tonic inhibitory currents control single cell excitability in dentate gyrus granule cells throughout postnatal development

Tonic inhibitory currents affected intrinsic properties like input resistance of dentate gyrus granule cells and therefore possibly influence the general excitability of the cell. Hence, the effect of tonic inhibitory currents on the excitability of a single granule cell was investigated by analyzing the effect of the GABA<sub>A</sub>- receptor blocker picrotoxin (100 μM) on the action potential parameters.

Action potentials were evoked by stepwise current injections (800 ms duration, 10 pA increment) in current clamp mode (see above) and the effect on the first triggered action potential was analyzed (p7/8 n = 7; p14/15 n = 12; p>45 n = 8). Picrotoxin application (100 μM) showed no significant effect on action potential amplitude (values obtained in picrotoxin normalized to values obtained in aCSF:  $0.85 \pm 0.05$ , p7/8;  $1.09 \pm 0.05$ , p14/15;  $0.83 \pm 0.05$ , p>45), action potential half width ( $0.83 \pm 0.1$ , p7/8;  $0.82 \pm 0.16$ , p14/15;  $1.2 \pm 0.16$ , p>45) and the velocity of action potentials (rate of depolarization:  $0.91 \pm 0.05$ , p7/8;  $1.6 \pm 0.35$ , p14/15;  $0.82 \pm 0.08$ , p>45; rate of repolarization:  $0.87 \pm 0.13$ , p7/8;  $1.2 \pm 0.16$ , p14/15;  $0.75 \pm 0.07$ , p>45). To simplify the diagram means values were displayed in Fig. 42, but also the paired test within absolute values obtained in one single cell showed no significant effects on these action potential parameters (see Tab. 5).

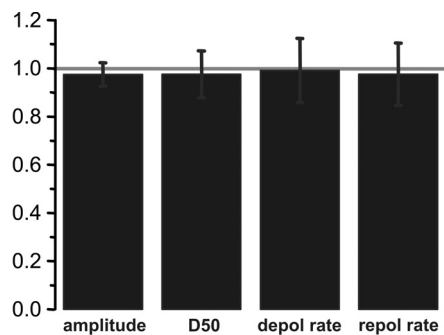


**Fig. 42 Action potential properties not affected by picrotoxin (100 μM).** Amplitude, action potential half width (AP D<sub>50</sub>) and velocity (rate of depolarization and repolarization) were not affected by application of 100 μM picrotoxin. Values obtained after picrotoxin application (bars) were normalized to values obtained in aCSF (line).

**Tab.5: Action potential properties are not affected by picrotoxin (100 μM)**

postnatal period	p 7/8, n = 7	p 14/15, n = 12	p > 45, n = 8
amplitude [mV], aCSF	79.7 ± 4.3	95.5 ± 6.0	131.7 ± 3.0
amplitude [mV], picrotoxin	69.4 ± 4.5	102.8 ± 6.3	110.8 ± 8.6
full width of half maximum [ms], aCSF	2.4 ± 0.3	2.6 ± 0.6	1.2 ± 0.04
full width of half maximum [ms], picrotoxin	2.4 ± 0.3	1.9 ± 0.3	1.4 ± 0.1
rate of depolarisation [V/s], aCSF	42 ± 11	129 ± 30	278 ± 16
rate of depolarisation [V/s], picrotoxin	42 ± 11	152 ± 32	228 ± 24
rate of repolarisation [V/s], aCSF	17 ± 4	49 ± 10	104 ± 6
rate of repolarisation [V/s], picrotoxin	16 ± 4	53 ± 10	85 ± 5

**Tab.5: Action potential properties are not affected by picrotoxin (100 μM).** Values obtained in aCSF and picrotoxin were not significantly different, tested with paired Student's t-test.

However, picrotoxin (100  $\mu$ M) clearly affects action potential threshold of dentate gyrus granule cells at p7/8 ( $-33.8 \pm 1.3$  mV in aCSF and  $-43.5 \pm 2.4$  mV in picrotoxin;  $p < 0.05$ ) and of mature cells aged  $p > 45$  ( $-47.7 \pm 2.4$  mV in aCSF and  $-55.8 \pm 2.2$  mV picrotoxin,  $p < 0.05$ ; Fig 43). Notably, action potential threshold of dentate gyrus granule cells at the end of the second postnatal week was not affected by application of picrotoxin ( $-37.8 \pm 2.6$  mV in aCSF and  $-38.1 \pm 2.1$  mV in picrotoxin, not significant; Fig 43).

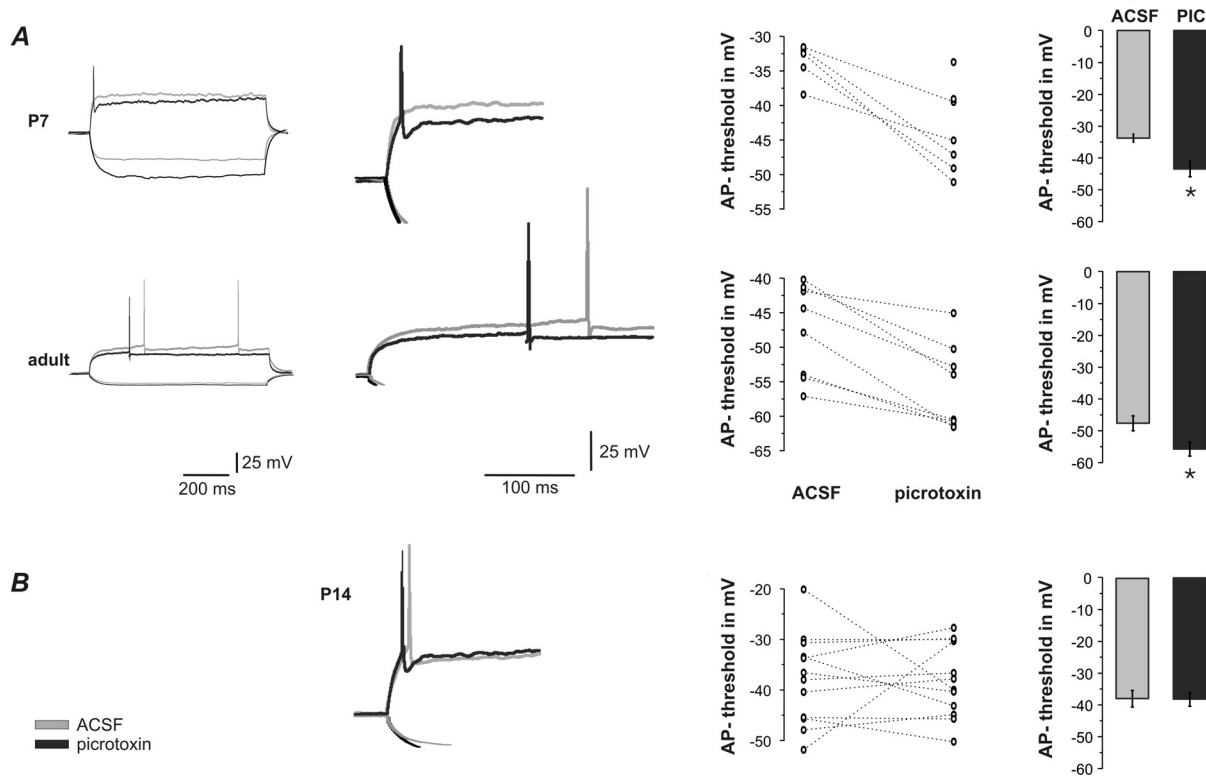


**Fig. 43 Effect of tonic inhibitory currents on action potential threshold.** **A** Picrotoxin application (100  $\mu$ M) lowered action potential threshold of dentate gyrus granule cells at p7/8 and of mature cells ( $p > 45$ ) significantly ( $p < 0.05$ ; paired Student's t-test). **B** Action potential threshold of p14/15 dentate gyrus granule cells were not altered by picrotoxin application.

Example raw data traces of cells at different maturational stages. Dot plot visualizes the decrease of AP-threshold after picrotoxin application, whereby interconnected dots represent the same cell in aCSF and after picrotoxin application. The bar diagram summarizes the mean values.

These results show that tonic inhibitory currents had a clear effect on the excitability of single dentate gyrus granule cells. Blocking tonic inhibitory currents led to a decrease of action potential threshold, which facilitated action potential release.

GABAergic tonic inhibition controlled single cell excitability by increasing action potential threshold and therefore inhibited the dentate gyrus on single cell level both, during early postnatal development and in the adult.

## Tonic inhibitory currents control network excitability in dentate gyrus granule cells throughout postnatal development

As tonic inhibitory currents were shown to control single cell excitability, it was of interest, whether tonic inhibitory currents also set network activity. Therefore, extracellular population spike recordings of dentate gyrus granule cells were performed in the submerged type chamber. Perforant path fibres were electrically stimulated at the hippocampal fissure (Fig. 44B). Control conditions were recorded in aCSF supplemented with GABA (2.5  $\mu$ M), subsequently phasic and tonic GABAergic currents were blocked by application of gabazine (200 nM) and picrotoxin (100  $\mu$ M), respectively.

Under control conditions usually one single population spike was elicited. Following gabazine perfusion the network disinhibited, an additional population spike occurred ( $n = 2.5 \pm 0.8$ , p7/8;  $n = 2.2 \pm 0.2$ , p14/15;  $n = 2.4 \pm 0.1$ , p>45; Fig. 44A,C). However, removal of tonic inhibitory currents by 100  $\mu$ M picrotoxin resulted in a complete disinhibition of the dentate gyrus network, manifested in multiple population spikes ( $n = 8.6 \pm 1.1$ , p7/8;  $n = 4.8 \pm 0.7$ , p14/15;  $n = 5.2 \pm 0.6$ , p>45; Fig. 44A,C). Furthermore, in some slices epileptic discharges could be observed upon picrotoxin application (data not shown). Astonishingly, the waveform of the disinhibited activity was very reproducible as shown in the overlay of consecutive traces (Fig. 44D).

Tonic inhibitory currents do not only reduce single cell excitability, but also had an effect on network excitability of mouse dentate gyrus. Blocking tonic inhibitory currents significantly disinhibited dentate gyrus network throughout postnatal development. Therefore, tonic inhibition was crucial for preventing overexcitation in dentate gyrus network upon incoming stimulation from perforant path.

To summarize, tonic inhibitory currents measured in dentate gyrus granule cells throughout postnatal development and in the adult were exclusively of GABAergic nature, predominantly mediated by  $\alpha_5$ - and  $\delta$ -subunit containing extrasynaptic GABA<sub>A</sub>-receptors. These receptors were previously shown to exhibit a high affinity for the ambient GABA in the extracellular space. The ambient GABA concentration is regulated by synaptic GABA release and the GABA transporter GAT-1, providing the main GABA source and GABA sink, respectively. Therefore, both processes influence tonic inhibitory currents in mouse dentate gyrus granule cells during postnatal development.

GABAergic tonic inhibitory currents had a clear effect on the excitability of single dentate gyrus granule cells. Tonic inhibition reduced excitability of the dentate gyrus on single cell level by increasing action potential threshold of dentate gyrus granule cells. Furthermore, tonic inhibitory currents regulated network excitability by preventing overexcitation of the dentate gyrus. Altogether, GABAergic tonic inhibition provided a powerful tool for regulating the excitation/inhibition balance at the hippocampal gate throughout development.

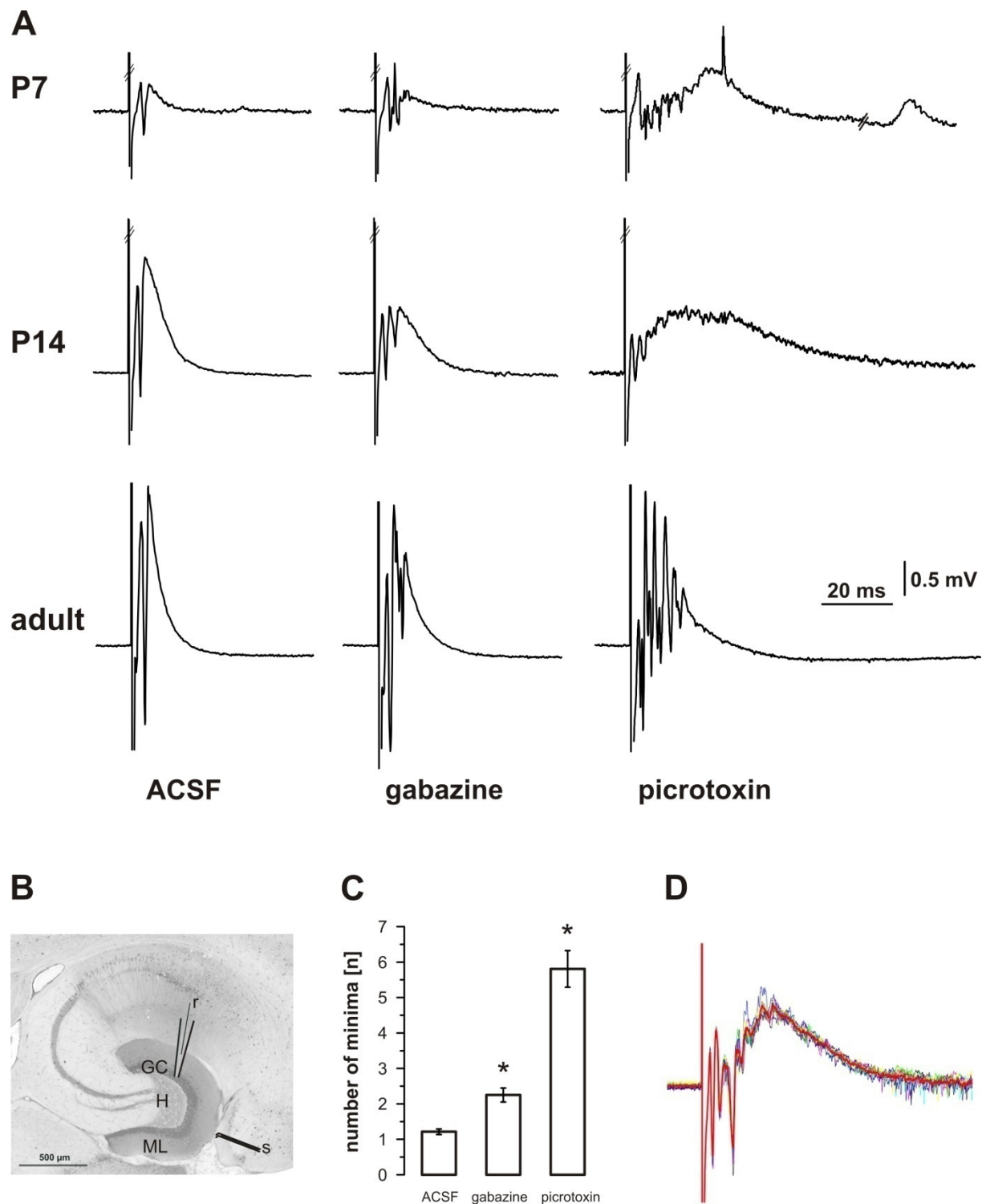


**Fig. 44 Effect of tonic inhibitory currents on network excitability.** **A** Raw data traces of population spikes recorded in dentate gyrus granule cell layer. Blocking GABAergic inhibition by subsequent application of gabazine (200 nM) and picrotoxin (100  $\mu$ M) continuously disinhibited dentate gyrus network throughout development. **B** Population spikes were recorded in granule cell layer (GC) by means of an extracellular recording electrode (r), stimulation electrode (s) was placed at the hippocampal fissure. **C** Disinhibition was quantified by counting the minima of the extracellular currents recorded. The differences obtained in different recording conditions were significant ( $p < 0.05$ ; paired Student's t-test). **D** Note that consecutively recorded traces were of similar appearance, even in picrotoxin (red line represents the mean).

# Discussion

The present thesis describes functional and morphological properties of interneurons and granule cell in developing mouse dentate gyrus, with special focus on inhibitory GABAergic currents. As the dentate gyrus receives strong excitatory cortical inputs via the perforant path, inhibition at the 'hippocampal gate' is important, especially during postnatal development (Hampson and Deadwyler, 1992; Sloviter, 1991).

GABAergic interneurons determine the excitation/inhibition balance through feedback or feedforward inhibition (Freund and Buzsaki, 1996; Somogyi and Klausberger, 2005; Soriano and Frotscher, 1989). They are also crucial for organizing network activity in the dentate gyrus. In the molecular layer of developing mouse dentate gyrus predominantly calretinin-positive cells were found. These GABAergic interneurons showed age-dependent changes of intrinsic and synaptic properties after the first postnatal week. The maturation of molecular layer interneurons went along with faster and larger action potentials, increased repetitive firing, and increased frequency of spontaneous postsynaptic inhibitory currents.

Age-dependent changes of intrinsic and synaptic properties were also found in developing dentate gyrus granule cells. Similar to interneurons, mature dentate gyrus granule cells exhibited faster and larger action potentials and showed an increased frequency of spontaneous postsynaptic inhibitory currents, though the integration of granule cells into the inhibitory synaptic network of dentate gyrus takes place after the second postnatal week.

The inhibitory control of network activity in the dentate gyrus is not only mediated by 'phasic' synaptic inhibitory events but also by 'tonic inhibition'. This long-lasting increase in chloride conductance (Nusser & Mody, 2002; Semyanov *et al.*, 2004) generates ~75% of the total inhibitory conductance received by hippocampal neurons (Mody & Pearce, 2004). Therefore it was important to ask how tonic inhibitory currents are mediated and whether they contribute to the excitability of the dentate gyrus granule cells, especially during postnatal development. GABAergic tonic inhibitory currents in granule cells were mediated by  $\alpha_5$ - and  $\delta$ -subunit containing extrasynaptic GABA<sub>A</sub>-receptors activated through ambient GABA in the extracellular space. The ambient GABA in the extracellular space is delivered by synaptic GABA release and regulated through GABA uptake by the GABA transporter-1.

Tonic inhibition influenced the excitation/inhibition balance of dentate gyrus throughout postnatal development. At the cellular level, this reduced excitability of the dentate gyrus granule cells by increasing the action potential threshold. Furthermore, tonic inhibitory currents regulated network excitability by preventing overexcitation of the dentate gyrus.

## Functional maturation of interneurons in molecular layer of dentate gyrus

The first part of the present thesis describes functional and morphological properties of developing interneurons in the molecular layer of the mouse dentate gyrus. Age-dependent changes of several intrinsic and synaptic properties have been found, most notably a faster waveform of action potentials, increased repetitive firing in older cells and a strong increase in synaptic input after the first postnatal week. This rather sharp transition coincides with the known maturation of synaptic inhibition in the hippocampus. After the first postnatal week, inhibitory potentials become hyperpolarizing (Rivera *et al.*, 1999). Within the first two postnatal weeks, many interneurons migrate towards their final position within the dentate gyrus (Dupuy-Davies & Houser, 1999; Morozov *et al.*, 2006). The development of typical fast action potential discharges and the increased synaptic integration may be important for the development of mature network functions. Heterogeneity of interneurons in this region was less pronounced than expected, both with respect to physiological parameters as well as to immunohistochemical stainings, which revealed that the majority of cells in the molecular layer express calretinin and are mainly negative for other typical marker proteins.

Action potential properties of interneurons depend on the expression pattern and density of voltage-gated ion channels. For example, fast spiking interneurons in the dentate express Kv3.1 and Kv3.2 (Martina *et al.*, 1998), which facilitate rapid repolarization and subsequent de-inactivation of sodium channels. Several neuronal subtypes show a functional maturation of action potentials similar to our present findings: depolarization and repolarization become faster, amplitude is enhanced and repetitive firing occurs (Zhang, 2004; Zhou & Hablitz, 1996). Interneurons in the dentate molecular layer follow the same scheme, reaching a typical mature discharge pattern within the second postnatal week. Trains of fast repetitive action potentials do occur in interneurons during certain high-frequency network oscillations, e.g. gamma- (Whittington & Traub, 2003), theta- (Buzsaki, 2002) or ripple-oscillations (Penttonen *et al.*, 1997; Ylinen *et al.*, 1995). Indeed, fast spiking of interneurons may be critical for the temporal organization of these network activity patterns. Therefore, the observed maturation of firing may mark the begin of adult network behaviour in the dentate gyrus, whereas at earlier stages other coordinated patterns of activity predominate, esp. early giant network discharges (Ben-Ari *et al.*, 1989; Cherubini *et al.*, 1991; Khazipov *et al.*, 1997).

Coinciding with the maturation of intrinsic discharge properties, an increase in synaptic activity was found, mainly expressed as an enhanced frequency of spontaneous IPSCs. Thus, at the time when interneurons reach their final position, they are increasingly integrated into the synaptic network of the dentate, which is characterized by particularly strong feedback inhibitory circuits (Hampson & Deadwyler, 1992; Sloviter, 1991). Surprisingly, spontaneous excitatory currents were not observed. In contrast, it was possible to elicit glutamatergic currents by electrical stimulation consistent with recent results (Chittajallu *et al.*, 2007). In most cells superimposed burst-like synaptic currents were observed, even at the lowest stimulation strength yielding regular responses, which is probably due to the network disinhibition in the presence of gabazine. The absence of spontaneous excitatory synaptic activity may be, at least in part, a consequence of the slicing procedure which is likely to disrupt many connections between neuronal somata in the entorhinal cortex and their target cells in the molecular layer. The data shows that excitatory synapses are present in molecular layer interneurons during the first two postnatal weeks, while spontaneous synaptic activity in slices from this region is largely restricted to GABAergic inhibitory currents.

Heterogeneity of interneurons in the hippocampal formation has become a major issue in recent years. It has been shown that different types of interneurons show distinct afferent and efferent connections, which are frequently targeted to specific postsynaptic neurons or subregions (e.g. distal dendrites) of their postsynaptic cells (Freund & Buzsaki, 1996; Somogyi & Klausberger, 2005). Moreover, the activation of interneurons during different states of the network, e.g. different types of oscillations, varies between subtypes (Somogyi & Klausberger, 2005). Besides their anatomy, interneurons can be subtyped based on the expression of certain markers, mostly calcium binding proteins and neuromodulatory peptides. Sections from the respective age-groups were stained for PV (Nitsch *et al.*, 1990), CR (Liu *et al.*, 1996a), CB (Celio, 1990) and SS (Naus *et al.*, 1988). The data shows that CR-positive multipolar cells form the majority of neurons in the middle position of the molecular layer at all ages studied. Recent work has also revealed interneurons expressing cholecystinin (CCK) in the dentate formation. However, these neurons migrate early towards the hilus and are largely absent from the molecular layer after the fourth day of postnatal development (Morozov *et al.*, 2006; Morozov & Freund, 2003).

In conclusion, the present data indicates that most of the developing interneurons in the middle portion of the molecular layer express calretinin. These findings point towards a rather low heterogeneity of the immunohistochemical profile of interneurons within the maturing molecular layer. The expression pattern of marker proteins changes through the first two postnatal weeks, probably due to both, changes in protein expression and cell migration. During the same time window, interneurons become integrated into synaptic networks and develop mature firing patterns.

## Functional maturation of dentate gyrus granule cells

During the first postnatal weeks, dentate gyrus granule cells developed in parallel to stratum moleculare interneurons. With ongoing development, action potentials became larger and faster and the inhibitory synaptic input on dentate gyrus granule cells increased. The discharge behavior of granule cells was shown to reach mature patterns after the second postnatal week and therefore matures later than interneurons. This consecutive maturation of interneurons and granule cells is in accordance to their successive generation (Altman & Bayer, 1990a; Altman & Bayer, 1990b). As the dentate gyrus is one of the regions in the mammalian brain where adult neurogenesis takes place, granule cells are of different developmental stages. However, the recorded granule cells from the outer granule cell layer should have already reached their definite position (Shapiro & Ribak, 2005) and they indeed showed the expected morphological maturation with ongoing postnatal development. Dentate gyrus granule cells exhibit their typical morphology already in immature tissue; though during the first postnatal weeks extensive dendritic growth takes place. Correspondingly, the input resistance decreased and membrane capacitance of dentate gyrus granule cells increased with ongoing development (Liu *et al.*, 2000; Liu *et al.*, 1996b). The heterogeneity of granule cells was less pronounced than expected, both with respect to their morphological shape and electrophysiological parameters.

The discharge behavior of dentate gyrus granule cells and of molecular layer interneurons showed a similar development. Mature granule cell action potentials became faster and larger and in contrast to interneuron action potentials exhibited a lower threshold with ongoing development. This finding

is in line with previously published data (Liu *et al.*, 2000; Liu *et al.*, 1996b). Action potential amplitudes of immature granule cells are comparable to action potential amplitudes of immature interneurons; while mature granule cells action potentials exhibited much bigger amplitudes than action potentials of mature stratum molecular interneurons. In general, principal cells show slower action potential waveforms than fast spiking interneurons, however this difference has not been found in the present study, which is probably due to the different recording conditions. Recordings of dentate gyrus granule cells were performed at body temperature, while interneurons were recorded at room temperature. Therefore, all biochemical and biophysical reactions were probably faster in the granule cells.

Similar, mature dentate gyrus granule cells showed an increased frequency of spontaneous postsynaptic inhibitory currents, which is indicating the ongoing integration of granule cells in the inhibitory synaptic network of dentate gyrus. GABA<sub>A</sub>-receptor-mediated events are present at all postnatal ages and their frequency increases during development in granule cells of dentate gyrus. GABAergic sIPSCs of immature granule cells display slower kinetics, but similar amplitudes compared with the adult (Hollrigel *et al.*, 1998). It has been shown, that there are early functional GABAergic synapses on immature granule cells (Hollrigel *et al.*, 1998). It may be of interest that both, discharge behavior and their integration in the inhibitory network of molecular layer interneurons, is completed during the second postnatal week. Simultaneously, dentate gyrus granule cells are integrated in the inhibitory network, though this was prior to full maturation of their action potential properties. It is likely that developmental processes of both, molecular interneurons and dentate gyrus granule cells, share similar mechanisms, including mutual interactions between developing interneurons and principal (granule) cells.

## Tonic inhibitory currents in dentate gyrus granule cells during postnatal development

Tonic inhibitory currents were present in dentate gyrus granule cells throughout postnatal development. In the adult, the detectable amount of tonic inhibition tended to smaller values than in the immature dentate gyrus. Dentate gyrus granule cells were inhibited by tonic currents before granule cells were integrated in the inhibitory synaptic network. In fact, synaptic GABA<sub>A</sub>-receptor subunits show augmented expression during the second postnatal week when synaptic receptor clustering takes place (Laurie *et al.*, 1992; Owens *et al.*, 1999).

Tonic inhibition is mediated by GABA<sub>A</sub>-receptors, which are rather homogeneously distributed over the cell membrane and do not colocalize with the synaptic GABA<sub>A</sub>-receptor anchoring protein gephyrin (Sassoe-Pognetto *et al.*, 2000). These high affinity extra- and perisynaptic receptors sense the low ambient GABA concentration in the extracellular space (Saxena & MacDonald, 1994; Wei *et al.*, 2003) and thereby mediate tonic inhibitory currents (Nusser *et al.*, 1998). In adult granule cells GABA<sub>A</sub>-receptor containing  $\alpha_5$ - and  $\delta$ -subunits are reported to mediate tonic inhibitory currents (Glykys *et al.*, 2008). These GABA receptor subunits are also expressed in the dentate gyrus throughout postnatal development (Laurie *et al.*, 1992). In this study, the  $\alpha_5$ -subunit was clearly shown to mediate about 50% of the tonic inhibition in granule cells - not only in the adult, but

throughout postnatal development. Here, the  $\delta$ -subunit was also necessary for tonic inhibition in dentate gyrus granule cells during postnatal development, which is similar to previous reports for the adult (Glykys *et al.*, 2008). The reduction of tonic inhibitory currents upon block of  $\alpha_5$ - and  $\delta$ -subunits, respectively, was not associated with changes in inhibitory postsynaptic currents, confirming the extrasynaptic localization of these receptors.

Recently, it has been discussed whether glycine receptors are involved in tonic inhibition in the dentate gyrus. There has been morphological and electrophysiological evidence for glycine receptor mediated inhibition in dentate gyrus (Danglot *et al.*, 2004; Ito & Cherubini, 1991). One has to take into account that in these studies glycine receptors were artificially stimulated by a high concentration of the transmitter (Chattipakorn & McMahon, 2003; Song *et al.*, 2006). However, in the present thesis the spontaneous mediated action of the glycine receptors was investigated. Here, glycinergic inhibition did not contribute to inhibitory currents in dentate gyrus; the block of glycine receptors did not affect phasic nor tonic inhibition.

GABAergic tonic inhibitory currents are mediated by the ambient transmitter in the extracellular space (Farrant & Nusser, 2005; Mody, 2001). Ambient GABA is found at micromolar concentrations in the extracellular space (Lerma *et al.*, 1986), but the source of the ambient GABA is rather undetermined. Synaptic GABA release by action potential-dependent mechanisms is discussed as one possible GABA source (Brickley *et al.*, 1996; Glykys & Mody, 2007; Kaneda *et al.*, 1995), also action-potential independent mechanisms are found, for example in cerebellar granule cells (Rossi *et al.*, 2003; Wall & Usowicz, 1997). The experiments showed that, synaptic spillover acts as a main source for ambient GABA in the extracellular space throughout postnatal development, although immature granule cells were less integrated in the synaptic network of dentate gyrus.

As GABA diffused in the extracellular space, the ambient GABA concentration is depending on the extracellular space volume fraction, which is diminished with age (Lehmenkuhler *et al.*, 1993), and the presence of a buffering system (Nicholson & Sykova, 1998; Vargova & Sykova, 2008). The most important component of the GABA buffering system is GABA transport. Removal of GABA and the possibility of inversed action (Gaspary *et al.*, 1998; Richerson & Wu, 2003) make the uptake system an effective regulator of GABA concentrations in the extracellular space. The present data shows, that in dentate gyrus granule cells, GABA transport provides a GABA sink and therefore regulates the ambient GABA concentration in the extracellular space throughout development.

Tonic inhibitory currents mediated by the ambient GABA in the extracellular space cause a long-lasting increase in chloride conductance in dentate gyrus granule cells (Nusser & Mody, 2002; Semyanov *et al.*, 2004). This continuous tonic GABAergic conductance controls the gain of the neuronal input-output-relation (Cavelier *et al.*, 2005; Chadderton *et al.*, 2004; Mitchell & Silver, 2003; Semyanov *et al.*, 2004). Here, tonic inhibitory currents reduced general excitability of the dentate gyrus at single cell level by increasing the action potential threshold of granule cells. This was observed for immature postnatal granule cells and in the adult. However, in granule cells at the end of the second postnatal week tonic inhibitory currents (though present) seemed to have no effect on the discharge behavior.

Further, in dentate gyrus adult neurogenesis had to be taken into account (Soriano *et al.*, 1989a; Soriano *et al.*, 1989b). Therefore, only cells with the adequate maturational stage (passive intrinsic parameters) were included in the analysis.

At the network level, tonic inhibition influenced network excitability throughout postnatal development. Tonic inhibitory currents prevented overexcitation of the dentate gyrus upon stimulation from perforant path. Blocking tonic GABAergic currents led to disinhibition of the dentate gyrus network, peaking in also observed epileptic discharges. This finding is in line with studies where the specific block of  $\alpha_5$ -subunit containing GABA<sub>A</sub>-receptors leads to hippocampal network hyperactivity (Glykys & Mody, 2006). Further, the localization of both, the  $\alpha_5$ -subunit and the  $\delta$ -subunits, are altered in a mouse model of epilepsy (Peng *et al.*, 2004; Zhang *et al.*, 2007). Already the fact that the reduction of tonic inhibitory currents by blocking the respective subunits was not associated with changes in inhibitory postsynaptic currents pointed towards a possible role of tonic GABA<sub>A</sub>-receptors in network activity. The inhibitory control of mouse dentate gyrus by tonic GABAergic currents is of particular importance as this region receives strong excitatory cortical inputs via the perforant path (Hampson and Deadwyler, 1992; Sloviter, 1991). During early postnatal development, where the dentate gyrus network is prone to seizures (Holmes *et al.*, 2002), the regulation of the excitation/inhibition balance at the hippocampal gate is necessary.

### Technical issues related to the recordings and measurements in this study

In general whole cell patch-clamp measurements and the recording of GABAergic currents is a rather easy task, if the appropriate recording conditions are chosen.

The constraints and limitations of whole cell patch-clamp measurements have already been discussed in the methods section. Here, I would just like to stress the consequences of diluting the cytosol during whole cell recordings. This method produces recording conditions, which can be easily controlled, but the configuration is still artificial. In hippocampal development neuronal intracellular chloride concentration decreases and the postsynaptic GABA responses change from depolarizing to hyperpolarizing (Ben-Ari, 2002; Leinekugel *et al.*, 1999). Therefore, an artificially set chloride concentration, where the intracellular chloride concentration equals the extracellular chloride concentration ('isochloride'), will never represent the natural situation. Especially, the result that GABAergic tonic currents are inhibitory throughout development has to be taken with care. Instead of whole cell patch clamp experiments, studies would have been more appropriate where the intracellular milieu is not changed. Therefore, in dentate gyrus granule cells, gramicidin perforated patch recordings have been tried out, unfortunately without any success. Hence, another method was chosen: the extracellular recordings in dentate gyrus granule cells. Here, the intracellular milieu of the cells was unaffected and the inhibitory nature of GABAergic tonic currents throughout postnatal development could be confirmed on network level.

It should be kept in mind, that the cellular network of the slice is an artificial preparation. The hippocampal slice is just a small part of the brain and many fiber connections to the hippocampal formation are harmed during the cutting procedure (see discussion about the absence of spontaneous excitatory synaptic activity in molecular layer interneurons). The level of tissue

oxygenation is important for a lively preparation exhibiting 'normal' cellular reactions and further, hypoxia shrinks the extracellular space (Nicholson & Sykova, 1998), which may lead to an increased extracellular GABA concentration. Therefore, the perfusion rate of the bath solution was kept at a high level, which in turn may wash out the ambient transmitter in the extracellular space, leading to a reduction of GABAergic currents. Particularly in the third part of the study, where extracellular GABA was analyzed as a mediator of tonic inhibitory currents, recording conditions were standardized by adding a defined transmitter amount. The extracellular solution was supplemented with micromolar levels of GABA, which is in the physiological range (Lerma *et al.*, 1986). Similar, the temperature conditions were brought to a more physiological level. At room temperature, the efficiency of amino acid transport is decreased (Asztely *et al.*, 1997; Mitchell & Silver, 2000). As GABA transport regulates the ambient GABA concentration, a decreased turnover could influence the magnitude of tonic inhibitory currents.

In addition to the artificial *in vitro* recording and the different temperature conditions, the drugs used in this study may have side effects. As examples side effects of two frequently used drugs are mentioned below:

The **neurobiotin** tracer used in the intracellular solution for staining electrophysiologically characterized neurons is shown to prolong the full width of half maximum of action potential significantly in rat cortical neurons. The passive intrinsic properties were not affected (Schlosser *et al.*, 1998). In the present study only cells with the same intracellular conditions were compared and therefore the results were valid. However, one has to be careful when comparing results of different studies with or without such drugs in the solution.

Another drug used in the present study is **CNQX**, which in first place blocks AMPA-receptor mediated events and thereby reduces cellular excitability of the recorded neurons. However, the frequency of inhibitory events increased in recorded interneurons of the present study. This increase in IPSC frequency has also been reported for hippocampal CA1 interneurons and CA3 pyramidal neurons during early postnatal development (Maccaferri & Dingledine, 2002; McBain *et al.*, 1992). This effect has to be taken into consideration when comparing IPSC frequencies of immature and mature neurons. As CNQX seems to affect specifically the immature inhibitory transmission, the IPSC frequency in these neurons would probably be even lower if it was investigated without CNQX interference. Therefore, the maturation of sIPSC frequency and the integration accompanying integration in the synaptic network of dentate gyrus would become more significant.

For possible side effects of the other drugs please see the appendix and also the results section (e.g. for picrotoxin).

In all conscience, technical limitations and constraints were taken into account during designing the experiments, data acquisition and analysis.

## Outlook

During the first two postnatal weeks, the discharge behavior and the synaptic properties of molecular layer interneurons and dentate gyrus granule cells mature. The dentate gyrus synaptic network establishes and both, molecular layer interneurons and dentate gyrus granule cells integrate into the network. During this period of time, inhibition in the dentate gyrus is mediated through the maturing synaptic inhibitory system and largely by tonic inhibitory currents.

The inhibitory control of the 'hippocampal gate' is of particular importance during postnatal development, where the dentate gyrus network is prone to seizures (Holmes *et al.*, 2002). Therefore, further investigations of tonic GABAergic currents and their effects at network level would be of interest, as they are responsible for generating a big part of the total inhibitory conductance in the hippocampus (Mody & Pearce, 2004). Adult mice deficient of  $\alpha_5$ - and  $\delta$ - GABA<sub>A</sub>-receptor subunits display spontaneous gamma oscillations *in vitro* (Glykys *et al.*, 2008) Here it would be interesting to see, whether blocking  $\alpha_5$ -subunits by the specific antagonist L655,708 elicits gamma oscillations also during early postnatal development. Subsequently applied picrotoxin may then evoke epileptic discharges by further altering dentate gyrus network oscillation. This would strengthen the role of tonic inhibition as the main regulator of excitation/inhibition balance at the hippocampal gate during postnatal development by calming network activity.

Tonic inhibition is also related to other processes. For example, the tonically activated  $\delta$ -subunit is highly sensitive to stress related neurosteroids (Stell *et al.*, 2003) and to ethanol (Mody *et al.*, 2007). Mouse knockout studies revealed a participation of tonic inhibition in memory related processes (Collinson *et al.*, 2002). In this context it would be feasible to perform hippocampal LTP experiments before and after blocking tonic inhibitory currents in mouse hippocampal slice cultures. Therefore, tonic inhibition could be blocked either unspecifically by washing in the different GABA<sub>A</sub>-receptor blockers or in a more specific manner by directly knocking down GABA<sub>A</sub>-receptors in dentate gyrus granule cells by means of a viral vector system.

# References

1. Acsady L, Kamondi A, Sik A, Freund T, & Buzsaki G (1998). GABAergic cells are the major postsynaptic targets of mossy fibers in the rat hippocampus. *J Neurosci* **18**, 3386-3403.
2. Alcantara S, Ferrer I, & Soriano E (1993). Postnatal development of parvalbumin and calbindin D28K immunoreactivities in the cerebral cortex of the rat. *Anat Embryol (Berl)* **188**, 63-73.
3. Altman J & Bayer SA (1990a). Migration and distribution of two populations of hippocampal granule cell precursors during the perinatal and postnatal periods. *J Comp Neurol* **301**, 365-381.
4. Altman J & Bayer SA (1990b). Mosaic organization of the hippocampal neuroepithelium and the multiple germinal sources of dentate granule cells. *J Comp Neurol* **301**, 325-342.
5. Anderson P, Bliss TV, & Skrede KK (1971). Lamellar organization of hippocampal pathways. *Exp Brain Res* **13**, 222-238.
6. Asztely F, Erdemli G, & Kullmann DM (1997). Extrasynaptic glutamate spillover in the hippocampus: dependence on temperature and the role of active glutamate uptake. *Neuron* **18**, 281-293.
7. Atack JR, Bayley PJ, Fletcher SR, McKernan RM, Wafford KA, & Dawson GR (2006). The proconvulsant effects of the GABAA alpha5 subtype-selective compound RY-080 may not be alpha5-mediated. *Eur J Pharmacol* **548**, 77-82.
8. Attwell D, Barbour B, & Szatkowski M (1993). Nonvesicular release of neurotransmitter. *Neuron* **11**, 401-407.
9. Ben-Ari Y (2002). Excitatory actions of gaba during development: the nature of the nurture. *Nat Rev Neurosci* **3**, 728-739.
10. Ben-Ari Y, Cherubini E, Corradetti R, & Gaiarsa JL (1989). Giant synaptic potentials in immature rat CA3 hippocampal neurones. *J Physiol* **416**, 303-325.
11. Ben-Ari Y, Gaiarsa JL, Tyzio R, & Khazipov R (2007). GABA: a pioneer transmitter that excites immature neurons and generates primitive oscillations. *Physiol Rev* **87**, 1215-1284.
12. Ben-Ari Y, Khalilov I, Represa A, & Gozlan H (2004). Interneurons set the tune of developing networks. *Trends Neurosci* **27**, 422-427.
13. Ben-Ari Y, Tseeb V, Ragozzino D, Khazipov R, & Gaiarsa JL (1994). gamma-Aminobutyric acid (GABA): a fast excitatory transmitter which may regulate the development of hippocampal neurones in early postnatal life. *Prog Brain Res* **102**, 261-273.
14. Brickley SG, Cull-Candy SG, & Farrant M (1996). Development of a tonic form of synaptic inhibition in rat cerebellar granule cells resulting from persistent activation of GABAA receptors. *J Physiol* **497 ( Pt 3)**, 753-759.

15. Buzsaki G (2002). Theta oscillations in the hippocampus. *Neuron* **33**, 325-340.
16. Caraiscos VB, Elliott EM, You-Ten KE, Cheng VY, Belelli D, Newell JG, Jackson MF, Lambert JJ, Rosahl TW, Wafford KA, MacDonald JF, & Orser BA (2004). Tonic inhibition in mouse hippocampal CA1 pyramidal neurons is mediated by alpha5 subunit-containing gamma-aminobutyric acid type A receptors. *Proc Natl Acad Sci U S A* **101**, 3662-3667.
17. Cavelier P, Hamann M, Rossi D, Mobbs P, & Attwell D (2005). Tonic excitation and inhibition of neurons: ambient transmitter sources and computational consequences. *Prog Biophys Mol Biol* **87**, 3-16.
18. Celio MR (1990). Calbindin D-28k and parvalbumin in the rat nervous system. *Neuroscience* **35**, 375-475.
19. Ceranik K, Bender R, Geiger JR, Monyer H, Jonas P, Frotscher M, & Lubke J (1997). A novel type of GABAergic interneuron connecting the input and the output regions of the hippocampus. *J Neurosci* **17**, 5380-5394.
20. Chadderton P, Margrie TW, & Hausser M (2004). Integration of quanta in cerebellar granule cells during sensory processing. *Nature* **428**, 856-860.
21. Chattipakorn SC & McMahon LL (2003). Strychnine-sensitive glycine receptors depress hyperexcitability in rat dentate gyrus. *J Neurophysiol* **89**, 1339-1342.
22. Chen L, Wang H, Vicini S, & Olsen RW (2000). The gamma-aminobutyric acid type A (GABAA) receptor-associated protein (GABARAP) promotes GABAA receptor clustering and modulates the channel kinetics. *Proc Natl Acad Sci U S A* **97**, 11557-11562.
23. Chen NH, Reith ME, & Quick MW (2004). Synaptic uptake and beyond: the sodium- and chloride-dependent neurotransmitter transporter family SLC6. *Pflugers Arch* **447**, 519-531.
24. Cherubini E, Gaiarsa JL, & Ben-Ari Y (1991). GABA: an excitatory transmitter in early postnatal life. *Trends Neurosci* **14**, 515-519.
25. Chittajallu R, Kunze A, Mangin JM, & Gallo V (2007). Differential synaptic integration of interneurons in the outer and inner molecular layers of the developing dentate gyrus. *J Neurosci* **27**, 8219-8225.
26. Danglot L, Rostaing P, Triller A, & Bessis A (2004). Morphologically identified glycinergic synapses in the hippocampus. *Mol Cell Neurosci* **27**, 394-403.
27. Demarque M, Represa A, Becq H, Khalilov I, Ben-Ari Y, & Aniksztejn L (2002). Paracrine intercellular communication by a Ca<sup>2+</sup>- and SNARE-independent release of GABA and glutamate prior to synapse formation. *Neuron* **36**, 1051-1061.
28. Dodt HU & Zieglgansberger W (1990). Visualizing unstained neurons in living brain slices by infrared DIC-videomicroscopy. *Brain Res* **537**, 333-336.
29. Dodt HU & Zieglgansberger W (1998). Visualization of neuronal form and function in brain slices by infrared videomicroscopy. *Histochem J* **30**, 141-152.
30. Dupuy ST & Houser CR (1997). Developmental changes in GABA neurons of the rat dentate gyrus: an in situ hybridization and birthdating study. *J Comp Neurol* **389**, 402-418.

31. Dupuy ST & Houser CR (1996). Prominent expression of two forms of glutamate decarboxylase in the embryonic and early postnatal rat hippocampal formation. *J Neurosci* **16**, 6919-6932.
32. Dupuy-Davies S & Houser CR (1999). Evidence for changing positions of GABA neurons in the developing rat dentate gyrus. *Hippocampus* **9**, 186-199.
33. Essrich C, Lorez M, Benson JA, Fritschy JM, & Luscher B (1998). Postsynaptic clustering of major GABAA receptor subtypes requires the gamma 2 subunit and gephyrin. *Nat Neurosci* **1**, 563-571.
34. Farrant M & Nusser Z (2005). Variations on an inhibitory theme: phasic and tonic activation of GABA(A) receptors. *Nat Rev Neurosci* **6**, 215-229.
35. Frahm C & Draguhn A (2001). GAD and GABA transporter (GAT-1) mRNA expression in the developing rat hippocampus. *Brain Res Dev Brain Res* **132**, 1-13.
36. Freund TF & Buzsaki G (1996). Interneurons of the hippocampus. *Hippocampus* **6**, 347-470.
37. Gaspary HL, Wang W, & Richerson GB (1998). Carrier-mediated GABA release activates GABA receptors on hippocampal neurons. *J Neurophysiol* **80**, 270-281.
38. Glykys J, Mann EO, & Mody I (2008). Which GABA(A) receptor subunits are necessary for tonic inhibition in the hippocampus? *J Neurosci* **28**, 1421-1426.
39. Glykys J & Mody I (2006). Hippocampal network hyperactivity after selective reduction of tonic inhibition in GABA A receptor alpha5 subunit-deficient mice. *J Neurophysiol* **95**, 2796-2807.
40. Glykys J & Mody I (2007). The main source of ambient GABA responsible for tonic inhibition in the mouse hippocampus. *J Physiol* **582**, 1163-1178.
41. Gozlan H & Ben-Ari Y (2003). Interneurons are the source and the targets of the first synapses formed in the rat developing hippocampal circuit. *Cereb Cortex* **13**, 684-692.
42. Hamill OP, Marty A, Neher E, Sakmann B, & Sigworth FJ (1981). Improved patch-clamp techniques for high-resolution current recording from cells and cell-free membrane patches. *Pflugers Arch* **391**, 85-100.
43. Hampson RE & Deadwyler SA (1992). Information processing in the dentate gyrus. *Epilepsy Res Suppl* **7**, 291-299.
44. Heinemann U, Beck H, Dreier JP, Ficker E, Stabel J, & Zhang CL (1992). The dentate gyrus as a regulated gate for the propagation of epileptiform activity. *Epilepsy Res Suppl* **7**, 273-280.
45. Hollrigel GS, Ross ST, & Soltesz I (1998). Temporal patterns and depolarizing actions of spontaneous GABAA receptor activation in granule cells of the early postnatal dentate gyrus. *J Neurophysiol* **80**, 2340-2351.
46. Holmes GL, Khazipov R, & Ben-Ari Y (2002). New concepts in neonatal seizures. *Neuroreport* **13**, A3-A8.
47. Holter NI, Zuber N, Bruehl C, & Draguhn A (2007). Functional maturation of developing interneurons in the molecular layer of mouse dentate gyrus. *Brain Res* **1186**, 56-64.

48. Huntsman MM, Porcello DM, Homanics GE, DeLorey TM, & Huguenard JR (1999). Reciprocal inhibitory connections and network synchrony in the mammalian thalamus. *Science* **283**, 541-543.
49. Ito S & Cherubini E (1991). Strychnine-sensitive glycine responses of neonatal rat hippocampal neurones. *J Physiol* **440**, 67-83.
50. Kaneda M, Farrant M, & Cull-Candy SG (1995). Whole-cell and single-channel currents activated by GABA and glycine in granule cells of the rat cerebellum. *J Physiol* **485 ( Pt 2)**, 419-435.
51. Katz LC & Shatz CJ (1996). Synaptic activity and the construction of cortical circuits. *Science* **274**, 1133-1138.
52. Kavanaugh MP, Arriza JL, North RA, & Amara SG (1992). Electrogenic uptake of gamma-aminobutyric acid by a cloned transporter expressed in *Xenopus* oocytes. *J Biol Chem* **267**, 22007-22009.
53. Kempermann G, Jessberger S, Steiner B, & Kronenberg G (2004). Milestones of neuronal development in the adult hippocampus. *Trends Neurosci* **27**, 447-452.
54. Khazipov R, Khalilov I, Tyzio R, Morozova E, Ben-Ari Y, & Holmes GL (2004). Developmental changes in GABAergic actions and seizure susceptibility in the rat hippocampus. *Eur J Neurosci* **19**, 590-600.
55. Khazipov R, Leinekugel X, Khalilov I, Gaiarsa JL, & Ben-Ari Y (1997). Synchronization of GABAergic interneuronal network in CA3 subfield of neonatal rat hippocampal slices. *J Physiol* **498 ( Pt 3)**, 763-772.
56. Klausberger T, Marton LF, O'Neill J, Huck JH, Dalezios Y, Fuentealba P, Suen WY, Papp E, Kaneko T, Watanabe M, Csicsvari J, & Somogyi P (2005). Complementary roles of cholecystikinin- and parvalbumin-expressing GABAergic neurons in hippocampal network oscillations. *J Neurosci* **25**, 9782-9793.
57. Kriegstein AR (2005). Constructing circuits: neurogenesis and migration in the developing neocortex. *Epilepsia* **46 Suppl 7**, 15-21.
58. Krosgaard-Larsen P, Frolund B, Liljefors T, & Ebert B (2004). GABA(A) agonists and partial agonists: THIP (Gaboxadol) as a non-opioid analgesic and a novel type of hypnotic. *Biochem Pharmacol* **68**, 1573-1580.
59. Kuenzi FM, Fitzjohn SM, Morton RA, Collingridge GL, & Seabrook GR (2000). Reduced long-term potentiation in hippocampal slices prepared using sucrose-based artificial cerebrospinal fluid. *J Neurosci Methods* **100**, 117-122.
60. Laurent G (2002). Olfactory network dynamics and the coding of multidimensional signals. *Nat Rev Neurosci* **3**, 884-895.
61. Laurie DJ, Wisden W, & Seeburg PH (1992). The distribution of thirteen GABAA receptor subunit mRNAs in the rat brain. III. Embryonic and postnatal development. *J Neurosci* **12**, 4151-4172.

62. LeBeau FE, Towers SK, Traub RD, Whittington MA, & Buhl EH (2002). Fast network oscillations induced by potassium transients in the rat hippocampus in vitro. *J Physiol* **542**, 167-179.
63. Lehmenkuhler A, Sykova E, Svoboda J, Zilles K, & Nicholson C (1993). Extracellular space parameters in the rat neocortex and subcortical white matter during postnatal development determined by diffusion analysis. *Neuroscience* **55**, 339-351.
64. Leinekugel X, Khalilov I, McLean H, Caillard O, Gaiarsa JL, Ben-Ari Y, & Khazipov R (1999). GABA is the principal fast-acting excitatory transmitter in the neonatal brain. *Adv Neurol* **79**, 189-201.
65. Leinekugel X, Khazipov R, Cannon R, Hirase H, Ben-Ari Y, & Buzsaki G (2002). Correlated bursts of activity in the neonatal hippocampus in vivo. *Science* **296**, 2049-2052.
66. Lerma J, Herranz AS, Herreras O, Abaira V, & Martin del RR (1986). In vivo determination of extracellular concentration of amino acids in the rat hippocampus. A method based on brain dialysis and computerized analysis. *Brain Res* **384**, 145-155.
67. Leuner B, Gould E, & Shors TJ (2006). Is there a link between adult neurogenesis and learning? *Hippocampus* **16**, 216-224.
68. Leutgeb JK, Leutgeb S, Moser MB, & Moser EI (2007). Pattern separation in the dentate gyrus and CA3 of the hippocampus. *Science* **315**, 961-966.
69. Leutgeb JK & Moser EI (2007). Enigmas of the dentate gyrus. *Neuron* **55**, 176-178.
70. Levi G & Raiteri M (1993). Carrier-mediated release of neurotransmitters. *Trends Neurosci* **16**, 415-419.
71. Li G & Pleasure SJ (2005). Morphogenesis of the dentate gyrus: what we are learning from mouse mutants. *Dev Neurosci* **27**, 93-99.
72. Liu X, Tilwalli S, Ye G, Lio PA, Pasternak JF, & Trommer BL (2000). Morphologic and electrophysiologic maturation in developing dentate gyrus granule cells. *Brain Res* **856**, 202-212.
73. Liu Y, Fujise N, & Kosaka T (1996a). Distribution of calretinin immunoreactivity in the mouse dentate gyrus. I. General description. *Exp Brain Res* **108**, 389-403.
74. Liu YB, Lio PA, Pasternak JF, & Trommer BL (1996b). Developmental changes in membrane properties and postsynaptic currents of granule cells in rat dentate gyrus. *J Neurophysiol* **76**, 1074-1088.
75. Maccaferri G & Dingledine R (2002). Complex effects of CNQX on CA1 interneurons of the developing rat hippocampus. *Neuropharmacology* **43**, 523-529.
76. Mager S, Naeve J, Quick M, Labarca C, Davidson N, & Lester HA (1993). Steady states, charge movements, and rates for a cloned GABA transporter expressed in *Xenopus* oocytes. *Neuron* **10**, 177-188.
77. Maguire JL, Stell BM, Rafizadeh M, & Mody I (2005). Ovarian cycle-linked changes in GABA(A) receptors mediating tonic inhibition alter seizure susceptibility and anxiety. *Nat Neurosci* **8**, 797-804.

78. Malchow RP & Ripps H (1990). Effects of gamma-aminobutyric acid on skate retinal horizontal cells: evidence for an electrogenic uptake mechanism. *Proc Natl Acad Sci U S A* **87**, 8945-8949.
79. Marti-Subirana A, Soriano E, & Garcia-Verdugo JM (1986). Morphological aspects of the ectopic granule-like cellular populations in the albino rat hippocampal formation: a Golgi study. *J Anat* **144**, 31-47.
80. Martina M, Schultz JH, Ehmke H, Monyer H, & Jonas P (1998). Functional and molecular differences between voltage-gated K<sup>+</sup> channels of fast-spiking interneurons and pyramidal neurons of rat hippocampus. *J Neurosci* **18**, 8111-8125.
81. Matyas F, Freund TF, & Gulyas AI (2004). Immunocytochemically defined interneuron populations in the hippocampus of mouse strains used in transgenic technology. *Hippocampus* **14**, 460-481.
82. McBain CJ, Eaton JV, Brown T, & Dingledine R (1992). CNQX increases spontaneous inhibitory input to CA3 pyramidal neurones in neonatal rat hippocampal slices. *Brain Res* **592**, 255-260.
83. McKernan RM & Whiting PJ (1996). Which GABAA-receptor subtypes really occur in the brain? *Trends Neurosci* **19**, 139-143.
84. Miles R, Toth K, Gulyas AI, Hajos N, & Freund TF (1996). Differences between somatic and dendritic inhibition in the hippocampus. *Neuron* **16**, 815-823.
85. Ming GL & Song H (2005). Adult neurogenesis in the mammalian central nervous system. *Annu Rev Neurosci* **28**, 223-250.
86. Mitchell SJ & Silver RA (2000). GABA spillover from single inhibitory axons suppresses low-frequency excitatory transmission at the cerebellar glomerulus. *J Neurosci* **20**, 8651-8658.
87. Mitchell SJ & Silver RA (2003). Shunting inhibition modulates neuronal gain during synaptic excitation. *Neuron* **38**, 433-445.
88. Mody I (2001). Distinguishing between GABA(A) receptors responsible for tonic and phasic conductances. *Neurochem Res* **26**, 907-913.
89. Mody I (2002). The GAD-given Right of Dentate Gyrus Granule Cells to Become GABAergic. *Epilepsy Curr* **2**, 143-145.
90. Mody I, Glykys J, & Wei W (2007). A new meaning for "Gin & Tonic": tonic inhibition as the target for ethanol action in the brain. *Alcohol* **41**, 145-153.
91. Mody I & Pearce RA (2004). Diversity of inhibitory neurotransmission through GABA(A) receptors. *Trends Neurosci* **27**, 569-575.
92. Mohler H (1992). GABAergic synaptic transmission. Regulation by drugs. *Arzneimittelforschung* **42**, 211-214.
93. Morozov YM, Ayoub AE, & Rakic P (2006). Translocation of synaptically connected interneurons across the dentate gyrus of the early postnatal rat hippocampus. *J Neurosci* **26**, 5017-5027.

94. Morozov YM & Freund TF (2003). Postnatal development and migration of cholecystokinin-immunoreactive interneurons in rat hippocampus. *Neuroscience* **120**, 923-939.
95. Moss SJ & Smart TG (1996). Modulation of amino acid-gated ion channels by protein phosphorylation. *Int Rev Neurobiol* **39**, 1-52.
96. Mozrzymas JW & Cherubini E (1998). Changes in intracellular calcium concentration affect desensitization of GABAA receptors in acutely dissociated P2-P6 rat hippocampal neurons. *J Neurophysiol* **79**, 1321-1328.
97. Mozrzymas JW, Zarnowska ED, Pytel M, & Mercik K (2003). Modulation of GABA(A) receptors by hydrogen ions reveals synaptic GABA transient and a crucial role of the desensitization process. *J Neurosci* **23**, 7981-7992.
98. Naus CC, Morrison JH, & Bloom FE (1988). Development of somatostatin-containing neurons and fibers in the rat hippocampus. *Brain Res* **468**, 113-121.
99. Navarro-Quiroga I, Hernandez-Valdes M, Lin SL, & Naegele JR (2006). Postnatal cellular contributions of the hippocampus subventricular zone to the dentate gyrus, corpus callosum, fimbria, and cerebral cortex. *J Comp Neurol* **497**, 833-845.
100. Neher E (1992). Correction for liquid junction potentials in patch clamp experiments. *Methods Enzymol* **207**, 123-131.
101. Neher E & Sakmann B (1992). The patch clamp technique. *Sci Am* **266**, 44-51.
102. Neher E & Sakmann B (1976). Single-channel currents recorded from membrane of denervated frog muscle fibres. *Nature* **260**, 799-802.
103. Nicholson C & Sykova E (1998). Extracellular space structure revealed by diffusion analysis. *Trends Neurosci* **21**, 207-215.
104. Nitsch R, Bergmann I, Kuppers K, Mueller G, & Frotscher M (1990). Late appearance of parvalbumin-immunoreactivity in the development of GABAergic neurons in the rat hippocampus. *Neurosci Lett* **118**, 147-150.
105. Nusser Z, Cull-Candy S, & Farrant M (1997). Differences in synaptic GABA(A) receptor number underlie variation in GABA mini amplitude. *Neuron* **19**, 697-709.
106. Nusser Z & Mody I (2002). Selective modulation of tonic and phasic inhibitions in dentate gyrus granule cells. *J Neurophysiol* **87**, 2624-2628.
107. Nusser Z, Sieghart W, & Somogyi P (1998). Segregation of different GABAA receptors to synaptic and extrasynaptic membranes of cerebellar granule cells. *J Neurosci* **18**, 1693-1703.
108. Owens DF & Kriegstein AR (2002). Is there more to GABA than synaptic inhibition? *Nat Rev Neurosci* **3**, 715-727.
109. Owens DF, Liu X, & Kriegstein AR (1999). Changing properties of GABA(A) receptor-mediated signaling during early neocortical development. *J Neurophysiol* **82**, 570-583.
110. Peng Z, Huang CS, Stell BM, Mody I, & Houser CR (2004). Altered expression of the delta subunit of the GABAA receptor in a mouse model of temporal lobe epilepsy. *J Neurosci* **24**, 8629-8639.

111. Penttonen M, Kamondi A, Sik A, Acsady L, & Buzsaki G (1997). Feed-forward and feed-back activation of the dentate gyrus in vivo during dentate spikes and sharp wave bursts. *Hippocampus* **7**, 437-450.
112. Pleasure SJ, Anderson S, Hevner R, Bagri A, Marin O, Lowenstein DH, & Rubenstein JL (2000). Cell migration from the ganglionic eminences is required for the development of hippocampal GABAergic interneurons. *Neuron* **28**, 727-740.
113. Quirk K, Blurton P, Fletcher S, Leeson P, Tang F, Mellilo D, Ragan CI, & McKernan RM (1996). [3H]L-655,708, a novel ligand selective for the benzodiazepine site of GABAA receptors which contain the alpha 5 subunit. *Neuropharmacology* **35**, 1331-1335.
114. Richerson GB & Wu Y (2003). Dynamic equilibrium of neurotransmitter transporters: not just for reuptake anymore. *J Neurophysiol* **90**, 1363-1374.
115. Rivera C, Voipio J, Payne JA, Ruusuvuori E, Lahtinen H, Lamsa K, Pirvola U, Saarma M, & Kaila K (1999). The K<sup>+</sup>/Cl<sup>-</sup> co-transporter KCC2 renders GABA hyperpolarizing during neuronal maturation. *Nature* **397**, 251-255.
116. Rossi DJ, Hamann M, & Attwell D (2003). Multiple modes of GABAergic inhibition of rat cerebellar granule cells. *J Physiol* **548**, 97-110.
117. Sassoe-Pognetto M, Panzanelli P, Sieghart W, & Fritschy JM (2000). Colocalization of multiple GABA(A) receptor subtypes with gephyrin at postsynaptic sites. *J Comp Neurol* **420**, 481-498.
118. Saxena NC & MacDonald RL (1994). Assembly of GABAA receptor subunits: role of the delta subunit. *J Neurosci* **14**, 7077-7086.
119. Schlosser B, ten BG, & Sutor B (1998). The intracellular tracer Neurobiotin alters electrophysiological properties of rat neostriatal neurons. *Neurosci Lett* **249**, 13-16.
120. Schousboe A & Redburn DA (1995). Modulatory actions of gamma aminobutyric acid (GABA) on GABA type A receptor subunit expression and function. *J Neurosci Res* **41**, 1-7.
121. Schwartz EA (1987). Depolarization without calcium can release gamma-aminobutyric acid from a retinal neuron. *Science* **238**, 350-355.
122. Scimemi A, Semyanov A, Sperk G, Kullmann DM, & Walker MC (2005). Multiple and plastic receptors mediate tonic GABAA receptor currents in the hippocampus. *J Neurosci* **25**, 10016-10024.
123. Semyanov A, Walker MC, & Kullmann DM (2003). GABA uptake regulates cortical excitability via cell type-specific tonic inhibition. *Nat Neurosci* **6**, 484-490.
124. Semyanov A, Walker MC, Kullmann DM, & Silver RA (2004). Tonic active GABA A receptors: modulating gain and maintaining the tone. *Trends Neurosci* **27**, 262-269.
125. Shapiro LA & Ribak CE (2005). Integration of newly born dentate granule cells into adult brains: hypotheses based on normal and epileptic rodents. *Brain Res Brain Res Rev* **48**, 43-56.
126. Sigworth FJ (1995). Design of the EPC-9, a computer-controlled patch-clamp amplifier. 1. Hardware. *J Neurosci Methods* **56**, ES.

127. Sloviter RS (1989). Calcium-binding protein (calbindin-D28k) and parvalbumin immunocytochemistry: localization in the rat hippocampus with specific reference to the selective vulnerability of hippocampal neurons to seizure activity. *J Comp Neurol* **280**, 183-196.
128. Sloviter RS (1991). Feedforward and feedback inhibition of hippocampal principal cell activity evoked by perforant path stimulation: GABA-mediated mechanisms that regulate excitability in vivo. *Hippocampus* **1**, 31-40.
129. Somogyi P & Klausberger T (2005). Defined types of cortical interneurone structure space and spike timing in the hippocampus. *J Physiol* **562**, 9-26.
130. Song W, Chattipakorn SC, & McMahon LL (2006). Glycine-gated chloride channels depress synaptic transmission in rat hippocampus. *J Neurophysiol* **95**, 2366-2379.
131. Soriano E, Cobas A, & Fairen A (1989a). Neurogenesis of glutamic acid decarboxylase immunoreactive cells in the hippocampus of the mouse. I: Regio superior and regio inferior. *J Comp Neurol* **281**, 586-602.
132. Soriano E, Cobas A, & Fairen A (1989b). Neurogenesis of glutamic acid decarboxylase immunoreactive cells in the hippocampus of the mouse. II: Area dentata. *J Comp Neurol* **281**, 603-611.
133. Soriano E, Cobas A, & Fairen A (1986). Asynchronism in the neurogenesis of GABAergic and non-GABAergic neurons in the mouse hippocampus. *Brain Res* **395**, 88-92.
134. Soriano E & Frotscher M (1989). A GABAergic axo-axonic cell in the fascia dentata controls the main excitatory hippocampal pathway. *Brain Res* **503**, 170-174.
135. Stell BM, Brickley SG, Tang CY, Farrant M, & Mody I (2003). Neuroactive steroids reduce neuronal excitability by selectively enhancing tonic inhibition mediated by delta subunit-containing GABAA receptors. *Proc Natl Acad Sci U S A* **100**, 14439-14444.
136. Stephenson FA (1995). The GABAA receptors. *Biochem J* **310 ( Pt 1)**, 1-9.
137. Stief F, Zuschratter W, Hartmann K, Schmitz D, & Draguhn A (2007). Enhanced synaptic excitation-inhibition ratio in hippocampal interneurons of rats with temporal lobe epilepsy. *Eur J Neurosci* **25**, 519-528.
138. Suzdak PD, Frederiksen K, Andersen KE, Sorensen PO, Knutsen LJ, & Nielsen EB (1992). NNC-711, a novel potent and selective gamma-aminobutyric acid uptake inhibitor: pharmacological characterization. *Eur J Pharmacol* **224**, 189-198.
139. Taylor J & Gordon-Weeks PR (1991). Calcium-independent gamma-aminobutyric acid release from growth cones: role of gamma-aminobutyric acid transport. *J Neurochem* **56**, 273-280.
140. Tossman U & Ungerstedt U (1986). Microdialysis in the study of extracellular levels of amino acids in the rat brain. *Acta Physiol Scand* **128**, 9-14.
141. Towers SK, LeBeau FE, Gloveli T, Traub RD, Whittington MA, & Buhl EH (2002). Fast network oscillations in the rat dentate gyrus in vitro. *J Neurophysiol* **87**, 1165-1168.

142. Tsubokawa H & Ross WN (1996). IPSPs modulate spike backpropagation and associated  $[Ca^{2+}]_i$  changes in the dendrites of hippocampal CA1 pyramidal neurons. *J Neurophysiol* **76**, 2896-2906.
143. Ueno S, Bracamontes J, Zorumski C, Weiss DS, & Steinbach JH (1997). Bicuculline and gabazine are allosteric inhibitors of channel opening of the GABAA receptor. *J Neurosci* **17**, 625-634.
144. Vargova L & Sykova E (2008). Extracellular space diffusion and extrasynaptic transmission. *Physiol Res*.
145. Wall MJ & Usowicz MM (1997). Development of action potential-dependent and independent spontaneous GABAA receptor-mediated currents in granule cells of postnatal rat cerebellum. *Eur J Neurosci* **9**, 533-548.
146. Wei W, Zhang N, Peng Z, Houser CR, & Mody I (2003). Perisynaptic localization of delta subunit-containing GABA(A) receptors and their activation by GABA spillover in the mouse dentate gyrus. *J Neurosci* **23**, 10650-10661.
147. Whittington MA & Traub RD (2003). Interneuron diversity series: inhibitory interneurons and network oscillations in vitro. *Trends Neurosci* **26**, 676-682.
148. Yang Z, Cromer BA, Harvey RJ, Parker MW, & Lynch JW (2007). A proposed structural basis for picrotoxinin and picrotin binding in the glycine receptor pore. *J Neurochem* **103**, 580-589.
149. Ylinen A, Bragin A, Nadasdy Z, Jando G, Szabo I, Sik A, & Buzsaki G (1995). Sharp Wave-Associated High-Frequency Oscillation (200-Hz) in the Intact Hippocampus - Network and Intracellular Mechanisms. *Journal of Neuroscience* **15**, 30-46.
150. Zhang N, Wei W, Mody I, & Houser CR (2007). Altered localization of GABA(A) receptor subunits on dentate granule cell dendrites influences tonic and phasic inhibition in a mouse model of epilepsy. *J Neurosci* **27**, 7520-7531.
151. Zhang ZW (2004). Maturation of layer V pyramidal neurons in the rat prefrontal cortex: intrinsic properties and synaptic function. *J Neurophysiol* **91**, 1171-1182.
152. Zhou FM & Hablitz JJ (1996). Postnatal development of membrane properties of layer I neurons in rat neocortex. *J Neurosci* **16**, 1131-1139.

**Books:**

Johnston D, Amaral DG, (1998). Hippocampus. Shepherd, G.M. (Hrsg.): The Synaptic Organisation of the Brain. 4., Oxford University Press, New York, Oxford, pp. 417-458

Numberger M, Draguhn A (1996). Patch-Clamp-Technik. Spektrum Akademischer Verlag GmbH Heidelberg, Berlin, Oxford.

Sakmann B, Neher E (1983). Single Channel Recording, Plenum New York.

# Appendix

A summary of the drugs used in the study - arranged from the companies' data sheets and interesting publications.

## *Drugs interfering with GABAergic neurotransmission*

A.1	gabazine (SR 95531 hydrobromide)	GABA <sub>A</sub> -receptor antagonist
A.2	picrotoxin	GABA <sub>A</sub> -receptor antagonist
A.3	L-655,708	GABA <sub>A</sub> -receptor antagonist, specific for $\alpha_5$ -subunit
A.4	THIP hydrochloride (gaboxadol)	agonist of $\delta$ -subunit containing GABA <sub>A</sub> receptors
A.5	CGP 55845A	GABA <sub>B</sub> -receptor antagonist
A.6	NNC-711	GAT-1 antagonist

## *Drugs interfering with excitatory glutamate receptors*

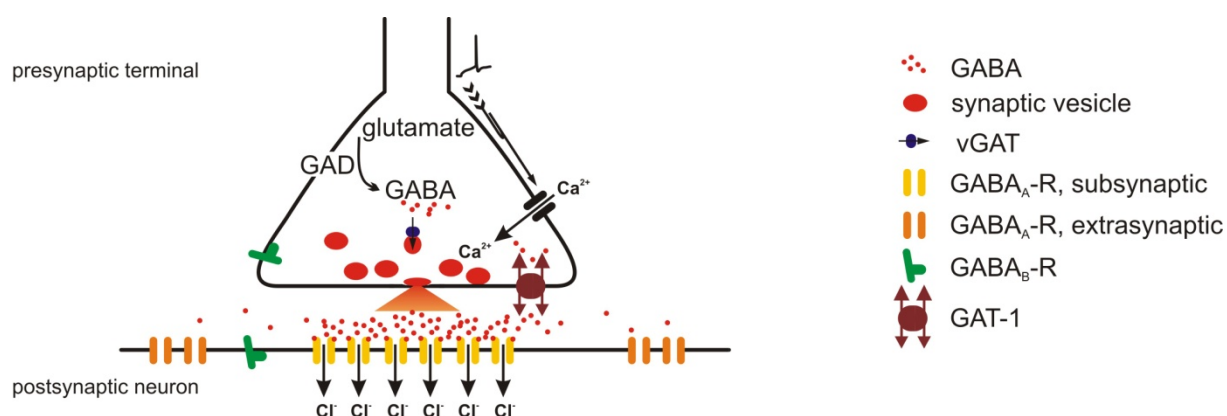
A.7	APV (DL-2-Amino-5-phosphonopentanoic acid)	NMDA receptor antagonist
A.8	CNQX (6-Cyano-7-nitroquinoxalin-2,3-dione)	AMPA/kainate receptor antagonist

## *Durg interfering with inhibitory glycine receptors*

A.9	Strychnine	glycine receptor antagonist
-----	------------	-----------------------------

## *Drugs interfering with synaptic release*

A.10	TTX	Selective inhibitor of Na <sup>+</sup> channel conductance
A.11	QX314 bromide	blocker of voltage-activated Na <sup>+</sup> channels

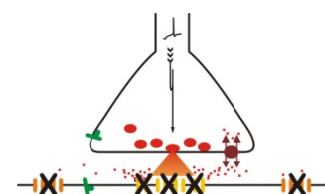


**The GABAergic synapse.** At the presynaptic terminal glutamate is metabolized into GABA by the Glutamic acid decarboxylase (GAD). The vesicular GABA transporter (vGAT) transports GABA into synaptic vesicles. Local action-potential triggered calcium ion influx leads to transmitter release into the synaptic cleft. At the postsynapse ligand-bound GABA<sub>A</sub>-receptor (GABA<sub>A</sub>-R) opens and chloride influx caused membrane hyperpolarization. GABA is translocated back in the presynapse by neuronal GABA-transporter (GAT-1). GABA<sub>B</sub>-receptors are located at pre- and postsynaptic sides (GABA<sub>B</sub>-R).

**Review:** Hevers W & Luddens H (1998). The diversity of GABAA receptors. Pharmacological and electrophysiological properties of GABAA channel subtypes. *Mol Neurobiol* **18**, 35-86.

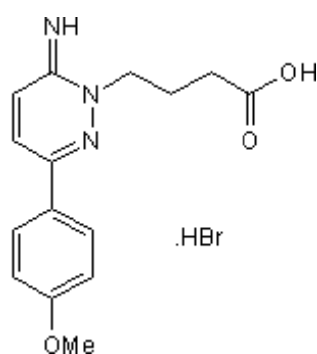
## A.1 gabazine (SR 95531 hydrobromide)

### *GABA<sub>A</sub>* -receptor antagonist



Gabazine is a selective, competitive GABA<sub>A</sub>-receptor antagonist. It displaces [3H]-GABA from rat brain membranes with a K<sub>i</sub> of 150 nM. Unlike bicuculline, gabazine selectively antagonises GABA-induced Cl<sup>-</sup> currents with little action on pentobarbitone-induced currents.

#### Molecular Structure:



6-imino-3-(4-methoxyphenyl)-1(6H)-pyridazinebutanoic acid hydrobromide

#### Physical and Chemical Properties:

Molecular Formula: C<sub>15</sub>H<sub>17</sub>N<sub>3</sub>O<sub>3</sub>.HBr

Molecular Weight: 368.23

CAS Number: [104104-50-9]

Physical Appearance: white solid

Solubility: Water to 25 mM  
Phosphate buffered saline to 5 mM  
Ethanol to 20 mM  
DMSO to 100 mM

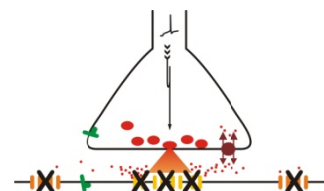
Gabazine stock solution (2mM in aqua bidest) was stored in small aliquots at -20°C and diluted to the final concentration of 200nM to 2µM in the recording solution.

#### References:

- Ito Y, Koshiha T, Doi M, Asami S, Fukuda H, & Murakoshi Y (1992). Characterization of antagonistic activity and binding properties of SR 95531, a pyridazinyl-GABA derivative, in rat brain and cultured cerebellar neuronal cells. *Synapse* **10**, 326-333.
- Luddens H & Korpi ER (1995). GABA antagonists differentiate between recombinant GABAA/benzodiazepine receptor subtypes. *J Neurosci* **15**, 6957-6962.
- Uchida I, Cestari IN, & Yang J (1996). The differential antagonism by bicuculline and SR95531 of pentobarbitone-induced currents in cultured hippocampal neurons. *Eur J Pharmacol* **307**, 89-96.
- Ueno S, Bracamontes J, Zorumski C, Weiss DS, & Steinbach JH (1997). Bicuculline and gabazine are allosteric inhibitors of channel opening of the GABAA receptor. *J Neurosci* **17**, 625-634.
- Wermuth CG, Bourguignon JJ, Schlewer G, Gies JP, Schoenfelder A, Melikian A, Bouchet MJ, Chantreux D, Molimard JC, Heaulme M, & . (1987). Synthesis and structure-activity relationships of a series of aminopyridazine derivatives of gamma-aminobutyric acid acting as selective GABA-A antagonists. *J Med Chem* **30**, 239-249.

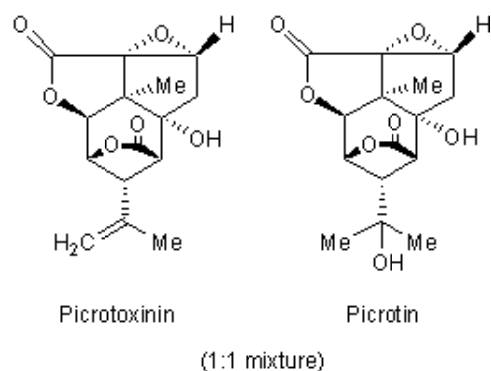
## A.2 *picotoxin*

### *GABA<sub>A</sub>-receptor antagonist*



Picrotoxin is a 1:1 mixture of picrotoxinin and picrotin. The GABA<sub>A</sub>-receptor antagonist is a potent CNS stimulant. Note that picrotoxin also inhibits glycine receptors, though in a use dependent manner (Wang *et al.*, 2007; Yang *et al.*, 2007).

#### Molecular Structure:



#### Physical and Chemical Properties:

Molecular Formula: C<sub>30</sub>H<sub>34</sub>O<sub>13</sub>

Molecular Weight: 602.59

CAS Number: [124-87-8]

Physical Appearance: White solid

#### **POTENT NEUROTOXIN – TREAT AS EXTREMELY POISONOUS**

Solubility: Ethanol to 50 mM  
DMSO to 10 mM  
Water to 1mM

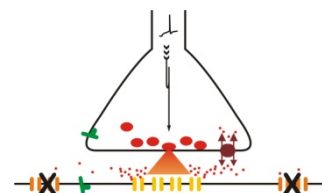
For pilot experiments picrotoxin was diluted in ethanol. The waveform of action potentials slowed down, an effect which appeared to be due to the solvent (Reynolds *et al.*, 1990). Further, ethanol was reported to act on GABA<sub>A</sub>-receptors, most notably on tonic inhibition (Mody *et al.*, 2007). Therefore, picrotoxin was dissolved in water. The stock solution (1 mM in aqua bidest) was stored at -20°C. Prior to use, a 'picrotoxin ACSF' was prepared by diluting the picrotoxin stock together with the stock solutions for the ACSF (all 1:10) up to the final picrotoxin concentration (100 μM).

#### References:

- Dillon GH, Im WB, Carter DB, & McKinley DD (1995). Enhancement by GABA of the association rate of picrotoxin and tert-butylbicyclophosphorothionate to the rat cloned alpha 1 beta 2 gamma 2 GABAA receptor subtype. *Br J Pharmacol* **115**, 539-545.
- Etter A, Cully DF, Liu KK, Reiss B, Vassilatis DK, Schaeffer JM, & Arena JP (1999). Picrotoxin blockade of invertebrate glutamate-gated chloride channels: subunit dependence and evidence for binding within the pore. *J Neurochem* **72**, 318-326.
- Mody I, Glykys J, & Wei W (2007). A new meaning for "Gin & Tonic": tonic inhibition as the target for ethanol action in the brain. *Alcohol* **41**, 145-153.
- Newland CF & Cull-Candy SG (1992). On the mechanism of action of picrotoxin on GABA receptor channels in dissociated sympathetic neurones of the rat. *J Physiol* **447**, 191-213.
- Reynolds JN, Wu PH, Khanna JM, & Carlen PL (1990). Ethanol tolerance in hippocampal neurons: adaptive changes in cellular responses to ethanol measured in vitro. *J Pharmacol Exp Ther* **252**, 265-271.
- Wang DS, Buckinx R, Lecorronc H, Mangin JM, Rigo JM, & Legendre P (2007). Mechanisms for picrotoxinin and picrotin blocks of alpha2 homomeric glycine receptors. *J Biol Chem* **282**, 16016-16035.
- Yang Z, Cromer BA, Harvey RJ, Parker MW, & Lynch JW (2007). A proposed structural basis for picrotoxinin and picrotin binding in the glycine receptor pore. *J Neurochem* **103**, 580-589.

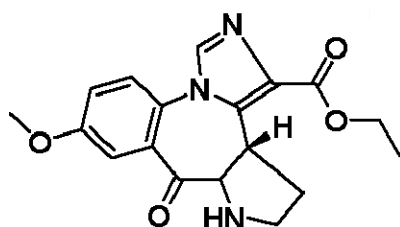
## A.3 L-655,708

*GABA<sub>A</sub>-receptor antagonist, specific for  $\alpha_5$ -subunit*



Novel ligand selective for the benzodiazepine site of GABA<sub>A</sub>-receptors which contain the  $\alpha_5$ -subunit (Quirk *et al.*, 1996).

## Molecular Structure



## Physical and Chemical Properties:

Molecular Formula C<sub>18</sub>H<sub>19</sub>N<sub>3</sub>O<sub>4</sub>

Molecular Weight 341.36

MDL number MFCD02684528

Physical Appearance: powder

Ethyl (S)-11,12,13,13a-

Tetrahydro-7-methoxy-9-oxo-9H-imidazo[1,5-a]pyrrolo[2,1c][1,4] benzodiazepine -1-carboxylate

Solubility: DMSO: 6 mg/mL  
insoluble in water

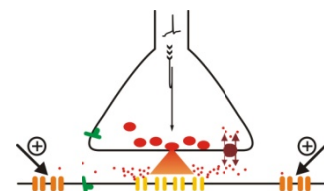
L655,708 was dissolved in DMSO (5 mM) and stored in small aliquots at -20°C. It was diluted to its final concentration of 500nM in the recording solution (use dilution series).

**Reference:**

- Quirk K, Blurton P, Fletcher S, Leeson P, Tang F, Mellilo D, Ragan CI, & McKernan RM (1996). [3H]L-655,708, a novel ligand selective for the benzodiazepine site of GABA<sub>A</sub> receptors which contain the alpha 5 subunit. *Neuropharmacology* **35**, 1331-1335.
- Mody I (2001). Distinguishing between GABA(A) receptors responsible for tonic and phasic conductances. *Neurochem Res* **26**, 907-913.
- Sur C, Fresu L, Howell O, McKernan RM, & Atack JR (1999). Autoradiographic localization of alpha5 subunit-containing GABA<sub>A</sub> receptors in rat brain. *Brain Res* **822**, 265-270.
- Sur C, Quirk K, Dewar D, Atack J, & McKernan R (1998). Rat and human hippocampal alpha5 subunit-containing gamma-aminobutyric AcidA receptors have alpha5 beta3 gamma2 pharmacological characteristics. *Mol Pharmacol* **54**, 928-933.

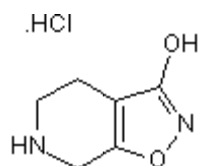
#### A.4 THIP hydrochloride (gaboxadol)

agonist of  $\delta$ -subunit containing GABA<sub>A</sub>-receptors



THIP hydrochloride is a systemically active GABA<sub>A</sub>-receptor agonist and GABA<sub>C</sub>-receptor antagonist. It displays antinociceptive, anticonvulsant and sedative effects. The hypnotic agent enhances delta activity within non-REM sleep in rats.

Molecular Structure:



Physical and Chemical Properties:

Molecular Formula: C<sub>6</sub>H<sub>8</sub>N<sub>2</sub>O<sub>2</sub>.HCl

Molecular Weight: 176.6

CAS Number: [64603-91-4]

4,5,6,7-Tetrahydroisoxazolo[5,4-c]pyridin-3-ol hydrochloride

Solubility: Water to 100 mM  
DMSO to 100 mM

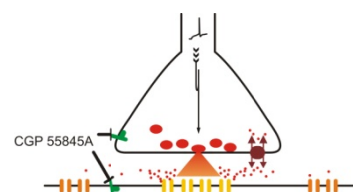
THIP was dissolved in water (100 mM) and stored in small aliquots at -20°C. It was diluted to its final concentration of 1  $\mu$ M in the recording solution (use dilution series).

#### References:

- Johnston GA (1996). GABA<sub>C</sub> receptors: relatively simple transmitter-gated ion channels? *Trends Pharmacol Sci* 17, 319-323.
- Krogsgaard-Larsen P & Falch E (1981). GABA agonists. Development and interactions with the GABA receptor complex. *Mol Cell Biochem* 38 Spec No, 129-146.
- Krogsgaard-Larsen P, Frolund B, & Liljefors T (2002). Specific GABA(A) agonists and partial agonists. *Chem Rec* 2, 419-430.
- Krogsgaard-Larsen P, Frolund B, Liljefors T, & Ebert B (2004). GABA(A) agonists and partial agonists: THIP (Gaboxadol) as a non-opioid analgesic and a novel type of hypnotic. *Biochem Pharmacol* 68, 1573-1580.
- Krogsgaard-Larsen P, Mikkelsen H, Jacobsen P, Falch E, Curtis DR, Peet MJ, & Leah JD (1983). 4,5,6,7-Tetrahydroisothiazolo[5,4-c]pyridin-3-ol and related analogues of THIP. Synthesis and biological activity. *J Med Chem* 26, 895-900.

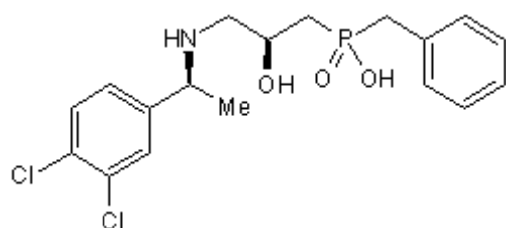
## A.5 CGP 55845A

### *GABA<sub>B</sub>*-receptor antagonist



Potent, selective GABA<sub>B</sub>-receptor antagonist (IC<sub>50</sub> = 6 nM).

Molecular Structure:



Physical and Chemical Properties:

Molecular Formula: C<sub>18</sub>H<sub>22</sub>Cl<sub>2</sub>NO<sub>3</sub>P

Molecular Weight: 402.26

CAS Number: [149184-22-5]

Physical Appearance: White solid

(2S)-3-[[[(1S)-1-(3,4-Dichlorophenyl)ethyl]amino]-2-hydroxypropyl](phenylmethyl)phosphinic acid

Solubility: DMSO to 100 mM

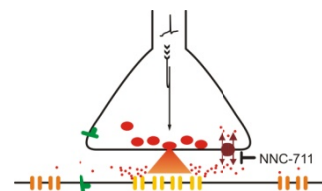
CGP 55845A stock solution (10mM in DMSO) was stored in small aliquots at -20°C and diluted to the final concentration of 5 μM in the recording solution (1 μM Prenosil *et al.*, 2006; 5 μM Scimemi *et al.*, 2005)

### References:

- Cunningham MD & Enna SJ (1996). Evidence for pharmacologically distinct GABAB receptors associated with cAMP production in rat brain. *Brain Res* **720**, 220-224.
- Davies CH, Pozza MF, & Collingridge GL (1993). CGP 55845A: a potent antagonist of GABAB receptors in the CA1 region of rat hippocampus. *Neuropharmacology* **32**, 1071-1073.
- Deisz RA (1999). The GABA(B) receptor antagonist CGP 55845A reduces presynaptic GABA(B) actions in neocortical neurons of the rat in vitro. *Neuroscience* **93**, 1241-1249.
- Prenosil GA, Schneider Gasser EM, Rudolph U, Keist R, Fritschy JM, & Vogt KE (2006). Specific subtypes of GABAA receptors mediate phasic and tonic forms of inhibition in hippocampal pyramidal neurons. *J Neurophysiol* **96**, 846-857.
- Scimemi A, Semyanov A, Sperk G, Kullmann DM, & Walker MC (2005). Multiple and plastic receptors mediate tonic GABAA receptor currents in the hippocampus. *J Neurosci* **25**, 10016-10024.

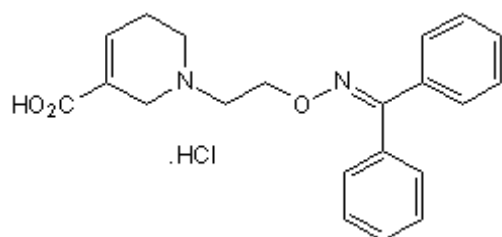
## A.6 NNC-711

### *inhibitor of GABA uptake by GAT-1*



Potent and selective inhibitor of GABA uptake by GAT-1 (IC<sub>50</sub> values are 0.04, 171, 1700 and 622  $\mu$ M for hGAT-1, rGAT-2, hGAT-3 and hBGT-1 respectively). Anticonvulsant following systemic administration in vivo.

#### Molecular Structure:



#### Physical and Chemical Properties:

Molecular Formula: C<sub>21</sub>H<sub>22</sub>N<sub>2</sub>O<sub>3</sub>.HCl

Molecular Weight: 386.88

CAS Number: [145645-62-1]

Physical Appearance: White solid

1,2,5,6-Tetrahydro-1-[2-[[[(diphenylmethylene)amino]oxy]ethyl]-3-pyridinecarboxylic acid hydrochloride

Solubility: Water to 10 mM  
Ethanol to 10 mM  
DMSO to 100 mM

NNC-711 stock solution (10 mM in aqua bidest) was stored in small aliquots at -20°C and diluted to the final concentration of 10  $\mu$ M in the recording solution.

#### References:

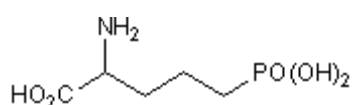
- Borden LA, Murali Dhar TG, Smith KE, Weinshank RL, Branchek TA, & Gluchowski C (1994). Tiagabine, SK&F 89976-A, CI-966, and NNC-711 are selective for the cloned GABA transporter GAT-1. *Eur J Pharmacol* **269**, 219-224.
- O'Connell AW, Fox GB, Kjoller C, Gallagher HC, Murphy KJ, Kelly J, & Regan CM (2001). Anti-ischemic and cognition-enhancing properties of NNC-711, a gamma-aminobutyric acid reuptake inhibitor. *Eur J Pharmacol* **424**, 37-44.
- Suzdak PD, Frederiksen K, Andersen KE, Sorensen PO, Knutsen LJ, & Nielsen EB (1992). NNC-711, a novel potent and selective gamma-aminobutyric acid uptake inhibitor: pharmacological characterization. *Eur J Pharmacol* **224**, 189-198.

## A.7 DL-2-Amino-5-phosphonopentanoic acid (APV)

### NMDA receptor antagonist

APV is a potent NMDA antagonist.

Molecular Structure:



DL-2-Amino-5-phosphonopentanoic acid

Physical and Chemical Properties:

Molecular Formula: C<sub>5</sub>H<sub>12</sub>NO<sub>5</sub>P

Molecular Weight: 197.13

CAS Number: [76326-31-3]

Physical Appearance: White solid

Solubility: Water to 10 mM  
1eq. NaOH to 100 mM

APV was dissolved in water (30 mM; encouraged by 1 eq. NaOH) and stored in small aliquots at -20°C. The stock solution was diluted to the final concentration of 30 μM in the recording solution.

### References:

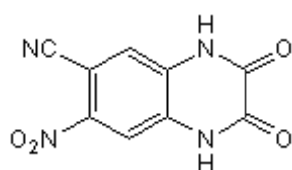
- Evans RH, Francis AA, Jones AW, Smith DA, & Watkins JC (1982). The effects of a series of omega-phosphonic alpha-carboxylic amino acids on electrically evoked and excitant amino acid-induced responses in isolated spinal cord preparations. *Br J Pharmacol* **75**, 65-75.
- Davies J & Watkins JC (1982). Actions of D and L forms of 2-amino-5-phosphonovalerate and 2-amino-4-phosphonobutyrate in the cat spinal cord. *Brain Res* **235**, 378-386.

## A.8 6-Cyano-7-nitroquinoxalin-2,3-dione (CNQX)

### *non-NMDA receptor antagonist*

CNQX is a Potent AMPA/kainate receptor antagonist and also an antagonist at glycine modulatory site on the NMDA receptor complex. Note, that CNQX increases IPSC frequency during early postnatal development (Maccaferri & Dingledine, 2002; McBain *et al.*, 1992).

Molecular Structure:



6-cyano-2,3 dihydroxy-7-nitro-quinoxaline

Physical and Chemical Properties:

Molecular Formula: C<sub>9</sub>H<sub>4</sub>N<sub>4</sub>O<sub>4</sub>

Molecular Weight: 232.16

CAS Number: [115066-14-3]

Physical Appearance: Cream solid

Solubility: DMSO to 100 mM

CNQX was actually dissolved in water (10 mM; encouraged by 1 eq. NaOH) and stored in small aliquots at -20°C. The stock solution was diluted to the final concentration of 20 μM in the recording solution.

### References:

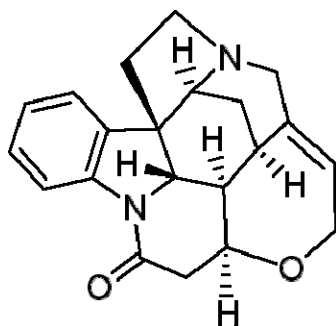
- Honore T, Davies SN, Drejer J, Fletcher EJ, Jacobsen P, Lodge D, & Nielsen FE (1988). Quinoxalinediones: potent competitive non-NMDA glutamate receptor antagonists. *Science* **241**, 701-703.
- King AE, Lopez-Garcia JA, & Cumberbatch M (1992). Antagonism of synaptic potentials in ventral horn neurones by 6-cyano-7-nitroquinoxaline-2,3-dione: a study in the rat spinal cord in vitro. *Br J Pharmacol* **107**, 375-381.
- Long SK, Smith DA, Siarey RJ, & Evans RH (1990). Effect of 6-cyano-2,3-dihydroxy-7-nitro-quinoxaline (CNQX) on dorsal root-, NMDA-, kainate- and quisqualate-mediated depolarization of rat motoneurons in vitro. *Br J Pharmacol* **100**, 850-854.
- Maccaferri G & Dingledine R (2002). Complex effects of CNQX on CA1 interneurons of the developing rat hippocampus. *Neuropharmacology* **43**, 523-529.
- McBain CJ, Eaton JV, Brown T, & Dingledine R (1992). CNQX increases spontaneous inhibitory input to CA3 pyramidal neurones in neonatal rat hippocampal slices. *Brain Res* **592**, 255-260.
- Watkins JC, Krosggaard-Larsen P, & Honore T (1990). Structure-activity relationships in the development of excitatory amino acid receptor agonists and competitive antagonists. *Trends Pharmacol Sci* **11**, 25-33.

## A.9 Strychnine

### *glycine receptor antagonist*

Strychnine is a glycine receptor antagonist binding to  $\alpha_1$ -subunit containing glycine receptors (Betz & Laube, 2006).

Molecular Structure:



(-)-Strychnine

Physical and Chemical Properties:

Molecular Formula  $C_{21}H_{22}N_2O_2$

Molecular Weight 334.41

CAS Number 57-24-9

Solubility: chloroform (clear to hazy)

Strychnine was diluted in water at 100  $\mu$ M and diluted to the final concentration in the recording solution (1  $\mu$ M).

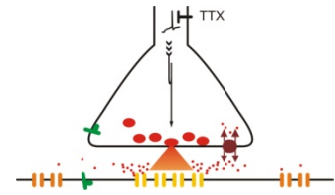
## References

Betz H & Laube B (2006). Glycine receptors: recent insights into their structural organization and functional diversity. *J Neurochem* **97**, 1600-1610.

White WF (1985). The glycine receptor in the mutant mouse spastic (spa): strychnine binding characteristics and pharmacology. *Brain Res* **329**, 1-6.

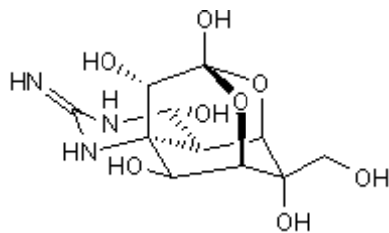
## A.10 TTX

### *selective inhibitor of Na<sup>+</sup> channel conductance*



The selective inhibitor of Na<sup>+</sup> channel conductance binds reversible and with a high affinity ( $K_d = 1\text{-}10$  nM). It blocks Na<sup>+</sup> channels in a use dependent manner.

#### Molecular Structure:



#### Physical and Chemical Properties:

Molecular Formula: C<sub>11</sub>H<sub>17</sub>N<sub>3</sub>O<sub>8</sub>

Molecular Weight: 319.27

CAS Number: [4368-28-9]

Octahydro-12-(hydroxymethyl)-2-imino-5,9:7,10a-dimethano-10aH[1,3]dioxocino[6,5d]pyrimidine-4,7,10,11,12-pentol

Solubility: Acidic buffer (pH 4.8) to 3 mM

TTX was dissolved in water (1 mM in aqua bidest.) and stored in small aliquots at -20°C. The stock solution was diluted to the final concentration of 0.5 μM in the recording solution.

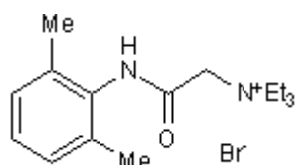
#### References:

- Gleitz J, Tosch C, Beile A, & Peters T (1996). The protective action of tetrodotoxin and (+/-)-kavain on anaerobic glycolysis, ATP content and intracellular Na<sup>+</sup> and Ca<sup>2+</sup> of anoxic brain vesicles. *Neuropharmacology* **35**, 1743-1752.
- Kao CY (1986). Structure-activity relations of tetrodotoxin, saxitoxin, and analogues. *Ann N Y Acad Sci* **479**, 52-67.
- Kao CY (1972). Pharmacology of tetrodotoxin and saxitoxin. *Fed Proc* **31**, 1117-1123.

### A.11 QX314 bromide

QX314 bromide membrane impermeable quaternary derivative of lidocaine, a blocker of voltage-activated Na<sup>+</sup> channels. Intracellular QX 314 bromide also inhibits calcium currents in hippocampal CA1 pyramidal neurons.

Molecular Structure:



Physical and Chemical Properties:

Molecular Formula: C<sub>16</sub>H<sub>27</sub>N<sub>2</sub>OBr

Molecular Weight: 343.31

CAS Number: [21306-56-9]

Physical Appearance: White solid

*N*-(2,6-Dimethylphenylcarbamoylmethyl)triethylammonium bromide

Solubility: Water to 100 mM

#### References:

- Strichartz GR (1973). The inhibition of sodium currents in myelinated nerve by quaternary derivatives of lidocaine. *J Gen Physiol* **62**, 37-57.
- Alreja M & Aghajanian GK (1994). QX-314 blocks the potassium but not the sodium-dependent component of the opiate response in locus coeruleus neurons. *Brain Res* **639**, 320-324.
- Perkins KL & Wong RK (1995). Intracellular QX-314 blocks the hyperpolarization-activated inward current I<sub>q</sub> in hippocampal CA1 pyramidal cells. *J Neurophysiol* **73**, 911-915.
- Talbot MJ & Sayer RJ (1996). Intracellular QX-314 inhibits calcium currents in hippocampal CA1 pyramidal neurons. *J Neurophysiol* **76**, 2120-2124.